Landbrugsministeriet
Statens Planteavlsforsøg

Proceedings from the workshop on remote sensing

Sostrup Castle, Grenå, May 6-7, 1991

Editors:
Anton Thomsen
The Danish Institute of Plant and Soil Science
Research Centre of Agriculture
Department of Agrometeorology
DK-8830 Tjele

Arne Jensen
Risø National Laboratory
Environmental Science and Technology Department
DK-4000 Roskilde

Henry E. Jensen
The Royal Veterinary and Agricultural University
Department of Agricultural Sciences
Section of Soil, Water and Plant Nutrition
DK-1871 Frederiksberg C

Tidsskrift for Planteavls Specialserie

Beretning nr. S 2207 - 1992

Landbrugsministeriet
Statens Planteavlsforsøg

Proceedings from the Workshop on Remote Sensing

Sostrup Castle, Grenå May 6-7, 1991

Editors
Anton Thomsen
The Danish Institute of Plant and Soil Science
Department of Agrometeorology

Arne Jensen
Risø National Laboratory
Environmental Science and Technology Department

Henry E. Jensen
The Royal Veterinary and Agricultural University
Section of Soil, Water and Plant Nutrion

Tidsskrift for Planteavls Specialserie

Beretning nr. S 2207 - 1992

Preface

Proceedings from the Workshop on Remote Sensing held at the Sostrup Castle, Grenå, May 6-7, 1991.

The workshop and the publication of the proceedings was partly funded by the Danish Agricultural and Veterinary Research Council (SJVF).

The workshop was organized jointly by the following Danish institutions:

- The Danish Institute of Plant and Soil Science, Ministry of Agriculture.
- Botanical Institute, University of Aarhus.
- The Royal Veterinary and Agricultural University, Copenhagen.

The workshop was planned in order to present the state of the art in remote sensing applications within the following disciplines:

- Spectral measurements and its application to monitoring crop conditions (biomass, LAI, plant diseases, etc.)
- Surface temperatures and its application to monitoring crop water status, stress, etc.
- Aerial photography and satellite imagery and its application to mapping of surface types, surface temperatures, etc.

In Denmark, a number of remote sensing research projects, mainly sponsored by government research councils, have been completed. The May workshop was the third and final workshop presenting results from these projects. It was the aim of the organizing committee to present the major results from Danish remote sensing research in a single publication.

The organizers would like to thank the workshop participants for their contributions to a successful workshop. The lively and enlightning contributions by Jürgen Schellberg of the University of Rheinischen Friedrich-Wilhelms, Germany and Michael A. Hardisky of the University of Scranton, USA are especially acknowledged.

Research Centre Foulum
February 1992

Anton Thomsen
Arne Jensen
Henry E. Jensen

Contents

Spectral images of plants, progress and prospects

Arne Jensen
Environmental Science and Technology Department
Risø National Laboratory, P.O. Box 49, DK-4000 Roskilde, Denmark

Introduction

For the application of remote sensing to e.g., ecosystem studies, crop inventories, yield prediction related to diseases and stresses, climate or soils, there are a number of constrains which often impede the transition from research to operational use of remote sensing techniques. Going from research projects to applications seems especially difficult for remote sensing techniques using space data, whereas the transition from airborne and near surface techniques to operational applications seem less problematic.

Remotely sensed information related to vegetation canopies can only be interpreted precisely if the mechanisms of interaction of electromagnetic radiation with the atmosphere, live and dead plant material and the soil are well known.

The optical properties of vegetation canopies show great spatial and temporal variations. These variations are caused by diurnal and seasonal changes in the physical and chemical environment and by the biological development of the canopy.

This short review will mainly consider problems related to plant canopies and data obtained by use of near surface remote sensing techniques.

Sampling frequency and spatial resolution

The potential of remote sensing in various disciplines is limited by spatial and temporal restrictions mainly because of limitations in current data handling systems, but also by limitations in spatial resolution of current techniques (Fig. 1).

Biological and agricultural applications of remote sensing require adequate temporal and spatial resolution. The frequency of the temporal sampling must be high enough to resolve the critical and indicative changes in plant canopies and other biological systems, which takes place over periods of a few days or less. Thus there should be an option of acquiring data every two or tree days even if this high sampling frequency only is needed during a relatively short period of time.

For applications of remote sensing carried out on the ground or from vehicles the spatial resolution is usually not a problem. However, it is important to stress that the total area sampled, perhaps by a number of subsamples, should be large enough to represent the plant community, crop or soil cover in question. In crops like wheat an area of about one meter in diameter is needed to represent the crop correctly.

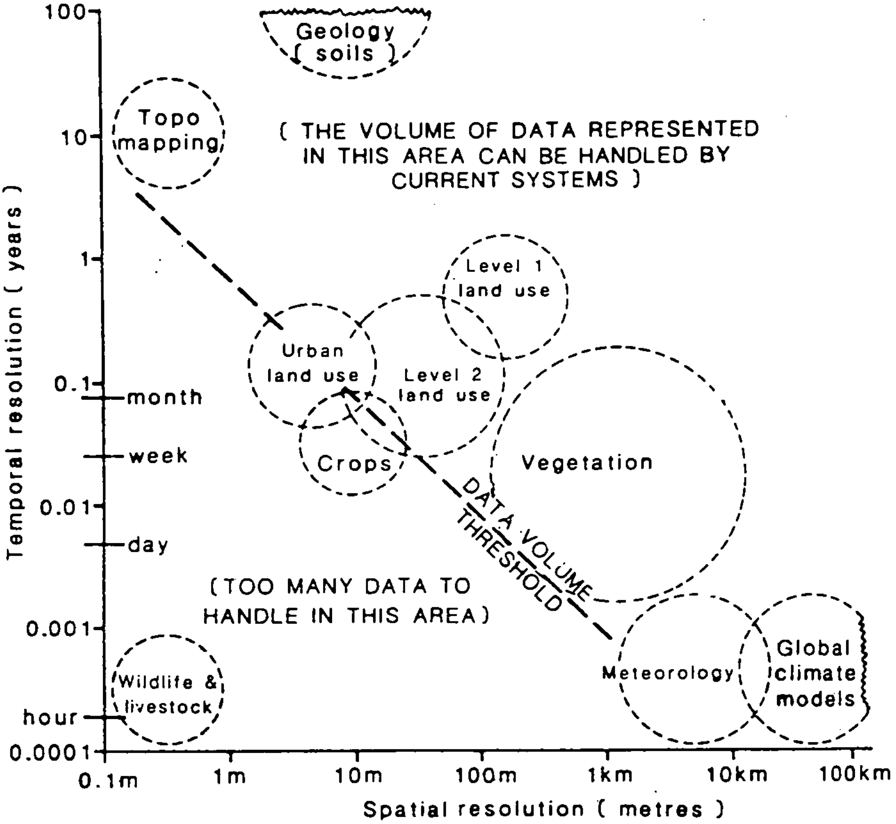

Figure 1: The requirements of agricultural applications with respect to spatial and temporal resolution of remote sensing systems compared with those of other users of remotely sensed data (redrawn from Allan 1990).

Biomass and plant production

Most green leaves strongly reflect (40-45 %) near infrared radiation (NIR; 700 to 1300 nm). In this wavelength interval of the spectrum, absorptance is low (5-10 %) and the percentage of radiation transmitted is similar to that which is reflected. Most green leaves strongly absorb 90 to 95 % red radiation (R; 625 to 680 nm). In the red part of the spectrum transmission is very low, 1 to 5 %, and the reflection from leaves is also low 5 to 10 %. Several authors have shown seasonal changes in red and infrared reflectance from canopies. Generally, as the amount of photosynthetic tissue increases during the growing season, the reflectance of the canopy declines in the red region and increases in the infrared region. From these observations the amount of photosynthetic tissue appears to be the major factor determining infrared reflectance of a canopy.

Several papers have demonstrated how remote sensing techniques can be used to estimate rates of dry matter accumulation in communities of natural plants, and in crop stands. During the growing season of 1977 the quantity of near infrared reflection from the vegetation in a salt marsh was used to predict the amount of standing crop of photosynthetic tissue in the plant community (figure 2). The predicted values was within 10 % of the measured values obtained by use of harvest techniques (Jensen, 1980). In addition the amount of reflected near infrared radiation was found to be strongly correlated with leaf area index of the canopy.

Later it became customary to work with wavebands just below and just above a wavelength of 700 nm to give a maximum discrimination between foliage, dead biomass and the underlying soil. The Normalized Difference

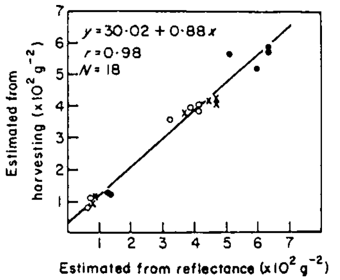

Figure 2: Relationships between predicted and observed values of the biomass of photosynthetic tissue (•), biomass of leaves of all species (×) and biomass of Halimione portulacoides leaves (o) in a salt marsh plant community (after Jensen 1980).

Vegetation Index was adopted for biomass determination NDVI= (IR - R) / (IR + R) together with the dry matter/ radiation quotient, *e*. During vegetative growth, many agricultural crops and some other vegetation types have remarkably similar values of *e*. A typical figure for C3 plants is 1.4 gram of dry matter for each MJ of total solar radiation intercepted (Monteith 1977). C4 species, for example maize, seem to exhibit somewhat larger values of *e*. It has been demonstrated that the Normalized Vegetation Index, NDVI, shows a strong near-linear relationship to the fraction of visible radiation intercepted by a vegetation canopy, and appears to be almost insensitive to variations in canopy geometry. Given daily mean values of incoming solar radiation and the fraction of radiation intercepted by the canopy several authors have demonstrated that remote sensing can be used to estimate rates of biomass accumulation by crop stands during vegetative growth. However, the existing models do not give good estimates of biomass accumulation early in the growing season when the leaf area index is low and radiation reflected by the soil surface interferes with the reflection from the foliage. Later in the growing season during the transition from the vegetative growth to senescence the models also loose sensitivity because of interference from dead plant material within the canopy, and from the soil, of which larger and larger proportions become exposed to the sensors during senescence.

Interference from soil, dead and senescent plant material

The reflectance of plant canopies depends on the amount of senescent and dead plant material, and on the percentage of ground cover as well as on the optical properties of the dead biomass and the soil background.

The effect of the soil background can clearly be seen up to a leaf area index of approximately 3, which corresponds to nearly complete canopy cover. At LAI values between 3 and 5 the near-infrared reflectance becomes increasingly saturated and the interference from the soil can be neglected. The reflectance from the soil background depends strongly on the moisture contents in the upper few millimetres of the soil profile (fig. 3), and the reflectance is inversely related to the moisture content of the soil. The reflectance from dead biomass also strongly depends on the water content, and the reflectance is inversely related to the moisture content of the dead biomass (figure 4).

In two natural plant communities (I_{low} & II_{high} in dead biomass) differing in the amount of dead plant biomass interfering with the NIR and R reflectance from the canopy, several normalisation indices (NIR blue^{-1}, NIR red^{-1}, VI, PI and NIR_{bio}) were tested. Positive relations between these indices and total live biomass and green biomass were observed, with values between 0.69 and 0.96. Inverse relations of an asymptotic nature were observed between dead biomass as a percentage of total biomass and of green biomass, with values between 0.90 and 0.91 (Lorenzen and Jensen 1988). A model discriminating live and dead aboveground biomass was developed to improve correlations between canopy reflectance and biomass variables. On the condition that the influence of NIR_{dead} on total NIR reflectance decreased as a proportion of dead biomass the following equation was developed

$$NIR_{bio} = NIR_{tot} - NIR_{tot}(d[a(NIR_{tot}red^{-1})^{b}]^{-1})$$

Normalizing the total NIR reflectance from the two different plant canopies with this equation the correlation in community I was unchanged, but the normalization nearly doubled the correlation coefficient between biomass and reflection in community II.

Crop diseases

Already in the 1920s remote sensing techniques were proposed as tools to forecast the dispersal of various diseases in crops (Taubenhous et al. 1929). Later Colwell (1956) among others described applications of aerial photography and false colour infrared films for detection and assessment of crop diseases. Attempts have also been made to use multispectral sensors and satellite images in detection of diseased crops (Kanemasu et al., 1974). However, detection and identification of crop diseases by use of spectral images seems very difficult because various diseases show several and similar symptoms. Powdery mildew is a very serious crop disease causing severe yield reduction in many important crops. Cereal mildew can now more or less be controlled by the use

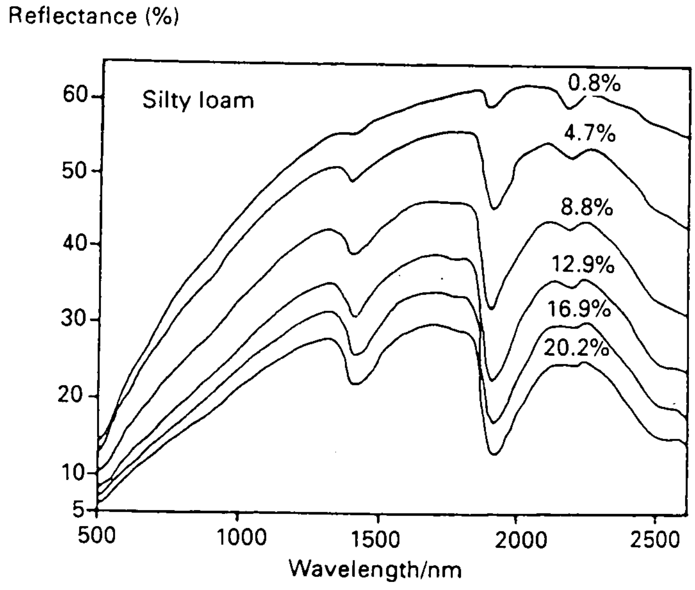

Figure 3: Reflectance spectra of a silty loam soil for different moisture contents (redrawn from Bowes and Hanks, 1965).

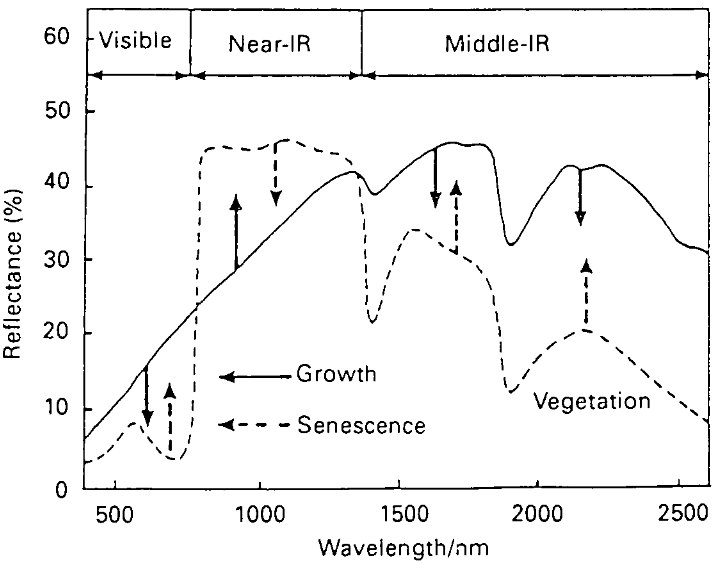

Figure 4: Diagram representing changes in plant canopy reflectance during growth and senescence (redrawn after Guyot 1989).

of fungicides, but especially in western Europe there is a growing environmental concern about the rather heavy use of chemicals for crop protection. Attempts have been made to develop methods for early warning of mildew infections, and to determine the optimal time for spraying crops to achieve the necessary yield protection using less fungicides.

Changes in spectral properties induced in barley were studied to identify the most important spectral regions, in the 400-1100 nm spectrum, to infected barley leaves (Lorenzen and Jensen 1989). Five spring barley lines were grown in a greenhouse and inoculated with powdery mildew. Three of the lines were highly susceptible to mildew and two lines were resistant (figure 5). During a 20-day period the spectral images of the leaves were recorded and related to infection, chlorophyll and water content of the leaves. The results from the experiment can be summarized as follows:

1. The spectral reflectance of control leaves and inoculated resistant leaves was very similar throughout the experimental period.

2. No changes in spectral reflectance from inoculated leaves were evident within the first 3 days after the inoculation.

3. Six days after inoculation, the susceptible lines showed significantly higher reflectance in the visible wavelenght region.

4. Ten days after inoculation, the susceptible lines showed significantly higher reflectance throughout the spectrum from 400 to 1100 nm as compared to control plants.

5. The difference in near infrared reflectance between control and infected plants were small and occurred several days later than changes in the visible region of the spectrum.

6. The difference in reflectance of blue and red wavebands between control and inoculated plants were highly correlated to the chlorophyll content of infected leaves.

The fact that no changes in the spectral reflectance from inoculated leaves were evident within the first three days after inoculation sets narrow limits to possible early warning systems based on spectral images of leaves in the 400 to 1100 nm waveband region.

It is surprising that significant changes in spectral reflectance of single leaves infected with mildew occur earlier in the visible region of the spectrum than in the infrared part of the spectrum. This observation makes possible early warning systems even more difficult because of the very weak reflectance from plant leaves in the visible part of the spectrum.

Nutrient and water status

There have only been a few attempts to asses the nitrogen status of plants using reflectance measurements (Plummer, 1988; Jensen et al. 1990). Different wavelengths have been proposed, but only low correlations have been found between the spectral reflectance and total plant nitrogen content. In spite of the poor direct relationship between reflectance and plant nitrogen, it may be possible to use reflectance measurements, since nitrogen availability has a profound effect on the leaf expansion rate and on the final leaf size of crops. Nitrogen fertilizers also increases the number of leaves per plant in crops. These higher numbers of leaves are due to increased branching or tiller survival and are not the

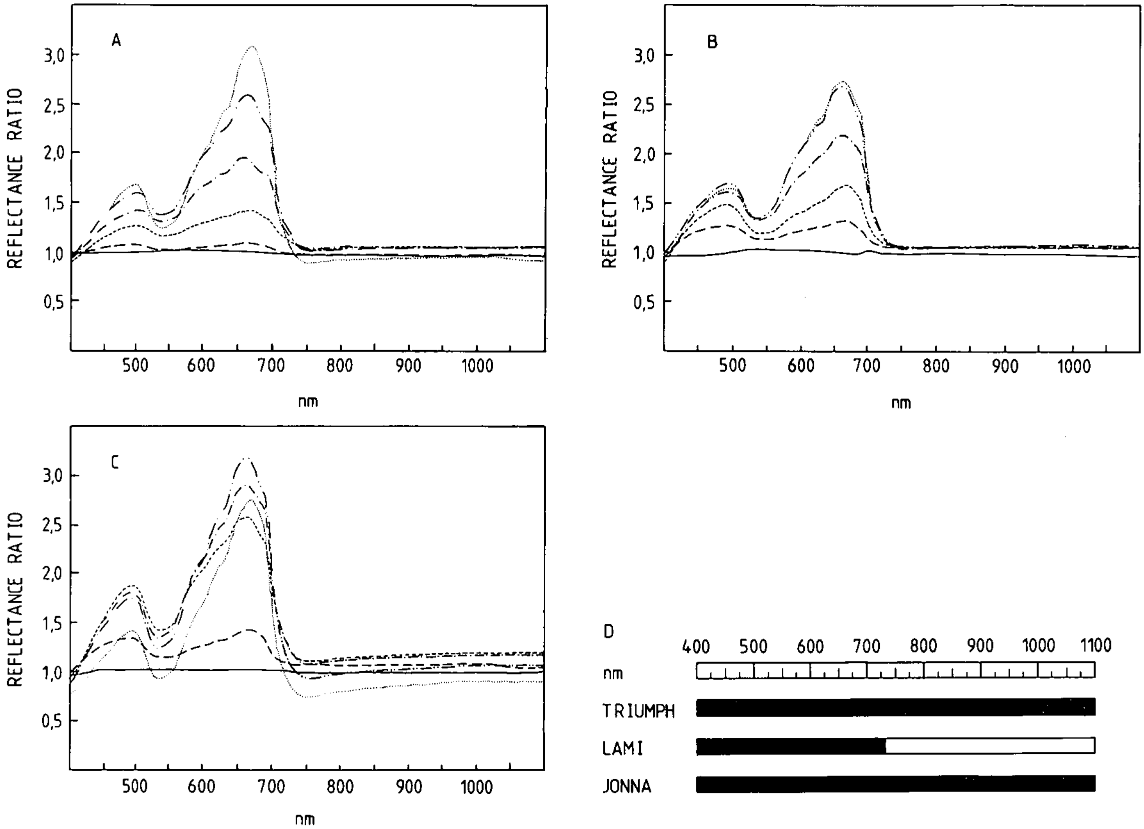

Figure 5: Ratios between the spectral reflectance of inoculated leaves and the reflectance of control leaves of the susceptible barley lines: A) Triumph; B) Lami; C) Jona. Three days (——), 6 days (– – –), 10 days (- - - -), 14 days (- · -), 17 days (- ·· -), and 20 days (···) after inoculation. D) Result of one way anova analysis classified after dates of the spectral reflectance of inoculated susceptible leaves during the experiment. Filled areas show the spectral regions where significant (P < 5 % =) changes were observed (redrawn from Lorenzen and Jensen 1989).

result of an increase in the rate of unfolding of leaves, which is controlled entirely by air and soil temperature. Other mineral nutrients can influence leaf expansion, but under intensive agriculture, where phosphorus, potassium and trace elements are maintained at optimal levels by fertilizer application, nitrogen is the most important nutrient controlling canopy development.

In a field experiment with barley grown at different nitrogen treatment levels the percentage nitrogen content of the crop was negatively correlated with the biomass accumulation, and the nitrogen content declined in an exponential manner. However, at any given chronological age the total plant nitrogen content and the accumulated biomass was strongly correlated in a curvilinear manner (figure 6). Thus on each sampling occasion the NIR and NIR/red reflectance was closely related to percentage of total plant nitrogen in a curvilinear manner similar to the relationship between accumulated biomass and percentage plant nitrogen. To create a model assessing percentage plant nitrogen by reflectance measurements, sequential information about reflectance and chronological age of the plants is needed. However, the chronological age is not the optimal way of describing the crop development in a biomass model, because the overall plant nitrogen status has a significant influence on the number of leaves and on the final leaf size in crops.

Data reduction and analysis

Enormous amounts of data are generated by instrumentations on satellites and near surface platforms, but only a small fraction is subsequently used. In general a disproportionate amount of energy seems to have been used on the data-collecting end of remote sensing and far too little effort is put into data analysis and into development of new hypotheses.

Unlike measurements from satellites data from near surface platforms in most cases have been intensively validated by "ground truth" data.

The traditional vegetation indices used for data reduction are all functionally equvalent, and in a helthy green vegetation there are well established correlatiions between biomass and these vegetation indices. But when chlorosis occurs in stressed or senessing vegetation these indices confound biomass variation with vegetation colour, and the limitations of these indices are clearly shown. Accurate monitoring and interpretation of vegetation stress by use of remote sensing techniques will require development of new methods or indices able to destinguis and quantify the different stresses.

In the future, imaging spectrometers will measure the reflected radiance in several hundred narrow wavebands. The potential information contained in these high resolution spectra is very high, but the realisation of this potential is not an easy task because of the volume of data involved.

Smoothing and filtering of the high resolution data are required in order to resolve the finer spectral features, but a variety of smoothing and curvefitting techniques are commersially available today.

Similary, differentiation is an well established technique in analytical chemistry used to resolve the components of a spectrum and to reduce the effects of background spectral interference. Differentiation is the basis for studies of the red-edge which should be explored systematically in more details in the future together with for firts derivity peaks at 1050, 1150, 1300 and 2300 nm which appear promising especially in relation to leaf water content.

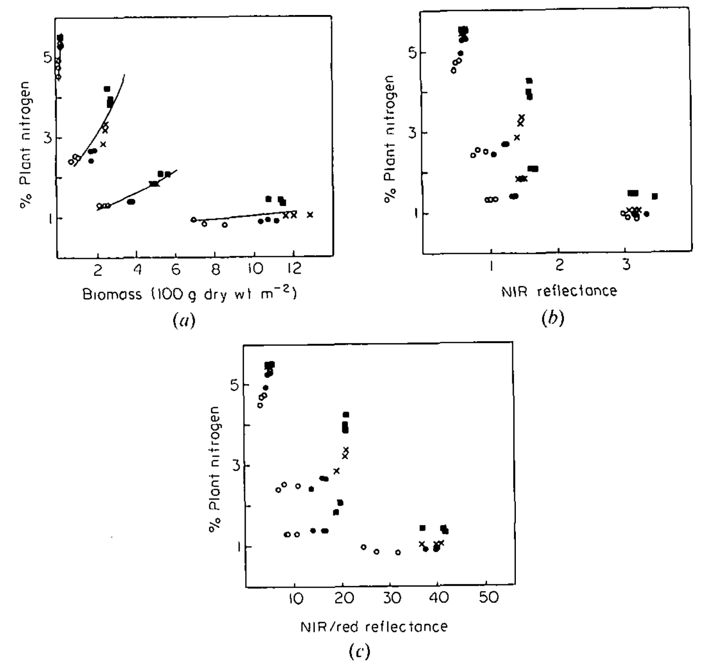

Figure 6: (a) Relationships between biomass and percentage nitrogen content of crops during the growing season. (b) Relationship between the NIR reflectance factor and percentage nitrogen content of crops during the growing season. (c) Relationships between the NIR/red reflectance factor and percentage nitrogen content of crops during the growing season. (o) data collected from 0 N plots; (•) data collected from 50 kg N/ha plots; (×) data collected from 100 kg N/ha plots; (■) data collected from 150 kg N/ha plots (redrawn from Jensen et al, 1990).

Remote sensing in management

In a world where combiners are equipped with yieldmonitors and Global Positioning Systems an attractive possibility is to offer the remote sensing technology to farmers. In an agricultural environment where there are increasing economic and legal constraints on the use of fertilizers and chemicals for crop protection, a tractor-mounted system to diagnose changes in foliage density and crop condition caused by diseases, or nutrient stress has considerable advantages. Dynamic detection of crop condition may allow immediate treatments in a differentiated manner, resulting in a much more effective use of fertilizers and chemicals, with significant benefit to both the farmer and the environment.

In the future "ultra low sensor platforms" such as tractors and combiners will make the full range of sensors and monitoring techniques available to solve the practical everyday problems of farmers and forrest managers.

Standardisation of methods and calibration of sensors

In the future we have to confront the problems of calibration of sensors over time, standardisation of methods and intercalibration of methods and sensors used for common purposes in collaborative projects.

It is a serious draw back for the advancement of remote sensing techniques that most of the remotely sensed information up to now have been collected with uncalibrated sensors only referring to internal unspecified or weakly defined standards, which in most cases makes it impossible to compare data obtained from two instruments or to compare the results from two different experiments. In the future tremendous amounts of work can be saved by standardization and intercalibration of both equipment and methods.

Concluding remarks

Several projects have demonstrated how remote sensing can be used to estimate rate of dry matter accumulation in plant communities and crops, but unfortunately this possibility is not yet widely used for practical purposes. As in many other cases it seems unreasonably difficult to make the transition from the research level to practical use of knowledge.

Radiometric estimation of the nitrogen content in barley has been demonstrated in a research project with crops grown in the field at different nitrogen levels, but the technique is not yet ready for practical use.

The development of diagnostic and early warning systems for crop diseases has not yet been successful, but work in this field of research should be intensified because of the very large economical and environmental potential in this area.

Reliable remote sensing techniques for grain yield prediction is not yet available, but may be within reach in a few years.

The use of radiation thermometers to measure the radiative temperature of soils and crops, and to assess rates of evaporations from crops have proven very difficult under temperate cloudy conditions with random fluctuations of solar radiation.

In a rapid developing field of research and technology it is dangerous to lecture about what may and may not be possible in the near future. Remote sensing is a rapid developing field of research, and the continuing development of sensor and computer technology makes it almost impossible to predict what remote sensing may be able to do for environmental science and technology in another 10 to 15 years.

In global ecology remote sensing the key issue is to identify and monitor physical, chemical and biological changes caused by industrial practices.

In agricultural remote sensing it is extremely important to identify and then to minimize damage to the environment caused by current agricultural practices, and to increase the quality and quantity of food production.

References

Allan, J.A. 1990. Sensors. platforms and applications; acquiring and managing remotely sensed data. In: Applications of Remote Sensing in Agriculture, (eds.) M.D. Steven and J.A. Clark, pp. 3-18, Butterworths, London.

Bowers, S.S. and Hanks, R.J. 1965. Reflection of radiant energy from soils. Soil Science, 100, 130-38.

Colwell, R.N. 1956. Determining the prevalence of certain cereal crop diseases by means of aerial photography. Hilgardia, 26, 223-286.

Guyot, G. 1989. Les signatures spectrales des surface naturelles. Télédétection Satellitaire, 5, Caen.

Jensen, A. 1980. Seasonal changes in near infrared reflectance ratio and standing crop biomass in a salt marsh community dominated by Halimione portulacoides (L.) Aellen. New Phytologist, 86, 57-67.

Kanemasu, E.T., Niblett, C.L., Manges, H., Lenhert, D., and Newman, M.A. 1974. Wheat: its growth and disease severity as deduced from ERTS-1. Remote Sensing of Environment, 3, 255-260.

Lorenzen, B. and Jensen, A. 1988. Reflectance of blue, green red and near infrared radiation from wetland vegetation used in a model discriminating live and dead above ground biomass. New Phytologist, 108, 345-355.

Lorenzen, B. and Jensen, A. 1989. Changes in Leaf Spectral Properties Induced in Barley by Cereal Powdery Mildew. Remote sensing of environment 27, 201-209.

Monteith, J.L. 1977. Climate and efficiency of crop production in Britain. Philosofical Transactions of the Royal Society of London, Series B, 281, 277-94.

Toubenhous, J.J., Ezekiel, W.N., and Neblette, C.B. 1929. Airplane photography in the study of cotton root rot. Phytopathology, 19, 1025-1029.

A spectral reflectance index as indicator for crop growth and development

C.T. Petersen
The Royal Veterinary and Agricultural University
Department of Agricultural Sciences
Section of Soil and Water and Plant Nutrition
Thorvaldsensvej 40, DK-1871 Frederiksberg C
Denmark

Summary

The reflectance in a near infrared band (NIR) and in a photosynthetically active band (PR) was followed intensively in spring barley, winter wheat, spring rape and perennial ryegrass during the 1986 growing season and in spring barley during the 1988 and 1990 growing seasons. A vegetation index was formed as the ratio between NIR and PR.

It is demonstrated that NIR/PR during the central four hours of the day was insensitive to changing solar elevation and largely independent of soil surface wetness and cloud cover, responding almost entirely to varying green crop cover. In barley, though, some minor dependence on soil surface wetness was found at sparse crop cover and a systematic dependence on cloud cover was found within a three week period after earing. Close correlations were found in barley during vegetative growth stages between NIR/PR and green leaf area index and between NIR/PR and intercepted photosynthetically active radiation.

Introduction

An important goal of agricultural remote sensing research is to spectrally estimate crop variables related to crop conditions which can subsequently be applied to evapotranspiration and crop growth models. Alternatively, spectral reflectance indices may be used directly in such models or simply as easily derived indicators of crop conditions which can support information about the crop obtained by more traditional means. However, the sensitivity of spectral reflectance measurements for crop evaluation depends entirely on the efficiency by which spectral responses due to vegetation changes can be separated from responses attributable to atmospheric conditions and to soil background.

Several spectral vegetation indices have been developed with the aim of minimizing the effect of irrelevant factors while enhancing certain aspects of the vegetation signal. Perry and Lautenschlager (1984) summarize and give references to the origin, derivation and motivation for some four dozen of such formula. One general class of indices comprise ratios of two or more band variables (Tucker, 1979) of which the near infrared to red reflectance ratio is one of the most simple. This index has been found quite effective in reducing spectral variation from soils devoid of vegetation due to fluctuating soil wetness (Colwell, 1974; Tucker, 1979). Whether soil influences are further reduced by the shielding effect of emerging vegetation is not clear, however. Huete (1987), working with cotton and four different soil backgrounds, thus reported on greatest soil brightness effects for middle to high (60-75 %) green crop cover, suggesting significant interactions between soil and vegetation spectra in producing composite canopy response. Changing cloud cover is generally assumed to disturb crop reflectance seriously due to changing influx geometry. Furthermore, unstable influx will complicate reflectance measurements.

This paper presents ground-based recordings in spring barley, winter wheat, spring rape and perennial ryegrass of a simple near infrared to photosynthetically active reflectance ratio which seems only slightly affected by varying soil surface wetness and atmospheric conditions.

Eksperimental approach

The field experiments were carried out at the Royal Veterinary and Agricultural University Experimental Farm at Tåstrup (55°40'N, 12°18'E) during the 1986, 1988 and 1990 growing seasons. In 1986 spring barley (cv. Lina), winter wheat (cv. Kraka), spring rape (cv. Topas) and perennial ryegrass (cv. Borvi) were grown with rows in the north-south direction. In 1988 spring barley (cv. Lina) was grown in a field with rows in the north-south direction as well as on two plots (50 N and 100 N) laid down in spring barley with rows in the east-west direction. In 1990 spring barley (cv. Lina) was grown in a field with rows in the north-south direction. All crops were planted with a 12 cm row spacing on a level sandy loam soil having about 2.0 % organic matter in the 20 cm top layer. Except from low nitrogen application (50 kg N ha^{-1}) to the 50 N barley plot in 1988 all crops were treated according to standard agricultural practices including weed and pest control when necessary.

Green leaf area index (GLAI) was determined once or twice per week. In 1986 the determinations were based, generally, on five 0.19 m^2 samples from each crop. Same method was employed in the field in 1988, but in the plots the determinations were based on three 0.10 m^2 samples. In 1986 and 1988 the sampling was carried out systematically around fixed radiometric sensors leaving circular areas undisturbed for collecting the spectral data. 15 m^2 was left undisturbed for this purpose in the barley plots in 1988 and 50 m^2 in all the other cases. In 1990 using portable radiometric equipment all determinations were based on one 0.36 m^2 sample taken directly below the radiometric sensors. Projected area measurements were carried out with an optically scanning leaf area meter with conveyer. Data on precipitation were obtained from the Climate and Water Balance Station at Tåstrup located on the experimental farm.

Spectral data were provided from serial manufactured quantum and near infrared sensors both equipped with a silicon photodiode and special interference filters. All sensors were cosine corrected and hemispherical. Thus, signals from the quantum sensors (LI-190S point sensors or 1 m long LI-191 SB line sensors) were proportional to the hemispherical photon flux density (μE $m^{-2}s^{-1}$) between approximately 400 and 700 nm, referred to as photosynthetically active radiation (PAR)(LI-COR, 1984). Signals from the near infrared sensors (LI-220S point sensors) were proportional to the hemispherical energy flux density (Wm^{-2}) between approximately 740 and 820 nm (LI-COR, 1979).

In 1986 and 1988 all sensors were placed at fixed positions in the crops in order to eliminate spatial variability. Simultaneous observations of incoming and reflected radiation were taken frequently each day in each crop during the entire growing season by using the two sensor types. In addition transmitted PAR was observed in barley using in each plot a line quantum sensor placed in the across row direction underneath the canopy. Each single observation was completed within less than 0.3 s and all four (or five) observations in each crop within about 1 s. In 1986 observations were taken and recorded every 10 min. In 1988 observations were taken every minute and average values were recorded every half hour. Reflection was measured from a level of 0.7-1.1 m above maximum crop height, the level being lowest in the two barley plots in 1988.

In 1990 sensors and datalogger were combined into a portable unit and observations were taken at different places from 1 m above the crop. Two identical black painted collimators were mounted on the vertically oriented downward facing sensors leaving a 55° field of wiev to the reflection measurements. All observations were taken between 1000 and 1400 hour DST. On a number of days with initially dry soil conditions about 5 mm of water was sprayed on the soil surface so that data were obtained from exactly the same locations with both a wet and a dry soil surface.

Calculations

All observations taken while it was raining and until two hours after the rain had stopped were rejected based on hourly precipitation data. In addition, PAR-transmission in the 50 N barley plot in 1988 had to be rejected due to instrument problems. Measures of reflectance in the near infrared and photosynthetically active band, NIR and PR were obtained as the ratio between reflection and influx. Relative PAR transmission, PT, was calculated by dividing transmitted PAR by the PAR influx.

Daily NIR/PR and PT average values were based generally in 1986 on 24 observations and in 1988 on 240 observations (8 half hour average values) taken between 1000 and 1400 hour DST. In 1990 NIR/PR values were based on five observations from each location.

Results and discussion

The NIR/PR index values shown in Fig. 1 and 2 form relatively smooth curves during the growing season. A similar smoothness of daily NIR/PR values plottet over the season as shown in Fig. 2 for the 100 N plot was found in the other two barley crops in 1988. NIR/PR increased in all crops with increasing amounts of green vegetation at the beginning of the growing season. For wheat and barley in 1986 and 1988 saturation was reached when green leaf area index reached about 3.5. NIR/PR saturation levels were different for the different cereal crops being especially low for the 50 N barley crop in 1988 (not shown) that clearly suffered from N deficiency. In 1990 using collimated sensors for the reflection measurements NIR/PR became saturated at a somewhat higher GLAI value (about 5.5). From time of saturation until beginning senescence (crop yellowing) the index was relatively insensitive to crop changes. Earing for example did not cause any significant change in average index values. In 1986 though there was a marked drop in index values around day no. 182, when the crops were short of water (Fig. 1). Cloudy weather and rain on day no. 187 was probably needed to

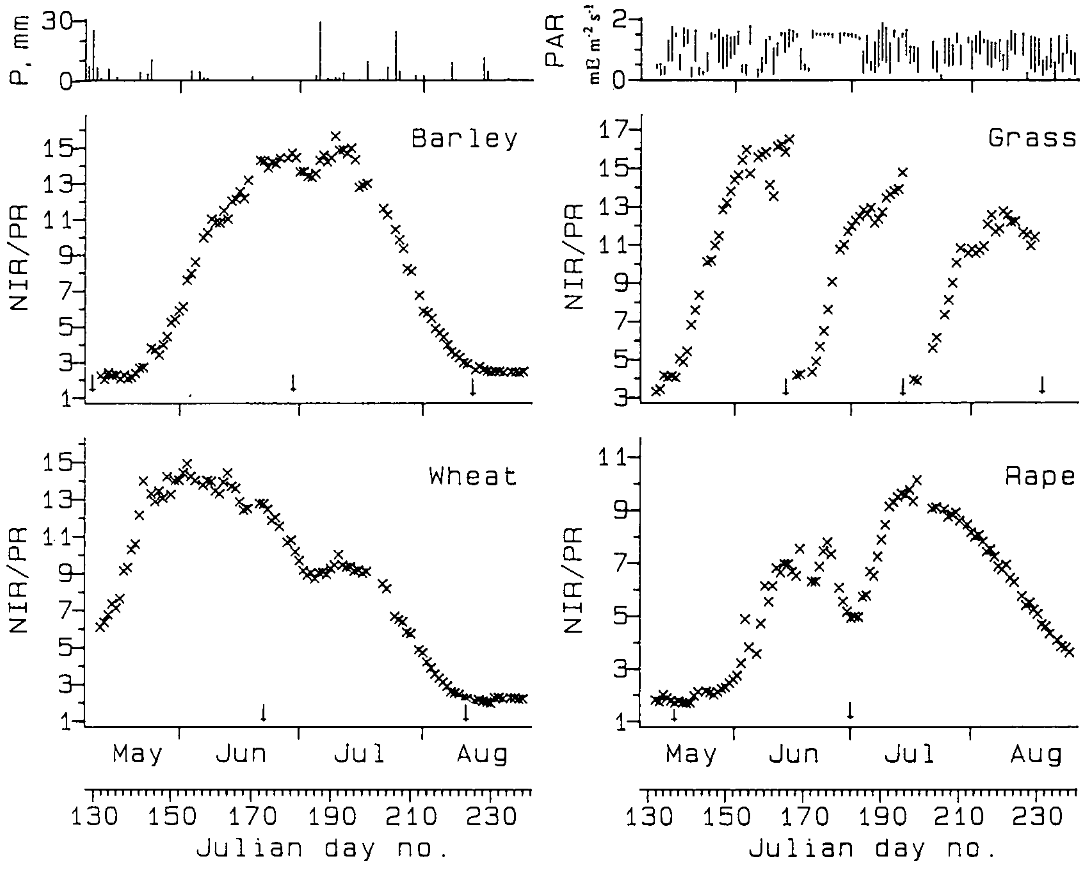

Figure 1: Daily precipitation (P). Daily PAR values (average ± std) and average NIR/PR values observed between 1000 and 1400 hour DST in spring barley, whinter wheat, perennial ryegrass and spring rape in 1986. ↓ marks emergence (barley, rape); start of earing and date when completely yellow (barley, wheat); maximum flowering (rape); three cuttings (grass).

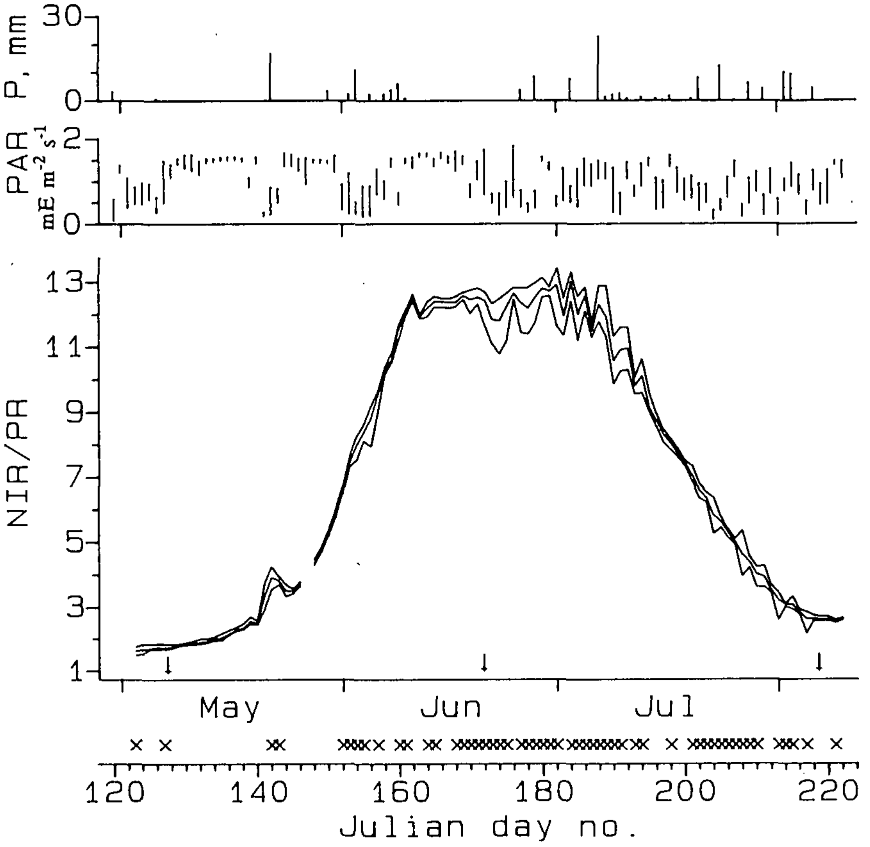

Figure 2: Daily precipitation (P). Daily PAR values (average ± std) and NIR/PR values (average value, minimum and maximum half hour average values) recorded between 1000 and 1400 hour DST in spring barley in 1988 (100 N plot). × marks days when the PAR influx corresponding to the minimum NIR/PR value was smaller than that corresponding to the maximum NIR/PR value. ↓ marks dates for emergence, start of earing and a completely yellow crop.

extend the growing season.

During senescence NIR/PR index values of wheat and barley decreased until almost exactly the day when green canopy parts were no longer visible. Completely yellow crops had NIR/PR values near 2.4. The grain yield (dry matter) was 5.6, 4.4 and 5.1 t ha^{-1}, respectively, for wheat and barley in 1986 and for the 100 N barley crop in 1988.

In rape during flowering the NIR/PR values dropped dramatically following increased PR values, irrespectively of the amount of green vegetation (Fig. 1). For unknown reasons the index was rather unstable just before flowering. The stage considered to be optimal for cutting to swath (1/3 of the seeds being brown, 1/3 being green and 1/3 being partly brown, partly green) corresponded to an index value of 3.5-4.0. The yield of seeds (dry matter) was 3.0 t ha^{-1}.

In perennial ryegrass (Fig. 1) at high biomass levels the index was sensitive to sudden architectural changes due to wind and heavy rain (second cutting) and to water deficiency (third cutting). The dry matter yield was 4.3, 4.4, and 3.1 t ha^{-1}, respectively, for the three cuttings.

Observations taken in 1986 above a bare soil surface with water content ranging from very wet to very dry showed a high positive correlation between NIR and PR. The daily NIR/PR average values varied between 1.8 and 2.2 being larger than 2.1 only when the soil was very wet. That explains the relatively stable development in index values when the crop cover was sparse. Fig. 3 shows a relatively fast increase in NIR and PR values after considerable amounts of rain. The potential evapotranspiration rate according to Penman was 2.1, 2.9 and 2.7 mm, respectively, for the three days considered in the figure.

At a GLAI value in barley of about 0.5 NIR/PR rose about 0.5 index units responding to 17 mm rain in the morning (Fig. 2, day no. 142). However, alternate wetting and drying of the soil surface at GLAI values around 1-2 between day no. 150 and 161 had very little influence on NIR/PR. Data from 1990 support this finding (Table 1). As a result of wetting the soil surface NIR/PR rose maximally 0.54 index units at a GLAI value of 0.35 while at GLAI values of 1.4 and larger there was no clear effect on NIR/PR.

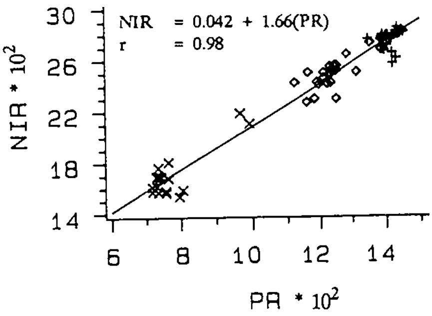

Figure 3: NIR versus PR for a bare soil surface in a condition ranging from very wet to dry. Data observed every 10 minute between 1000 and 1400 hour DST over a three day drying period after 10 mm of rain. ×, ◇ and +: 1st, 2nd and 3rd day, respectively.

Photosynthetically active radiation (PAR) varied considerably from day to day due to varying cloud cover (Fig. 1 and 2). Generally, however, this variation is not to any large extent reflected in the daily NIR/PR values which can be seen by comparing the PAR plots with the smooth NIR/PR curves. The somewhat smoother NIR/PR average curve for barley in Fig. 2 compared with Fig. 1 may be ascribed to much more observations in 1988. The range of daily half hour NIR/PR average values observed between 1000 and 1400 hour DST were very narrow during most of the 1988 season (Fig. 2). So, accurate av-

Table 1: Effect, D, of wetting a dry soil surface at different GLAI in spring barley in 1990 on NIR/PR (D =NIR/PR$_{wet}$−NIR/PR$_{dry}$). Average of 3 determinations.

Date	20.04	03.05	08.05	15.05	19.05	25.05	31.05	08.06
GLAI	0.00	0.35	0.70	0.86	1.4	1.7	2.6	3.5
D	0.31	0.54	0.42	0.23	-0.01	0.13	-0.07	0.02

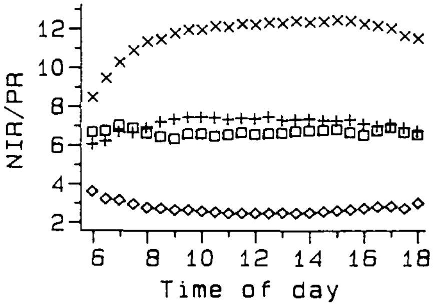

Figure 4: Half hour average NIR/PR values recorded between 0600 and 1800 hour DST in the 100 N barley plot in 1988. Data from four relatively clear days at four different stages of development, Julian day no. 140 (◇), 152 (□), 164 (×) and 200 (+).

erage NIR/PR values can be based on much less than 240 readings, generally. The need for replicates is, however, dependent on both the sensing system, the weather situation and the stage of crop development.

Detailed correlation analyses made for all barley crops for 24 single days with varying influx (clouds) selected over the season showed that NIR/PR was almost completely uncorrelated to PAR between 1000 and 1400 hour DST, except within a period of about three weeks after start of earing. In this period greater variability was observed in NIR/PR (Fig. 2) due, primarily, to fluctuating PR values, and NIR/PR was positively correlated to PAR. A similar picture was not observed in wheat.

Both NIR and PR rose on clear days with decreasing solar elevation. This trend was less pronounced, however, for bare soil and at sparse crop cover. NIR/PR varied much less than NIR and PR, relatively, during the central hours of the day, especially for crops with rows in the north-south direction at medium to dense crop cover. Thus, NIR/PR of bare soil and of completely yellow barley crops did not vary systematically over the day between 0600 and 1800 hour DST neither on overcast nor on relatively clear days. At low GLAI values around 0.5 during vegetative stages of growth NIR/PR tended to rise in the morning and late in the afternoon with decreasing sun height (Fig. 4, day no. 140; Fig. 5), whereas for medium to dense green crop cover (GLAI> 1.7) and during senescence there was a trend in the opposite direction (Fig. 4, day no. 164 and 200; Fig. 5). The systematic dependence on sun height was in no crops and at no stage of development much larger than shown in Fig. 4. For the time interval between 1000 and 1400 hour DST on clear days the NIR/PR variability was generally very small compared to the variability caused by the crop development (Fig. 2). Thus, between 1000 and 1400 hour DST the systematic variation in NIR/PR due to clouds and direction of direct insolation was negligible.

NIR/PR was closely correlated to GLAI during vegetative stages of growth (Fig. 6). The shown regression equation is based on 1990 data and covers the whole period from emergence till earing. Data from 1986 and 1988 (excluding the 50 N plot) are in close accordance with the 1990 data for GLAI val-

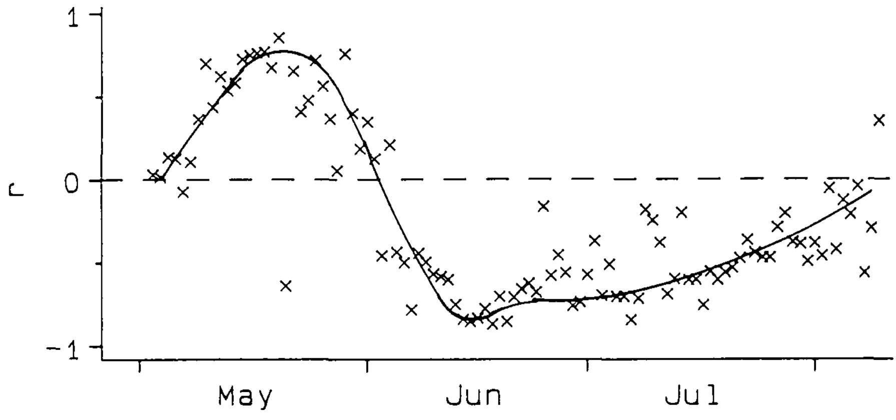

Figure 5: Daily coefficients of correlation, r, between NIR/PR and the absolute time difference (min) between noon (maximum sun height) and time of observation. Data from the 100 N spring barley plot in 1988 recorded between 0600 and 1800 hour DST.

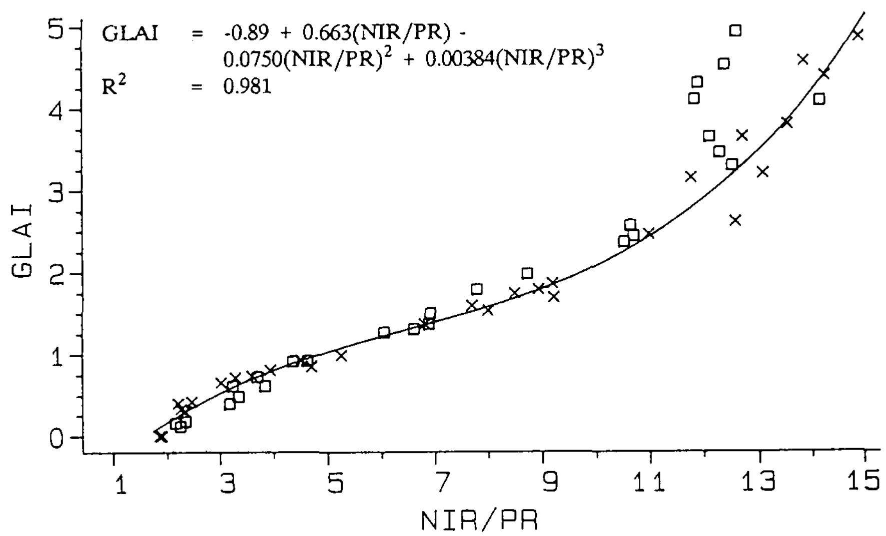

Figure 6: Green leaf area index (GLAI) versus NIR/PR from emergence untill earing of spring barley. Data from 1986 and 1988 (excluding the 50 N plot) (□) and from 1990 (with NIR/PR values measured above a dry soil surface) (×). The regression equation and the curve are based on the 1990 data, only.

ues less than 3.5, but not for GLAI values larger than 3.5 where NIR/PR became saturated. This difference between saturation levels may probably be ascribed to the sensing system using collimated sensors for the reflection measurements in 1990. NIR/PR values were at all GLAI values lower in the 50 N plot than in the other barley crops indicating that the shown regression equation cannot be used independently of N level. During senescence NIR/PR and GLAI was much less closely correlated due in part, probably, to difficulties in separating green and yellow plant parts. The smoothness of the NIR/PR curves during this period indicates, however, that such a relation may exist, although some minor disturbance is to be expected from dead plant parts located, primarilly, in the lower vegetation layers. Other close relationships between GLAI and different spectral vegetation indices have been documented for several crops during vegetative growth stages (e.g. Tucker, 1979; Ahlrichs and Bauer, 1983; Redelfs et al., 1987).

Kumar and Monteith (1981) theroretically derived that relative PAR-interception can be estimated in homogenous plant stands with horizontal foilage acting as perfectly diffuse surfaces from the ratio between reflectance in a near infrared and a visible band. Asrar et al. (1984) further developed these considerations for canopies with leaves inclined at different angles concluding, though, that a near infrared to visible reflectance ratio would not be perfectly suited for estimating relative PAR-interception due to assumed non linearity and dependence on solar elevation. For the present NIR/PR index the independence of solar elevation within the central four hours of day has already been demonstrated. A period of 31 days in spring covering the largest increase of NIR/PR values were chosen from the three barley data sets including transmitted PAR measurements. During this period the fraction of incoming PAR not reaching the ground, (1-PT), observed in the field crops in 1986 and 1988 was closely and linearly correlated to NIR/PR (Fig. 7). Both data sets fitted the same equation. PAR-interception in the 100 N barley plot, however, was obviously higher for medium NIR/PR values than predicted by the shown linear relationship. This might be explained by lower light transmission at noon when rows are running east-west or nearly perpendicular to the direction to the sun. The non linear relationship found in the 100 N plot resembles more the one proposed by Asrar et al. (1984).

References

Ahlrichs, J.S. and Bauer, M.E. (1983). Relation of agronomic and multispectral reflectance characteristics of spring wheat canopies. Agron. J. 75: 987-993

Asrar, G., Fuchs, M., Kanemasu, E.T. and Hatfield, J.L. (1984). Estimating absorbed photosynthetic radiation and leaf area index from spectral reflectance in wheat. Agron. J. 76: 300-306.

Colwell, J.E. (1974). Vegetation canopy reflectance. Rem. Sens. Env. 3: 175-183.

Huete, A.R. (1987). Soil-dependent spectral response in a developing plant canopy. Agron. J. 79: 61-68.

Kumar, M. and Monteith, J.L. (1981). Remote sensing of crop growth. In: Plants and the Daylight Spectrum (ed. by H. Smith), pp. 133-144. Academic Press, London.

LI-COR (1979). Light sensors and accessories. Brochure RSI-279. LI-COR Inc., Lincoln, Nebraska.

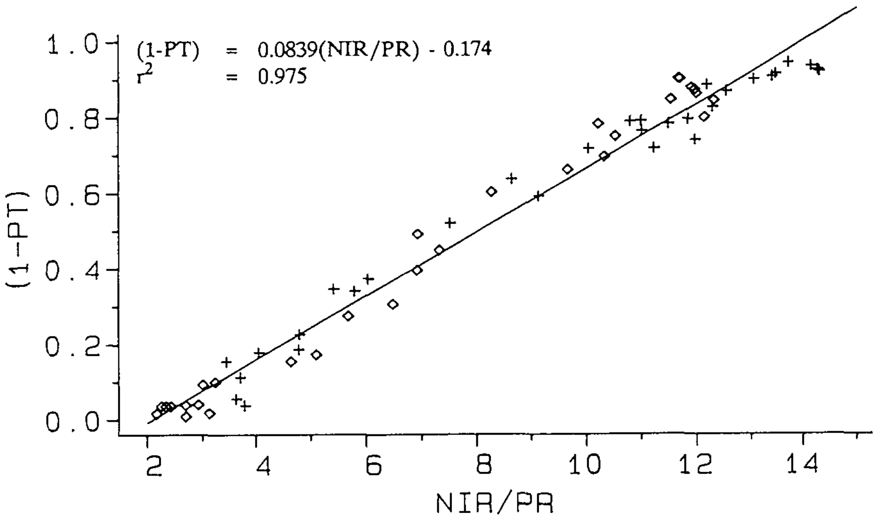

Figure 7: Relative PAR-interception, (1-PT) versus NIR/PR in spring barley with rows in the north-south direction in 1986 (+) and 1988 (◇) during the 31 days with largest NIR/PR increase.

LI-COR (1984). Radiation measurement instruments. LI-COR Inc., Lincoln, Nebraska.

Perry, C.R. and Lautenschlager, L.F. (1984). Functional equivalence of spectral vegetation indices. Rem. Sens. Env. 14: 169-182.

Redelfs, M.S., Stone, L.R., Kanemasu, E.T. and Kirkham, M.B. (1987). Greennessleaf area index relationships of seven row crops. Agron. J. 79: 254-259.

Tucker, C.J. (1979). Red and photographic infrared linear combinations for monitoring vegetation. Rem. Sens. Env. 8: 127-150.

Estimation of Leaf-Area-Index (LAI) from Radiation Measurements

Anton Thomsen
Dept. of Agrometeorology, Research Centre Foulum
P.O. Box 25, DK-8830 Tjele

Abstract

Measurements of canopy spectral reflectance and light transmittance were made in spring barley research plots. Three N application rates provided data for a range of growth conditions. Canopies were sampled weekly for laboratory measurements of area indices. Radiation measurements were made continuously with self-recording instruments and biweekly with hand carried instruments. Laboratory measurements were used to evaluate the following indirect methods of LAI determination:

1. Spectral indices calculated from spectral reflectance at visible and reflected infrared wavelengths,

2. gap fractions calculated from canopy diffuse transmittance obtained using a fisheye sensor, and

3. canopy transmittance measured using line sensors.

Results show that all three methods can provide reliable data on leaf-area-index. Unlike transmittance measurements spectral indices are mostly sensitive to the amount of green canopy material, allowing this method to be used for detection of plant stress caused by e.g. nitrogen starvation or pathogens.

Introduction

Knowledge of canopy structure is required for detailed modelling of crop microclimate, growth, water balance, etc. Crop canopies are higly dynamic over time and measurements need to be repeated frequently (e.g. weekly) if the full growth cycle is to be represented.

Canopy structure can simply be defined as the spatial arrangement of canopy material (see e.g. Norman and Campbell, 1989, for an introduction to canopy structure). In the present workshop paper, only the measurement of the area of canopy material (not its orientation)-specifically the area index of green leaves and stems (Green Crop-Area-Index, GCAI)-will be considered.

Traditionally, LAI is measured using direct methods. Typically, a representative sample of plants is clipped individually or within a small area. In the laboratory the area of detached leaves, stems, etc. can then be measured using a suitable planimeter. The data presented in this paper were obtained from measurements on four rows of spring barley clipped within a rectangular 0.25 m^2 area.

Direct methods of canopy measurements are time consuming and usually destructive in nature, and alternative indirect methods are in high demand, especially if frequent measurements are to be made. A recent survey of indirect methods can be found in Norman and Campbell (1989). At the Department of Agricultural Meteorology the following indirect methods have been pursued for routine measurements of LAI: Measurements of canopy spectral reflectance and measurements of canopy gap fractions. Spectral methods are based on the absorption and scattering of light of visible (VIS) and near infrared (NIR) wavelengths. Especially spectral vegetation indices calculated as ratios of NIR and VIS reflectance have been found to be highly correlated with measurements of green LAI or CAI (Petersen, 1989). Gap fraction methods rely on measurements of gaps (fraction of canopy openings) as a function of view angle. Leaf-area-index (actually CAI) is calculated from averages of gap fractions using a model of radiation transfer in crop canopies and numerical inversion procedures (Welles, 1990; Welles and Norman, 1991).

Experimental approach

All measurements were made in a spring barley experiment located at Research Center Foulum (near Viborg in Central Jutland) during the summer of 1990. The experiment included 18 15 m × 3 m plots treated identically except for N fertilization rates. Plots were subjected to three N-rates: 0 kg, 50 kg, and 100 kg/ha. Plot orientation was approximately East-West. Individual plots were organized as 10 m × 3 m areas for non-destructive measurements. The remaining 5 m were used for destructive sampling for laboratory analysis.

Laboratory measurements

Beginning in late April, plots were sampled at weekly intervals for laboratory measurement of areas of green canopy material (leaves, stems and heads). Wire frames were used to define 0.25 m^2 areas to be clipped and bagged for immediate laboratory analysis. Areas of canopy material were measured using a LI-COR LI-3100 area meter. Until maximum GLAI was reached during the middle of June six plots (two from each N-level) were sampled every week. From that time and until late July only three plots were sampled each week. Figure 1 shows the development in total green crop-area-index (GCAI) during most of the growth period. It is seen how the three N application rates resulted in an approximately 3:1 ratio in maximum attained crop-area-index.

Spectral measurements

Spectral data were obtained with a Cropscan multiband radiometer (Pederson and Nutter, 1982). Measurements were made biweekly whenever possible in all 18 plots. Four measurements were averaged for each plot. Additionally, individual measurements were made over each area to be clipped for laboratory measurements.

The Cropscan instrument measures spectral reflectance in eight narrow (10 nm) wavebands in the visible and reflected infrared spectra by simultaneously determining irradiance and reflected radiance. Spectral reflectance is calculated by the instrument and stored in annotated files. Of the eight bands available only two bands centered around 700 (VIS) and 800 (NIR) nanometers were used for calculating two dimentional vegetation indices. (The visible Cropscan band centered around 650 nm would have been prefered instead of the 700 nm band but showed signs of degradation possibly due to filter aging).

Gap fraction measurements

Gap fractions at five zenith angles were measured using the LAI-2000 Plant Canopy Ana-

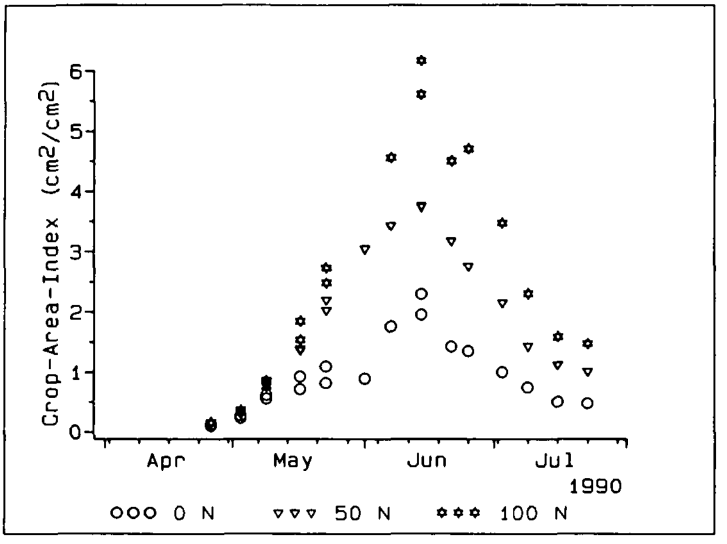

Figure 1: Laboratory measurements of green crop-area-index (leaves + stems, CAI) for a spring barley experiment in 1990. Four rows within a 0.25 m^2 rectangular area clipped, bagged and taken to the laboratory for analysis. Symbols indicate N application rate (0, 50 and 100 kg ha^{-1}).

lyzer recently developed by LI-COR (LI-COR Technical Report # 102; Welles, 1990). The instrument uses a fisheye sensor to measure diffuse radiation levels in five circular bands centered around the vertical. Relative radiation levels (= gap fractions) at the five angles are calculated from a reference reading made above the canopy immediately before making a reading at ground level. Gap fraction data can be inverted to yield an estimate of leaf-area-index (actualy total canopy area) and foliage inclination angle using numerical techniques (Norman and Campbell, 1989; Welles, 1990). The LAI-2000 calculates and displays running estimates of LAI while in use. Data are also written to annotated files that can be further processed by PC software accompanying the instrument. To avoid direct sunlight, measurements were made just before sunset or during cloudy conditions.

Measurements with radiation line sensors

At the south end of the 18 plots in the barley field surrounding the experiment, fixed instrumentation was installed for making automated measurements of light levels above and below the canopy. Photosynthetically active radiation (PAR) levels above the canopy were measured using a point sensor (LI-190). PAR levels below the canopy were measured using a line sensor (LI-191). Both instruments are manufactured by LI-COR. Total shortwave radiation was also measured above and below the canopy using tube solarimeters (TSL) manufactured by Delta-T Devices. Only mean data values recorded during the central four hours of the day were used in the analysis discussed later.

Results and discussion

Cropscan reflectance measurements

Individual Cropscan measurements made over the 0.25 m^2 sampling areas and laboratory measurements of leaf and stem areas were used to relate spectral indices to LAI and total crop area (CAI). Only data obtained before heading (medio June) were used in the analysis. The analysis was restricted to the pre-heading period when all (most) leaves are still green in order to compare Cropscan and LAI-2000 measurements. Spectral indices have been found to be well correlated to active plant tissue (Wiegand and Richardson, 1990; Jensen et al., 1990) whereas the LAI-2000 senses total CAI. In order to compare the two instruments Cropscan measurements were calibrated against total green CAI (GCAI) instead of just GLAI.

Figures 2 and 3 show the main results from the calibration of spectral indices against laboratory measurements. Figure 2 shows laboratory measurements of CAI plotted against the NIR/Red ratio derived from Cropscan measurements made over individual clipping areas. A second order polynomial is fitted to the data. The plot includes all data recorded up to the end of June after CAI has peaked (see Fig. 1) and lower leaves are becoming senescent. The plot shows that the relationship between CAI and spectral index breaks down at a CAI value of approximately 1 for 0 N plots, 3 for 50 N plots, and 5 for 100 N plots. Figure 3 is identical to Fig. 2 except that only data up to (but not including) heading during the second week of June are included. It is seen that a single polynomial provides a reasonable fit to the combined data. Regressing against LAI instead of CAI improved the fit only marginally (std. = 0.18 instead of 0.25) making it resonable to estimate CAI from spectral measurements.

The use of the normalized vegetation index (NDVI) was explored using the same data. It was found that 'saturation' limits for NDVI were approximately 0.75 for 0 N, 1.75 for 50 N, and 2.75 for 100 N plots. Consequently, the simple ratio index was used in the further analysis.

LAI-2000 leaf area measurements

Leaf area development in all 18 plots was measured on five dates from medio May until the last week of June after heading. The LAI-2000 outputs LAI directly without requiring any form of calibration.

The instrument was programmed to use four sets of measurements per plot. Each set of measurements included one reference reading above the canopy and two readings below the canopy. The total number of measuremnts per plot consequently four above and eight below the canopy. The instrument averaged measurements to a single LAI estimate for each plot. The LAI-2000 measurements were again averaged to give a LAI estimate for each N-level on each date. In Fig. 4 LAI-2000 measurements (treatment averages) are plotted together with the laboratory point measurements of crop-area-index (CAI). Except for a few (possibly) atypical point measurements (compare also with Fig. 1) there is a high degree of agreement between LAI-2000 estimates and laboratory measurements.

Comparison of Cropscan and LAI-2000 measurements

To compare CAI estimates from spectral methods (Cropscan) and gap fraction methods (LAI-2000) frequent Cropscan measurements of reflectance were obtained for all

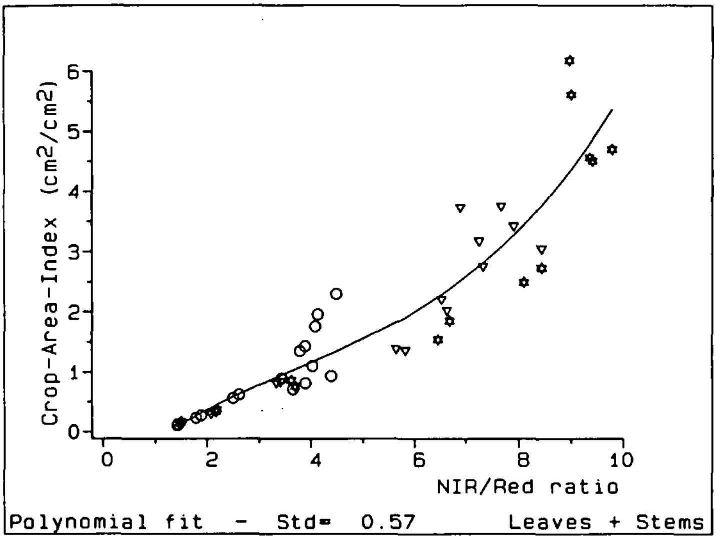

Figure 2: Polynomial regression relationship between laboratory measurements of CAI and NIR/Red spectral reflectance ratios. Spectral data recorded before 0.25 m^2 areas were clipped and analyzed in the laboratory. Data includes all measurements made during April, May, and June of 1990. Symbols etc. same as used in Fig. 1.

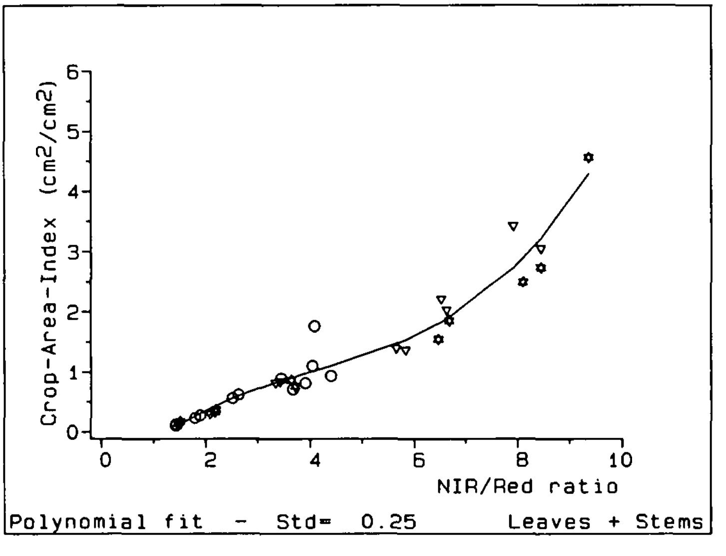

Figure 3: Same as Fig. 2 except that only data collected before heading (medio June) included. The least squares fitted polynomial used for calculating CAI from spectral measurements.

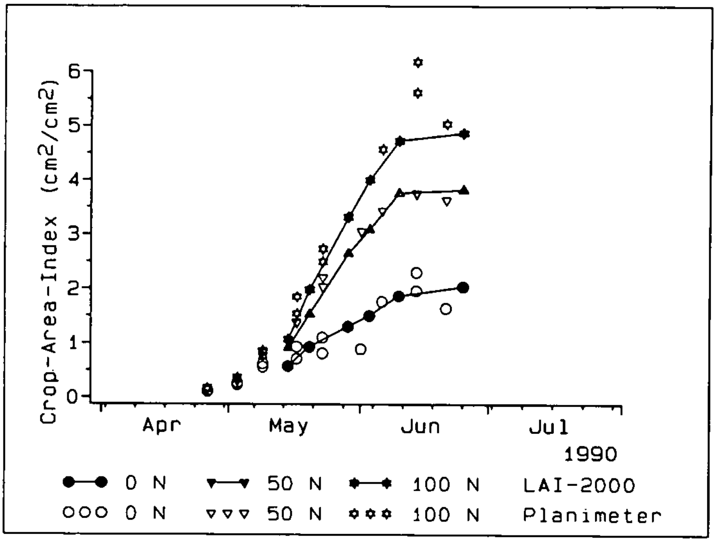

Figure 4: Laboratory measurements of point values of CAI (see Fig. 1) and treatment averages of CAI measured using the LAI-2000 instrument. Each LAI-2000 measurement shown calculated as the mean of 6 individual CAI estimates for plots within treatment.

plots during the entire season. Four measurements per plot were averaged into mean VIS (700 nm) and NIR (800 nm) reflectance values. Spectral indices calculated from mean reflectance values were recalculated into CAI values using the calibration (polynomial) shown in Fig. 3. The two estimates of CAI development are plotted together in Fig. 5. The plot shows that CAI growth curves obtained from Cropscan measurements are not nearly as smooth as LAI-2000 measurements. Figure 5 also shows the 'saturation' levels for Cropscan measurements as previously discussed. It is believed that the low saturation levels for low N rates is caused by low chlorophyll levels and possibly early senescence of lower leaves.

Line sensor transmittance measurements

The calculation of LAI from canopy transmission measurements is discussed by e.g. Walker et al., 1987. The approach used by Walker et al. requires an estimate of direct and diffuse radiation components.

During this study only total incident and transmitted radiation was measured using PAR (Photosynthetically Active Radiation) sensors and tube solarimeters (total shortwave radiation) therefore, a simpler approach was needed. The best correlation between transmittance measurements and crop-area-index estimates (LAI-2000) was obtained by simply fitting an exponential function to the data. Figure 6 shows plots of CAI estimated by the LAI-2000 instrument and CAI calculated from measurements of PAR transmittance and the fitted model. It was found that the best fit was obtained when only days with low irradiance (diffuse conditions) were

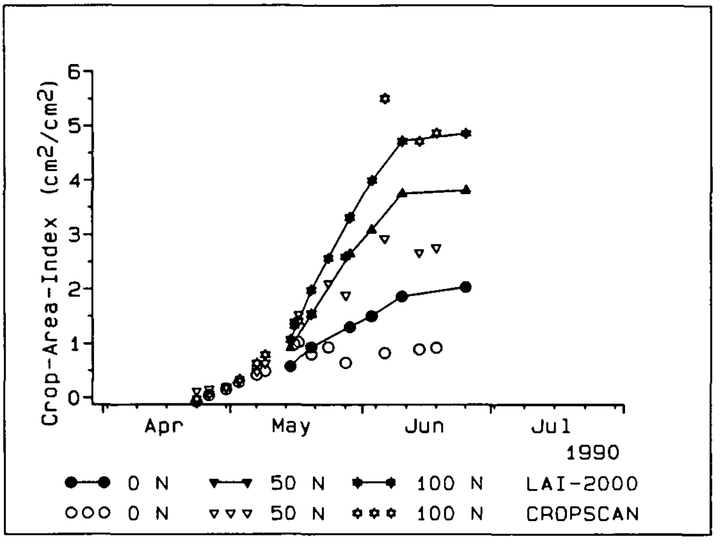

Figure 5: Treatment averages of CAI measured using the Cropscan and LAI-2000 instruments. Sampling as discussed in Fig. 4. Cropscan reflectance measurements calibrated using polynomial shown in Fig. 3.

included in the analysis. In Fig. 6 only days when near noon PAR irradiance was less than 350 μmol m^{-2} s^{-1} have been included. By analyzing the data recorded using Delta-T tube solarimeters sensing total incident and transmitted shortwave radiation results very similar to the results shown in Fig. 6 were obtained.

- Results obtained using the new LAI-2000 instrument are especially encouraging for further use of the instrument in field experiments. The possibility of obtaining rapid CAI estimates without prior calibration is a unique feature of the instrument. The need for diffuse light conditions does, however, limit the number of useful hours on most days.

Conclusions

Keeping the limitations of a single spring barley experiment in mind the following main conclusions have been drawn:

- The area of canopy surfaces (leaves + stems, CAI) for the pre-heading period can be reliably estimated using the three methods investigated: Canopy reflectance, gap fractions, and canopy transmittance.

- Estimation of the area of green canopy material is possible with instruments based on canopy reflectance measurements. Therefore, these instruments can be used during the entire growing season and in stressed crops for monitoring the 'size' of the active part of the canopy. This sensitivity provides the basis for the use of spectral indices in e.g. studies related to photosynthesis and crop yield (Wiegand and Richardson, 1990).

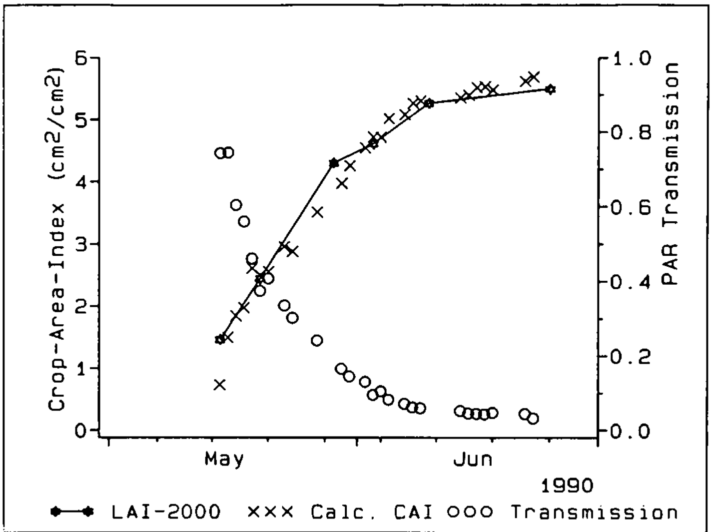

Figure 6: Development in CAI measured using LAI-2000, relative canopy PAR transmission measured using point and line sensors, and CAI values calculated from transmittance measurements. Calculations based on least squares fitted exponential relationship between PAR transmittance and LAI-2000 CAI measurements. Only days with low ($< 350\mu$mol m^{-2} s^{-1}) PAR irradiance included.

- Combined use of more than one type of instrument should be considered for new monitoring possibilities, improved data quality, and labor savings. As an example of this approach the difference between LAI-2000 and Cropscan estimates of CAI (see Fig. 5) might prove useful in photosynthesis, transpiration, and evaporation studies.

References

Jensen, A., Lorenzen, B., Østergård, H.S. and Hvelplund E.K. (1990). Radiometric estimation of biomass and nitrogen content of barley grown at different nitrogen levels. Int. J. Remote Sensing 11(10): 1809-1820.

LAI-2000 Plant Canopy Analyzer. Technical Report # 102. LI-COR, Inc. Lincoln, Nebraska, USA.

Norman, J.M. and Campbell G.S. (1989). Canopy structure. In: Plant Physiological Ecology: Field methods and instrumentation. (eds. R.W. Pearcy, J. Ehlringer, H.A. Mooney and P.W. Rundel), Chapman and Hall, London and New York. pp. 301-325.

Pederson, V.D. and Nutter F.W. (1982). Low-cost, portable multispectral radiometer for assessment of onset and severity of foliar disease of barley. Proc. of International Society for Optical Engineering (SPIE) 356: 126-130.

Petersen, C. (1989). A spectral reflectance index of developing crops largely independent of cloud cover and soil surface wetness. Acta Agric. Scand. 39:465-476.

Walker, G.K., Blackshaw, R.E. and Dekker J. (1988). Leaf Area and Competition for Light between Plant Species using Direct Sunlight Transmission. Weed Technology 2: 159-165.

Welles, J. (1990). Some indirect methods of estimating canopy structure. In: Instrumentation for studying vegetation canopies for remote sensing in optical and thermal infrared regions. (eds. J. Norman and N. Goel), Harwood Academic Publishers GmbH, London. pp. 31-43.

Welles, J. and Norman, J.M. (1991). Instrument for Indirect Measurement of Canopy Architecture. Agron. J. 83: 818-825.

Wiegand, C.L. and Richardson, A.J. (1990). Use of Spectral Vegetation Indices to Infer Leaf Area, Evapotranspiration and Yield: I. Rationale. Agron. J. 82: 623-629.

Multispectral radiometry
A source of additional data in field fungicide trials

J.G. Hansen*, L.N. Jørgensen** and J. Simonsen**
*Dept. of Agrometeorology, Danish Institute of Plant and Soil Science
Research Center Foulum, P.O. Box 25 8830 Tjele, Denmark
**Dept. of Plant Pathology, Danish Institute of Plant and Soil Science
Lottenborgvej 2, 2800 Lyngby, Denmark

Abstract

During the 1990 and 1991 growing seasons four field fungicide trials were monitored by multispectral radiometry and visual disease assessment. Spectral reflectance data were found to be highly correlated to disease assessments and grain yields. The area under the normalized difference curve (AUNDC) from heading to soft dough could explain 93-99 percent of the variation in grain yield after harvest. With a simple yield loss function the use of NIR/Red vegetation index was found to be a better predictor of yield loss than using NDVI or NIR reflectance. Multispectral radiometry as a supplement to traditional assessment and monitoring methods is discussed.

Introduction

During the last 15 years several investigators have reported significant correlations between spectral reflectance and green leaf biomass (Curran, 1983; Petersen, 1989). In field fungicide trials other variables influencing growth such as nutrient levels, soil water availability, solar radiation etc. is assumed to be equal. The difference in spectral reflectance between plots has therefore been used to describe the disease impact on crop growth (Sharp et al., 1985; Pederson, 1986; Nilsson, 1991; Hansen, 1991). Because the green leaf area index (GLAI) is essential in yield formation, single date or integrated spectral reflectance measurements has been used in yield estimation or yield loss prediction (Aase et al., 1984; Tucker et al., 1980; Hansen, 1991).

It is the aim of this paper to describe how spectral radiometry can be a source of additional data in field fungicide trials. In a similar approach Hansen (1991) analyzed results from three winter wheat fungicide trials with yellow rust. This paper includes results from four trials with wheat and barley, each with one dominant disease.

Materials and methods

During the 1990 and 1991 growing seasons four fungicide trials were monitored by traditional methods and by multispectral radiometry. All trials consisted of four replications of a randomized block design with 25-30 m^2 plots. The trials were designed to test the effectiveness of different fungicides or different control strategies using reduced dosages and disease models.

In each field experiment one disease was dominating: 1) Yellow rust (*Puccinia striiformis*) in winter wheat (Sleipner), 2) leaf blotch (*Rhyncosporium secalis*) in winter barley (Pastoral), 3) leaf stripe (*Drechslera graminea*) in spring barley (Golf and Triumph) and 4) Septoria spp. (*Septoria tritici; Septoria nodorum*) in winter wheat (Pepital). The fungicide application scheme for the winter wheat experiment with Septoria spp. is shown in Table 1.

During the period from May to the end of July the leaf diseases were assessed visually at 7-14 days intervals as disease severity or disease incidence (Nutter et al., 1991). Early in the season mildew occured at low levels ($< 2 - 10$ %) on lower leaves in all trials, but these attacks did not spread to the upper leaves. Each plot was harvested mid-August, and the grain yield adjusted to 85 percent dry matter. Grain yields are expressed as hkg/ha. Growth stages are after Zadoks et al. (1974).

During the season each plot was monitored three to six times with a handheld multispectral radiometer of the type CROPSCAN (Pederson, 1982, Nutter, 1989, Hansen, 1991). Four measurements (0.75 m^2) per plot were made to account for interplot variation in disease development and crop growth.

Different investigators have used different spectral bands and vegetation indexes to describe the relationship between reflectance and disease and yield respectively. Commonly used are the NIR band alone (Nutter, 1989; Clevers and Sibma, 1990), the band ratio NIR/Red (Petersen, 1989) and the Normalized Difference index, NDVI (NIR - Red)/(NIR + Red)(Curran, 1983; Sharp et al., 1985). Spectral measurements during the season of NIR, NIR/Red and NDVI were compared and related to disease assessments and grain yield by correlation and regression methods (SAS Institute Inc., 1988). In addition the Area Under the NIR/Red Curve (AUNRC) and the Area Under the Normalized Difference Curve (AUNDC) were related to grain yield after harvest.

Based on the work of Waggoner and Berger (1987), Hansen (1991) suggested to use spectral reflectance data for yield loss estimation, YLE (%), using a simple yield loss function:

$$YLE = [1 - (AUNRC/AUNRC_{\text{healthy}})] \times 100$$

where AUNRC healthy is the area under the NIR/RED curve of the "most healthy crop". In this approach AUNRC's are the areas under the NIR/Red curves for other treatments than the "most healthy crop".

Results

The fungicide application scheme and grain yield of the wheat experiment are shown in Table 1. Because the correlation between spectral data, disease severity and grain yield show the same tendencies in all trials, only figures for the winter wheat experiments with Septoria spp. is included. Figure 1 shows the development of Septoria spp. in the 12 plots. Figure 2a-c shows the progress of NIR, NIR/Red and NDVI respectively. Figure 3 shows the relationship between spectral reflectance and disease data. Figure 4 shows the relationship between spectral reflectance data and grain yields. Dates of application according to growth stages in Table 1 are shown in the figures as needles. The relationship between spectral reflectance data, disease severities and grain yields respectively are shown as correlation coefficients in Table 2.

Table 1: Fungicide application scheme in winter wheat (Pepital) at Foulum 1991. The dominant disease were Septoria spp. The disease development is shown in Figure 1.

Plot no.	Fungicide	l/ha	Application at growth stage		Grain yield and yield increase (hkg/ha)	rel.
1	Untreated				69.0	100
2	Bayfidan	2 × 0.5	30-31	51-59	2.3	103
3	Tilt 250ec	2 × 0.5	30-31	51-59	7.2	110
4	Alto 240 SL	2 × 0.25	30-31	51-59	1.9	103
5	Folicur 250 EW	2 × 1.0	30-31	51-59	6.7	110
6	DPX H 6573	2 × 0.8	30-31	51-59	9.9	114
7	Sportak 45ec	2 × 1.0	30-31	51-59	8.8	113
8	RPAN 10064 B	2 × 1.0	30-31	51-59	6.2	109
9	Corbel	2 × 1.0	30-31	51-59	2.3	103
10	Tilt Top	2 × 1.0	30-31	51-59	7.7	111
11	Matador	2 × 1.0	30-31	51-59	8.1	112
12	Tiptor	2 × 1.0	30-31	51-59	9.2	113
				LSD95	1.8	
				LSD95(excl. untreated)	1.8	

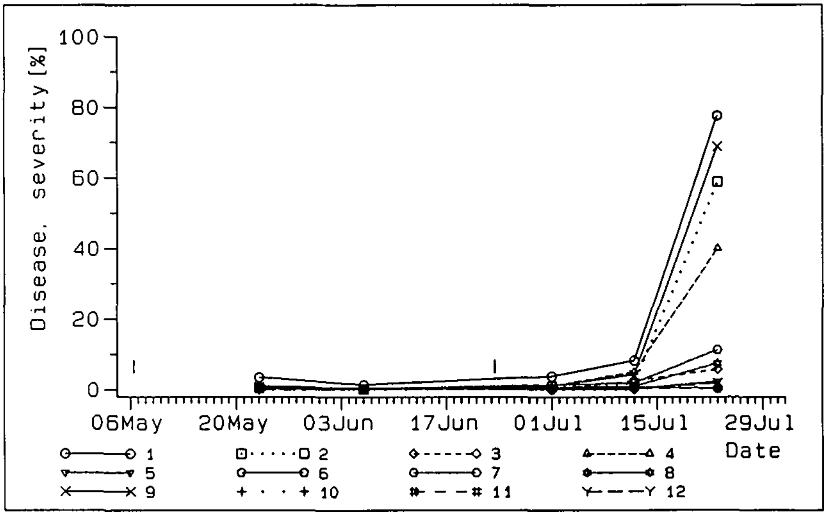

Figure 1: Winter wheat with Septoria spp. Disease progress. | = fungicide application according to scedule (Table 1).

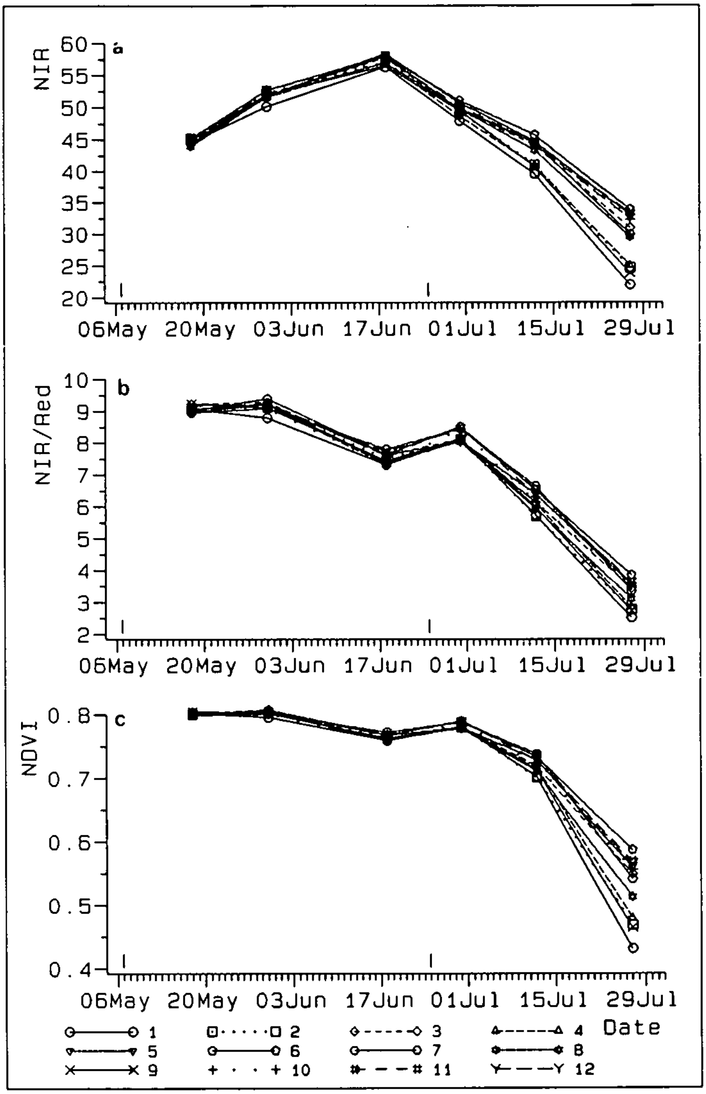

Figure 2: Winter wheat with Septoria spp. (a) NIR-progress, (b) NIR/Red-progress and (c) NDVI-progress. | = fungicide application according to scedule (Table 1).

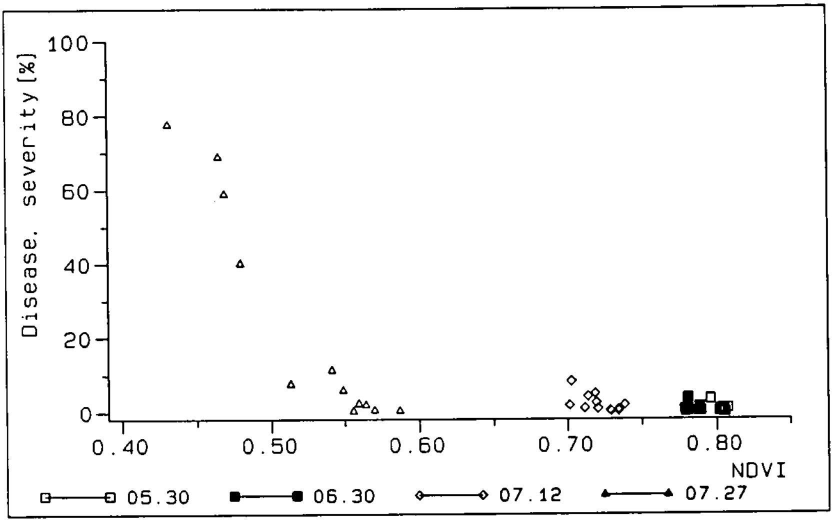

Figure 3: Winter wheat with Septoria spp. NDVI versus disease severity, % on May 30, June 30, July 12 and July 27 (Table 1).

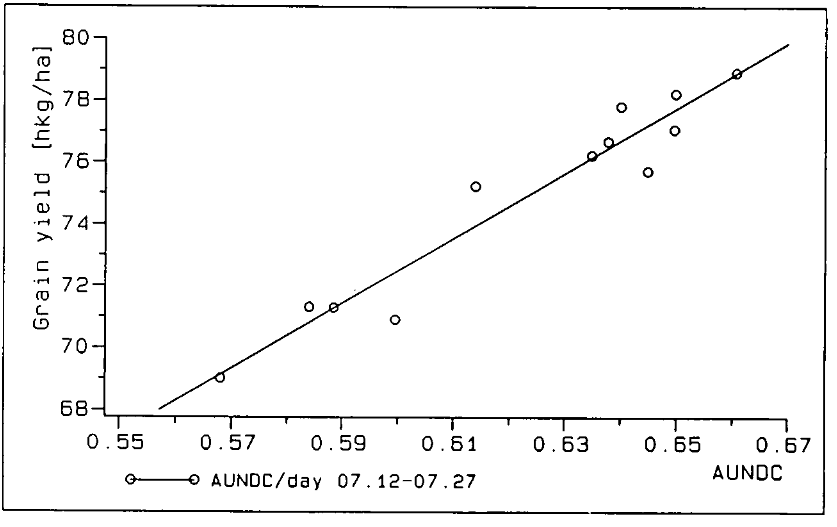

Figure 4: Winter wheat with Septoria spp. AUNDC/day for the period July 12 to July 27 versus grain yield, kg/ha. R^2=0.93 (Table 3).

Table 2: Correlation coefficients for spectral reflectance data and disease severity, % and grain yield, hkg/ha respectively. AUDPC (Area Under the Disease Progress Curce). AUNRC (Area Under The NIR/Red Curve). AUNDC (Area Under the Normalized Difference Curve.

Spectral index	Date	Growth stage Zadoks	Disease severity, %	Grain yield hkg/ha
Septoria spp. in winter wheat. Foulum, 1991				
Disease	May23	34	-	-0.63*
Disease	Jun06	45	-	-0.64*
Disease	Jul01	65	-	-0.66*
Disease	Jul12	75	-	-0.82**
Disease	Jul23	85	-	-0.93***
NIR	May18	32	-	-0.20 n.s.
NIR	May30	39	-0.78**	0.68*
NIR	Jun18	59	-	0.72**
NIR	Jun30	65	-0.75**	0.78**
NIR	Jul12	75	-0.84***	0.98***
NIR	Jul27	85	-0.97***	0.95***
NIR/Red	May18	32	-	-0.31 n.s.
NIR/Red	May30	39	-0.69*	0.63*
NIR/Red	Jun18	59	-	0.70*
NIR/Red	Jun30	65	-0.24 n.s.	0.70*
NIR/Red	Jul12	75	-0.58*	0.84***
NIR/Red	Jul27	85	-0.93***	0.96***
NDVI	May18	32	-	-0.32 n.s.
NDVI	May30	39	-0.70*	0.63*
NDVI	Jun18	59	-	0.70*
NDVI	Jun30	65	-0.24 n.s.	0.70*
NDVI	Jul12	75	-0.58*	0.84***
NDVI	Jul27	85	-0.95***	0.96***
AUDPC	May23-Jun06	34-45	-	-0.64*
AUDPC	Jun06-Jul01	45-65	-	-0.67*
AUDPC	Jul01-Jul12	65-75	-	-0.80**
AUDPC	Jul12-Jul27	75-85	-	-0.93***
AUNRC	May18-May30	32-39	-	0.52 n.s.
AUNRC	May30-Jun18	39-59	-	0.81**
AUNRC	Jun18-Jun30	59-65	-	0.82**
AUNRC	Jun30-Jul12	65-75	-	0.83***
AUNRC	Jul12-Jul27	75-85	-	0.95***
AUNDC	May18-May30	32-39	-	0.52 n.s.
AUNDC	May30-Jun18	39-59	-	0.81**
AUNDC	Jun18-Jun30	59-65	-	0.83***
AUNDC	Jun30-Jul12	65-75	-	0.85***
AUNDC	Jul12-Jul27	75-85	-	0.96***

Only for the Wheat-Septoria experiment results of correlations from all dates are given. The multiple correlation coefficients (R^2) for reflectance data and grain yield are given in Table 3.

Discussion

The relationship between spectral reflectance and disease impact on crop growth in the four field fungicide trials was analyzed by correlation and linear regression based on the near linear relation between spectral reflectance and GLAI's below 4 (Petersen, 1989; Curran, 1983). This approach seems to be appropriate because:

a) disease impact on crop growth normally reduce GLAI,

b) foliar diseases such as Septoria spp. and Rhynchosporium normally develops in epidemics after heading, when GLAI decreases because of *natural* age dependent senescens and

c) GLAI during the period of grain filling normally are relative low.

Spectral reflactance and foliar diseases

In the wheat-Septoria trial the epidemic disease development started in plot 1, 2, 4 and 9 after flowering, mid-July (Table 1 and Figure 1). Other treatments kept the disease at low levels at least until last week of July. The split in two groups between treatments were detected by NIR reflectance on July 12 (Figure 2a) and by NDVI on July 27 (Figure 2c). Correlation to disease severity was significant except at full flowering for the band ratios including NIR and Red reflectance (Table 2 and Figure 3. This is probably due to an influence on red reflectance of the changing colour and head structure during flowering, because the correlation for NIR reflectance seems not to be affected in the same way (Table 2). The correlation between reflectance and disease severity was highest after flowering where Septoria spp. developed on the upper two leaves (Tabel 2 and Figure 3).

Figure 3 shows, that NDVI on July 12 and especially on July 27 are different for plots with no or low disease level. Because the time from Septoria spp. infection to visual symptoms are 10-25 days this could be an expression of the non-visual disease impact on crop growth.

In the wheat trial only NIR reflectance was able to detect maximum GLAI mid June (Figure 2a-c). One reason for that is, that NIR reflectance reaches an asymptote at a higher GLAI than the two band ratios. This was found in a test plot with winter wheat, where spectral reflectance was related to GLAI measured in the laboratory (not published). Red reflectance had a local maximum on June 18 and local minimum at flowering June 30 (not published). This is the reason for the local minimum and maximum of the NIR/Red reflectance on June 18 and June 30 respectively (figure 2b).

Spectral reflectance and grain yield estimation

During the period from flowering (June 30) to soft dough (July 27) spectral reflectance correlation to grain yields was high. On July 12 correlation for NIR was significantly higher than for the two indices (Table 2).

Single date spectral measurements during the period after flowering were as highly correlated to grain yield as were integrated indices (Table 2). Integration of spectral measurements during the period of grain filling, although, seems to be a more appropriate ap-

Table 2: ..... continued.

Spectral index	Date	Growth stage Zadoks	Disease severity, %	Grain yield hkg/ha
Yellow rust (*Puccinia striiformis*) in winter wheat. Støvring, 1990				
NIR	Jul11	85	-0.95***	0.99***
NIR/Red	Jul11	85	-0.94***	0.97***
NDVI	Jul11	85	-0.94***	0.99***
AUNRC	Jun28-Jul11	75-85	-	0.98***
AUNDC	Jun28-Jul11	75-85	-	0.99***
Leaf Blotch (*Rhynchosporium secalis*) in winter barley. Spørring, 1991				
NIR	Jul08	85	-0.86***	0.81**
NIR/Red	Jul08	85	-0.91***	0.94***
NDVI	Jul08	85	-0.92***	0.94***
AUNRC	Jun09-Jul08	65-85	-	0.94***
AUNDC	Jun09-Jul08	65-85	-	0.97***
Leaf stripe (*Drechslera graminea*) in barley. Foulum, 1991				
NIR	Jul04	59	-0.94***	0.96***
NIR/Red	Jul04	59	-0.98***	0.91**
NDVI	Jul04	59	-0.99***	0.90**
AUNRC	Jul04-Jul12	59-69	-	0.97***
AUNDC	Jul04-Jul12	59-69	-	0.97***

*, **, *** indicated significance at the 0.05, 0.01 and 0.001 level respectively. Not significant (n.s.).

Table 3: Multiple correlation coefficients (R^2) for reflectance data and grain yield.

Disease	Index	Period	R^2
wheat Septoria spp.,	AUNDC	Jul12-Jul27	0.93***
wheat yellow rust,	AUNDC	Jun28-Jul11	0.99***
barley leaf stripe,	AUNDC	Jul04-Jul12	0.94***
barley leaf blotch,	AUNDC	Jun09-Jul08	0.94***

proach than the use of a single date measurement, because integration takes account of the variation in disease epidemics during that period.

The highest correlation to grain yield were found for AUNDC calculated for the period July 12 to July 27 (Tabel 2 and Figure 4). The AUNDC's calculated for the period July 12 to July 27 could explain 93 percent of the variation in grain yield using linear regression (Figure 4). The correspondingly calculated AUDPC's (July 12 to July 23) explained only 87 percent (R^2) of the variation in grain yield.

Grain yield can be estimated by a regression function based on spectral reflectance measurements and grain yield determination in a part of the plots or in a few test plots with plants grown under similar conditions. In Hansen (1991) several types of regression models are discussed.

Spectral reflectance and yield loss prediction

With a simple yield loss function based on integration of spectral reflectance data during the growing season, a prediction of yield loss in percent were calculated using different periods of integration. The integrated NIR/Red vegetation index was found to be a better predictor of yield loss than NDVI or NIR reflectance Figure 5. The yield loss prediction based on spectral reflectance can be used as an alternative to grain yield determination after harvest.

Conclusions

Relative reflectance between plots in fungicide trials can be used as a measure of the varying disease epidemic impact on crop growth.

Visual disease assessment is subjective and the quality of disease data are depending on method and the experience of the person conducting the survey. Spectral reflectance data can be used for intertrial calibration and for calibration between trials and methods.

Measurements of spectral reflectance during the period of flowering should be analyzed carefully. A negative influence of red reflectance on correlations to both disease and grain yield after harvest was found.

Spectral reflectance data was stronger correlated to grain yield than disease data.

No single reflectance index was the best in all situations. Only NIR reflectance could detect maximum GLAI in healthy plots. Multidate integration using AUNDC or AUNRC instead of single date reflectance measurements is suggested for yield modelling and yield loss prediction. The period from ended flowering to soft dough is suggested. Yield loss prediction or yield estimation based on spectral reflectance can be an alternative to grain yield determination by traditional plot harvesting.

Spectral reflectance do not distinguish between different diseases, and the method can only be a supplement to traditional plant pathology methods.

References

Aase, J.K., Siddoway, F.H. and Millard, J.P. (1984). Spring wheat leaf phytomass and yield estimates from airborne scanner and hand-held radiometer measurements. Int. J. Remote Sensing 5: 771-781.

Clevers, J.G.P.W. and Sibma, L. (1990). Estimation of dry matter yield of silage maize by means of multispectral aerial photography. Nethl. J. of Agric. Sci. 38: 653-659.

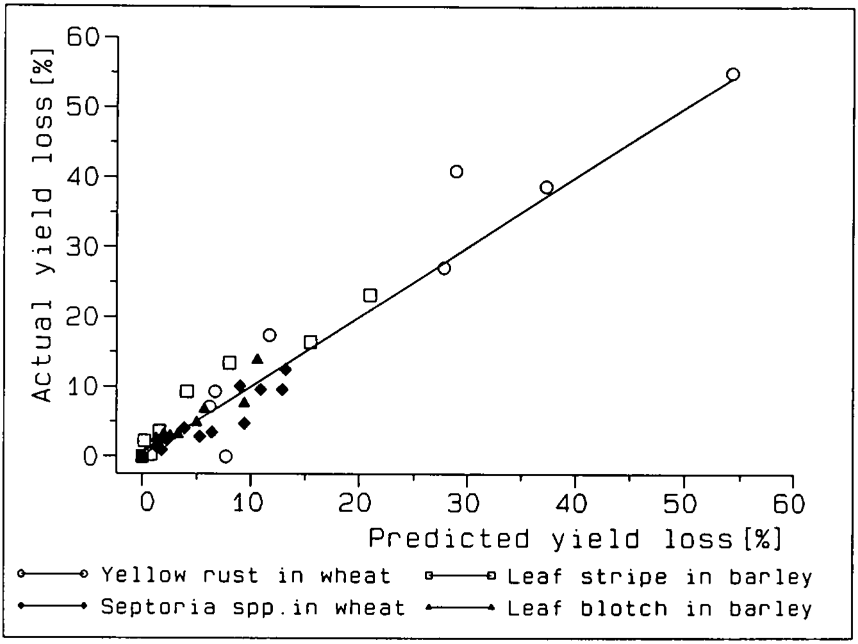

Figure 5: Predicted versus actual grain yield loss (%) for four field fungicide experiments. Grain yield loss, YLE (%), is estimated by the function: YLE = [1 - (AUNRC/AUNRC healthy)] × 100. AUNRC is Area Under the NIR/Red Curve. The period of integration (AUNRC) for the wheat yellow rust experiment is May 28 to July 11. For the leaf stripe barley experiment, July 4 to July 12. For the Septoria wheat experiment, June 30 to July 27 and for the leaf blotch barley experiment, June 9 to July 8. The line is the 1:1 line.

Curran, P.J. (1983). Multispectral remote sensing for the estimation of green leaf area index. Phil. Trans. R. Soc. Lond. A 309: 257-270.

Hansen, J.G. (1991). Use of multispectral radiometry in wheat yellow rust experiments. OEPP/EPPO Bull. 21, 651-658.

Nilsson, H.E. (1991). Hand-held radiometry and IR-thermography of plant diseases in field plot experiments. Int. J. Remote Sensing 12(3): 545-557.

Nutter, F.W.Jr. (1989). Detection and measurement of plant disease gradients in peanut with a multispectral radiometer. Phytopathology 79: 958-963.

Nutter, F.W., Teng, P.S. and Shokes, F.M. (1991). Disease assess ment terms and concepts. Plant Disease, 75(11) 1187-1188.

Pederson, V.D. and Nutter, F.W. Jr. (1982). Low-cost, portable multispectral radiometer for assessment of onset and severity of foliar disease of barley. Proc. Int. Soc. Opt. Eng. 356: 126-130.

Pederson, V.D. (1986). Estimation of efficacy of foliar fungicides on Barley by multispectral radiometry. Phytopathology 76(9): 957.

Petersen C. (1989). A spectral reflectance index of developing crops largely independent of cloud cover and soil surface wetness. Acta Agric. Scand. 39: 465-476.

SAS Institute Inc. (1988). SAS/STAT User's Guide, Release 6.03 Edition. Cary(US)

Sharp, E.L., Perry, C.R., Sharen, A.L., Boatwright, G.O., Sands, D.C., Lautenschlager, L.F., Yahyaoui, C.M. and Ravet, F.W. (1985). Monitoring ceral rust with a spectral radiometer. Phytopathology 75: 936-939.

Tucker, C.J., Holben, B.N., Elgin J.H.Jr. and McCurthrey, J.E. (1980). Relationship of spectral data to grain yield variation. Photogram. Engin. and Remote Sensing 46(5): 657-666.

Waggoner, P.E. and Berger, R.D. (1987). Defoliation, disease and growth. Phytopathology 77: 393-398.

Zadoks, J.C., Chang, T.T. and Konzak, C.F. (1974). A decimal code for the growth stages of cereals. Weed Research 14: 415-421.

Assessing leaf area index and light interception from spectral reflectance measurements

Svend Christensen
Research Centre for Plant Protection, Department of Weed Control
Flakkebjerg, DK-4200 Slagelse
Denmark

Summary

The advantage of measuring the spectral reflection of solar radiation from a canopy lies especially in the prospect of obtaining fast and accurate non-destructive information about photosynthetic activity of a crop.

In the presented paper the theoretical relationship between spectral reflectance and LAI, and spectral reflectance and PAR interception is described. The results showed that the correlation between spectral reflectance and LAI is sensitive to different soil types, soil humidities, instrumentation and to varying extinction of leaves caused by variation in canopy structure or leaf angles. Thus, the relationship between the spectral reflectance and PAR interception is preferable, because the effect of varying extinction is eliminated in this approach. However, the influence of soil type, soil humidity and instrumentation has to be calibrated with measurements from a bare soil and an infinite LAI.

A procedure to predict PAR interception from the spectral reflectance measurements is described and used to compare the indices, NDVI and RVI. The results showed no significant differences in PAR interception predicted from the two indices.

Introduction

The interception of photosynthetically active radiation (PAR) is the major parameter for describing the photosynthetic activity of a crop. Usually PAR interception is derived from assessments of leaf area index (LAI) and the extinction of the leaves, or measured with quantum sensors at the soil surface. Both methods require adequate sampling techniques with several replications which is rather time-consuming.

The objective of this paper is to describe a more accurate and efficient approach where the LAI or PAR interception is obtained from measurements of spectral reflectance.

The approach is based on the relationship between the reflectance of near infrared and red radiation from the canopy and LAI. The effect of canopy structure (extinction coefficient) is simulated. Further, the relationship between the spectral reflectance and the fraction of intercepted PAR (f_{PAR}) is derived.

The relationship between spectral reflectance and f_{PAR} was validated in Christensen & Goudriaan (submitted 1991) where the description, the instrumentation and the results of a field experiment including different spring barley cultivars are presented.

Finally, a comparative analyses of the relative vegetation index (RVI) and the normalized difference vegetation index (NDVI) is performed.

Vegetation indices

Several investigators have shown that the fraction of reflected red (ρ_r) and near infrared (ρ_i) radiation from the canopy contains significant information about the crop due to the contrast between the soil background and the vegetation (Bunnik, 1981; Tucker, 1979; Allrichs & Bauer, 1983; Petersen, 1989). Various combinations of ρ_i and ρ_r have been considered, but the normalized difference vegetation index

$$NDVI = \frac{(\rho_i - \rho_r)}{(\rho_i + \rho_r)} \tag{1}$$

and the relative vegetation index

$$RVI = \frac{\rho_i}{\rho_r} \tag{2}$$

are the most functional ones (Wiegand, 1990).

Deriving LAI from vegetation indices

The reflectance (ρ_i and ρ_r) from a canopy is influenced by the reflectance from the canopy itself and from the soil. The soil reflectance changes due to variations in humidity (Heute et al., 1985), but decreases with increasing LAI. The ρ_i and ρ_r are given by

$$\rho_r = \frac{\rho_{r,\infty} + \frac{(\rho_{r,\infty} - \rho_{r,s})}{(\rho_{r,s} - \frac{1}{\rho_{r,\infty}})} \cdot \frac{\exp(-2 \cdot K_r \cdot LAI)}{\rho_{r,\infty}}}{1 + \frac{(\rho_{r,\infty} - \rho_{r,s})}{\rho_{r,s} - \frac{1}{\rho_{r,\infty}}} \cdot \exp(-2 \cdot K_r \cdot LAI)} \tag{3}$$

and

$$\rho_i = \frac{\rho_{i,\infty} + \frac{(\rho_{i,\infty} - \rho_{i,s})}{(\rho_{i,s} - \frac{1}{\rho_{i,\infty}})} \cdot \frac{\exp(-2 \cdot K_i \cdot LAI)}{\rho_{i,\infty}}}{1 + \frac{(\rho_{i,\infty} - \rho_{i,s})}{\rho_{i,s} - \frac{1}{\rho_{i,\infty}}} \cdot \exp(-2 \cdot K_i \cdot LAI)} \tag{4}$$

(Goudriaan, 1977) where the parameters $\rho_{r,\infty}$ and $\rho_{i,\infty}$ are the red and near infrared reflectance at infinite LAI. The $\rho_{r,s}$ and $\rho_{i,s}$ represent the red and near infrared reflectance from a bare soil. K_i and K_r are the near infrared and red extinction coefficients. Knowing the parameters K_i, K_r, $\rho_{i,s}$, $\rho_{r,s}$, $\rho_{i,\infty}$ and $\rho_{r,\infty}$ (Table 1), the indices NDVI and RVI (Eqn. 1 and 2) are a function of LAI (Eqn. 3 and 4). The variability of the parameter values in Table 1 is discussed in the next section.

As seen in Fig. 1 both indices are nonlinear functions of the LAI (cf. Choudhury 1987, Asrar et al. 1984). The intercept at the vertical axis is the RVI or NDVI value from a bare soil. Both indices are ceiling at large LAI, but NDVI is ceiling at lower LAI than RVI.

The relationship between LAI and the indices depends on the extinction coefficients K_i and K_r. Fig. 1 shows that the indices are ceiling at lower LAI with increasing extinction coefficients. Thus, it is inappropriate to describe the relationship empirically by measurements of RVI and LAI, because the estimated parameters depend on the canopy structure, e.g. species and varieties.

Deriving PAR interception from vegetation indices

Instead of obtaining LAI from RVI or NDVI, a more appropriate approach is to derive the fraction of intercepted PAR (f_{PAR}) from the indices. Goudriaan (1977) showed that the ratio between PAR transmitted by a canopy

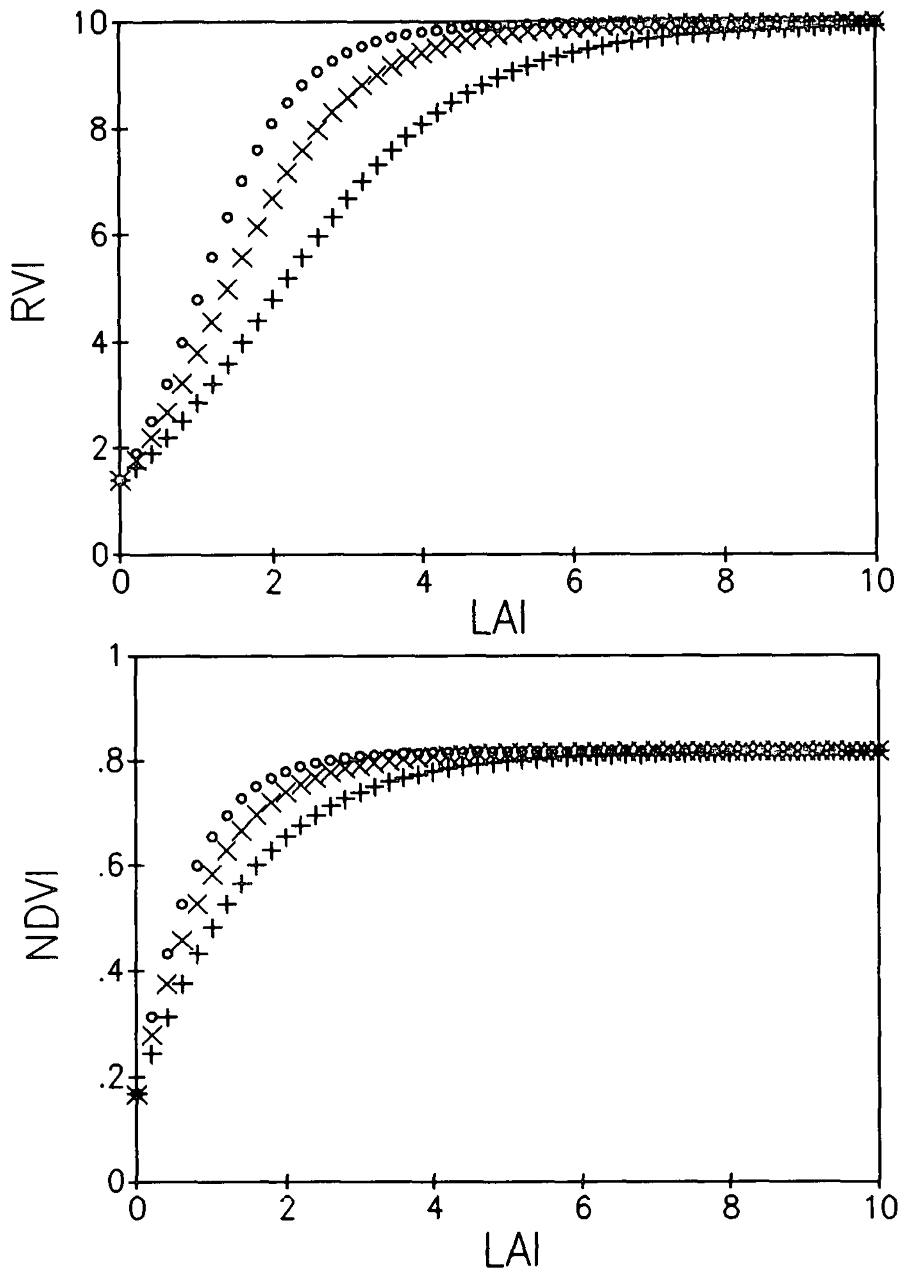

Figure 1: The relationship between RVI, NDVI and LAI at varying extinction coefficient. The values are calculated from Equation 3 and 4 using the parameter values in Table 1 and the extinction coefficient: Symbol o: $K_r = 0.8$ and $K_i = 0.4$. Symbol $\times$: $K_r = 0.6$ and $K_i = 0.3$. Symbol $+$: $K_r = 0.4$ and $K_i = 0.2$.

Table 1: The deduced parameter values in Equation 3, 4 and 7.

	Near infra-red	Red	Ratio
Extinction coefficient	$K_i = 0.35$	$K_r = 0.70$	$\frac{K_i}{K_r} = 0.5$
Reflectance at infinite LAI	$\rho_{i,\infty} = 0.400$	$\rho_{r,\infty 1} = 0.040$	$\frac{\rho_{i,\infty}}{\rho_{r,\infty 1}} = 10.0$
Reflectance from bare soil	$\rho_{i,s} = 0.28$	$\rho_{r,s} = 0.20$	$\frac{\rho_{r,s}}{\rho_{i,s}} = 1.4$

and incoming PAR decreases approximately exponentially with increasing LAI

$$\frac{S_{s,PAR}}{S_{0,PAR}} = \exp(-K_{PAR} \cdot LAI) \qquad (5)$$

where K_{PAR} is the extinction coefficient for PAR radiation. The fraction of intercepted PAR is then

$$f_{PAR} = 1 - \exp(-K_{PAR} \cdot LAI) \qquad (6)$$

Assuming that the extinction coefficient of red radiation K_r equals the extinction coefficient of PAR

$$f_{PAR} = 1 - \exp(-K_r \cdot LAI) \qquad (7)$$

f_{PAR} can be calculated for different LAI. Using Equation 3 and 4 to calculate RVI or NDVI at different LAI the relationship between RVI or NDVI and f_{PAR} can be described with a parametric plot (Fig. 2).

Fig. 2 shows that both indices are non-linear functions of the f_{PAR} (cf. Choudhury 1987, Asrar et al. 1984). The intercept at the horizontal axis is the RVI or NDVI value from a bare soil. The NDVI is ceiling at a lower f_{PAR} ratio than the RVI.

Comparing the relationship between RVI and f_{PAR} with the relationship between RVI and LAI a very convenient result is obtained, because the influence of varying extinction coefficients (different direction of incoming radiation, canopy structure and pigment density) are eliminated in the relationship between RVI and f_{PAR} (Fig. 2). The dotted line in Fig. 2 demonstrates that the PAR interception and the vegetation index are the same at a LAI=0.6, LAI=0.8 and LAI=1.2 when the extinction coefficients are $K_r = 0.8$, $K_r = 0.6$ and $K_r = 0.4$ respectively. The same result is obtained for the NDVI (Fig. 2).

However, the relationship between RVI or NDVI and f_{PAR} is influenced by varying $\frac{K_i}{K_r}$, $\frac{\rho_{i,s}}{\rho_{r,s}}$ and $\frac{\rho_{i,\infty}}{\rho_{r,\infty}}$ ratios. Rodskjer (1972) found that the $\frac{K_i}{K_r}$ ratio was a constant. Christensen & Goudriaan (submitted 1991) showed that the relationship shown in Fig. 2 was the same for different cultivars of spring barley which indicate that the assumption of constant $\frac{K_i}{K_r}$, $\frac{\rho_{i,s}}{\rho_{r,s}}$ and $\frac{\rho_{i,\infty}}{\rho_{r,\infty}}$ ratios is reasonable. Similar results are reported in Daughtry et al. (1983), Asrar et al. (1984), Gallo et al. (1985) in other cropping systems.

However, the correlation shown in Fig. 2 might change due to variation in soil brightness throughout the growing season. Wiegand et al. (1990) also reported that instrumentation (sensor type) influenced the $\frac{\rho_{i,s}}{\rho_{r,s}}$ and $\frac{\rho_{i,\infty}}{\rho_{r,\infty}}$ ratio. Thus, the influence of the soil and the instrumentation has to be eliminated by adjusting the parameters in Table 1 with

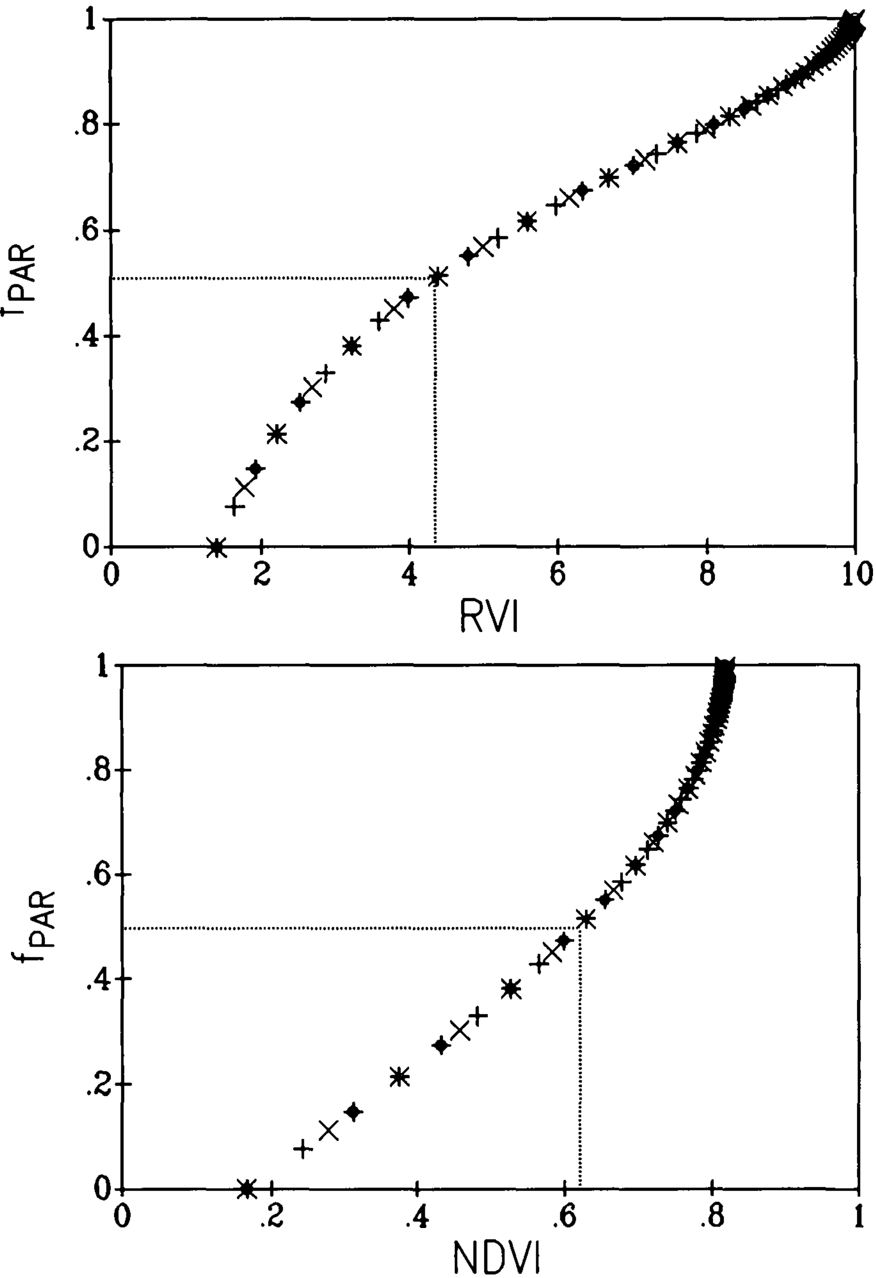

Figure 2: The correlation between f_{PAR} and RVI, NDVI. The values are calculated from Equations 3, 4 and 7 using the parameter values in Table 1. The symbols represent the correlation with the extinction coefficients given in Fig. 1. The dotted line illustrates the effect of different extinction of a similar LAI.

reference measurements on a bare soil and at an infinite LAI.

Predicting PAR interception

Because RVI or NDVI and f_{PAR} cannot be expressed explicitly in each other, estimation of f_{PAR} from RVI or NDVI is only possible with an empirical approximation to the theoretical relationship (Christensen & Coudriaan, submitted 1991). Aiming at an accurate description of the theoretical relationship a polynomial regression is acceptable. Equation (8) and (9) fitted the curves shown in Fig. 2 exactly.

$$f_{PAR} = -0.758 + 0.804 \cdot RVI - 0.238 \cdot RVI^2 + (4.04 \cdot 10^{-2}) \cdot RVI^3 - (3.48 \cdot 10^{-3}) \cdot RVI^4 + (1.19 \cdot 10^{-4}) \cdot RVI^5 \quad (8)$$

and

$$f_{PAR} = -1.769 + 23.51 \cdot NDVI - 114.86 \cdot NDVI^2 + 271.11 \cdot NDVI^3 - 300.32 \cdot NDVI^4 + 126.82 \cdot NDVI^5 \quad (9)$$

Comparison of RVI and NDVI

Using the polynomial regression on the relationship shown in Fig. 2 a comparative analyses of the predicted values of f_{PAR} from RVI and NDVI is possible. As seen in Fig. 3 the predicted values from both indices lies along the 1:1 line which demonstrates that there is no difference in f_{PAR} calculated from the two indices. A regression analyses showed that the line cut through the origin and that the slope was 1. Thus, RVI should be used because of simplicity.

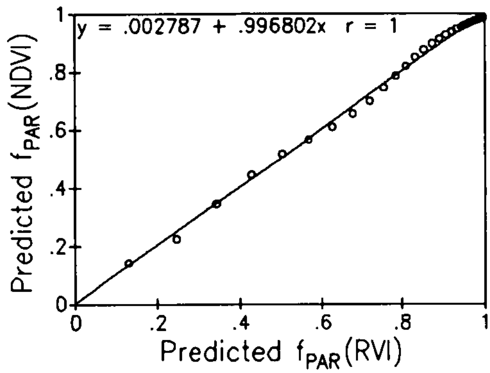

Figure 3: The correlation between predicted f_{PAR} from RVI and NDVI (Equation 8 and 9).

References

Asrar G., Fuchs M. Kanemasu E.T. and Hatfield J.L. (1984): Estimating absorbed photosynthetic radiation and leaf area index from spectral reflectance in wheat. Agron. J. 76: 300-306.

Ahlrichs J.S. and Bauer M.E. (1983): Relation of agronomic and multispectral reflectance characteristics of spring wheat canopies. Agron. J. 75: 987-993.

Bunnik N.J.J. (1981): Fundamentals of remote-sensing. Relations between spectral signatures and physical properties of crops. In: Application of remote sensing to agricultural production forecasting, (ed. Berg.), A.A.A. Balkemu, Rotterdam: 47-81.

Choudhury B.J. (1987): Relationships between vegetation indices, radiation absorption, and net photosynthesis evaluated by a sensitivity analysis. Rem. Sens. Env. 22: 209-233.

Christensen S. and Goudriaan J. (submitted 1991): Deriving biomass from spectral reflectance ratio. Rem. Sens. Env.

Daughtry C.S.T., Gallo K.P. and Bauer M.E. (1983): Spectral estimates of solar radiation intercepted by corn canopies. Agron. J. 75: 527-531.

Gallo K.P., Daughtry C.S.T. and Bauer M.E. (1985): Spectral estimation of absorbed photosynthetically active radiation in corn canopies. Rem. Sens. Env. 17: 221-232.

Goudriaan J. (1977): Crop micrometeorology: a simulation study. Simulation Monographs, Pudoc Wageningen. pp. 247.

Huete A.R., Jackson R.D. and Post D.F. (1985): Spectral response of a plant canopy with different soil backgrounds. Rem. Sens. Env. 17: 37-53.

Petersen C. (1989): A spectral reflectance index of developing crops largely independent of cloud cover and soil surface wetness. Acta Agric. Scand. 39: 465-476.

Rodskjer N. (1972): Measurements of solar radiation in barley and oats. Swedish J. of Agriculture Research 2: 71-81.

Tucker C.J. (1979): Red and photographic infrared linear combinations for monitoring vegetation. Rem. Sens. Env. 8: 127-150.

Wiegand C.L., Gerbermann, A.H., Gallo K.P., Blad B.L. and Dusek D. (1990): Multisite analyses of spectral-biophysical data for corn. Rem. Sens. Env. 33(1): 1-16.

Crop Canopy Temperature and Meteorological Conditions

H. Svendsen, H.E. Jensen, S.E. Jensen and V.O. Mogensen
The Royal Veterinary and Agricultural University
Department of Agricultural Sciences
Section of Soil and Water and Plant Nutrition
Thorvaldsensvej 40, DK-1871 Frederiksberg C
Denmark

Introduction

During the recent decades crop canopy temperature has been used as an indicator of plant water stress. The crop canopy temperature is a result of the energy fluxes through the soil-plant-atmosphere boundary layers. These fluxes are induced by the meteorological conditions. Evapotranspiration is one of the fluxes and it has long been recognized that it should be possible to estimate a relationship between crop canopy temperature and plant water status.

Ehrler (1973) suggested that leaf-air temperature differences could be used as a guide to irrigation scheduling. Later Jackson et al. (1981) and Idso et al. (1981) have developed a crop water stress index based on relationships between the crop canopy-air temperature difference and vapour pressure deficit.

Such models in which the crop canopy-air temperature difference in some way is normalized with respect to the meteorological conditions make it possible to estimate plant water status by using thermal infrared sensors.

Thermal infrared sensors can be used on a laboratory scale as handheld instruments from short distances or can be placed in satellites. Satellite based measurements make it possible to estimate plant water status on a regional basis with a minimum of work. However, special calibration techniques must be used to eliminate the atmospheric influence on the signals.

The model of Jackson et al. (1981) and Idso et al. (1981) was originally developed and verified under arid conditions. The present study is concerned with crop canopy temperatures of crops grown under different irrigation regimes in a temperate humid climate. The temperatures are measured from short distances.

Measurement of surface temperatures.

With thermal infrared sensors radiation from a surface can be measured. This radiation is composed of emitted radiation from the surface and radiation from the surroundings reflected by the surface. The emitted radiation depends on the surface temperature and on the wavelength band according to Planck's radiation equation and on the emissivity. In

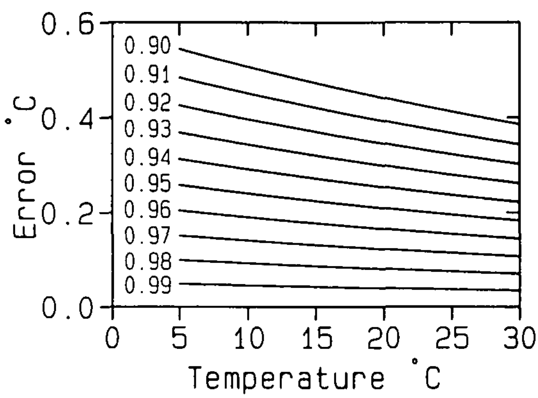

Figure 1: Expected temperature error vs. crop surface temperature calculated for various values of crop emissivity when neglecting clear sky radiation assumed to be 10 Wm^{-2}.

field measurements simultaneously values of reflected radiation are not known and by neglecting this term an error is introduced in the determination of true surface temperatures.

In this study surface temperatures are measured by both a handheld thermometer (Everest Interscience Model 110) and two continously measuring thermometers (Heiman Model KT 15). All instruments use the wavelength band 8-14 μm which is selected because of the maximum atmospheric transmission. In all measurements a view angle of 45° was used and the measurements were started when total plant cover was reached.

Svendsen et al. (1990) reported an analysis of the temperature error for surface temperatures between 0 and 30 °C for different emissivities neglecting clear sky radiation assumed to be 10 Wm^{-2}. The result are shown in Fig. 1. The temperature error depends on both true temperature and on the emissivity of the leaf.

Out of 34 plant species studied (Idso et al., 1969) it was found that 32 had single leaf emissivities >0.95. Fuchs and Tanner (1966) and Blad and Rosenberg (1976) have reported values of 0.976 and 0.971, respectively.

Supposing emissivities >0.96 it is concluded that the temperature error to be expected from neglect of clear sky radiation in crop canopy temperature determination is < 0.2°C.

Theoretical considerations

Relationships between crop canopy surface temperature and agrometeorological variables may be derived from the steady state energy balance equation for a crop, Eq. (1), in which R_n is net radiation, G is soil heat flux, H is sensible heat flux and λE is latent heat flux as E is evapotranspiration and λ is the heat of vaporization.

$$R_n = H + G + \lambda E \tag{1}$$

The flux of sensible heat can be written as Eq. (2) in which T_c is crop canopy surface temperature, T_a is air temperature, r_a is aerodynamic resistance to vapour transport, ρ is air density and C_p is heat capacity of the air. The flux of latent heat can be written as Eq. (3) in which e_c^* is saturated vapour pressure at the temperature T_c, e_a is actual vapour pressure of the air, is the crop canopy resistance to vapour transport and γ is the psychrometer constant.

$$H = \rho C_p(T_c - T_a)/r_a \tag{2}$$

$$\lambda E = \rho C_p(e_c^* - e_a)/\gamma(r_a + r_c)) \tag{3}$$

By assuming soil heat flux G to be negligible Eq. (1), (2) and (3) can be combined

(Jackson et al. 1981) to give Eq. (4) which relates the temperature difference $(T_c - T_a)$ between the crop canopy surface and the air to vapour pressure deficit $(e_a^* - e_a)$, net radiation R_n, aerodynamic resistance r_a and crop canopy resistance r_c. It is realized that aerodynamic resistance is closely related to wind speed and that the crop canopy resistance is closely related to the crop water status. In Eq. (4) Δ is the slope of the saturated vapour pressure at $\frac{1}{2}(T_c + T_a)$.

$$\begin{aligned} T_c - T_a &= \frac{R_n r_a}{\rho C_p} \frac{\gamma(1 + r_c/r_a)}{\Delta + \gamma(1 + r_c/r_a)} \\ &- \frac{(e_a^* - e_a)}{\Delta + \gamma(1 + r_c/r_a)} \end{aligned} \tag{4}$$

For a crop subjected to severe water stress the crop canopy resistance will assume a very high value in relation to the aerodynamic resistance. In this case Eq. (4) can be approximated by Eq. (5). In a diagram in which $(T_c - T_a)$ is plotted versus $(e_a^* - e_a)$ the result is a horizontal line with intercept A.

$$A = T_c - T_a = \frac{R_n r_a}{\rho C_p} \tag{5}$$

For a crop well supplied with water the crop resistance is designated r_{cp}. In this case Eq. (6) is obtained in which $\gamma^* = \gamma(1 + r_{cp}/r_a)$.

$$B = T_c - T_a = \frac{R_n r_a}{\rho C_p} \frac{\gamma^*}{\Delta + \gamma^*} - \frac{e_a^* - e_a}{\Delta + \gamma^*} \tag{6}$$

In a diagram in which $(T_c - T_a)$ is plotted versus $(e_a^* - e_a)$ the result is a line with an intercept of $R_n r_a \gamma^* / (\rho C_p(\Delta + \gamma^*))$ and with a slope of $-1/(\Delta + \gamma^*)$.

A certain range of R_n, T_a, e_a, r_a and r_{cp} may be encountered under actual conditions for crop canopy surface temperature determinations. Under such conditions Eq. (5) and (6) describe regions rather than lines (O'toole and Real, 1984). The upper base line may then be defined as the line through the mean intercept of the upper region and the lower base line as the best fit line through the lower region.

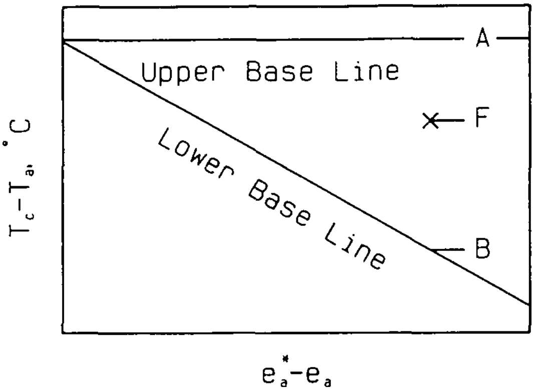

Figure 2: Theoretical upper and lower base lines for use to define the crop water stress index $CWSI$.

Upper and lower base lines are exemplified in Fig. 2. For actual climatic conditions the positions on the upper and lower base lines are designated A and B, respectively. For a crop with temperature difference $F = T_c - T_a$ the crop water stress index CWSI can be defined as Eq. (7) (Idso et al., 1981).

$$CWSI = \frac{F - B}{A - B} \tag{7}$$

The $CWSI$ may be related to the relative evapotranspiration E_a/E_p by Eq. (8). This equation represents an implecit relation between crop canopy surface temperature and the crop water status. For climatic conditions where Eq. (5) and (6) can be estimated with sufficient accuracy crop canopy surface temperatures have the potential for characterizing crop water status.

$$CWSI = 1 - E_a/E_p \quad (8)$$

Theoretical base lines for Danish climatical conditions, for r_a values encountered for various crops under actual wind conditions (Jensen et al., 1990) and for r_{cp} values covering a range of different crops (O'toole & Real, 1984; Jensen et al., 1990) have been analyzed (Svendsen et al., 1991). These theoretical base lines are estimated for selected values of R_n, r_a and r_{cp} in such a way that T_a and e_a are limited by minimum and maximum encountered values during the period 1955-79 under Danish climatic conditions. Limits for upper base line region can be found by Eq. (5) whereas limits for lower base line region may be found by an iterative procedure using Eq. (6). In this procedure T_a is varied at constant e_a and e_a is varied at constant T_a for fixed values of selected R_n, r_a and r_{cp}. By combination of the regions the base lines under varying climatic conditions can be found.

Experiment

The experimental part of the present work was conducted during 1986 and 1987 under Danish climatic conditions using a field lysimeter with a sandy soil as well as with a sandy loam soil. Test crops were in 1986 barley (Hordeum distichum L. cv. Lina) and rape (Brassica napus oleitera L. cv. Topas) and in 1987 perennial rye grass (Lolium perenne L. cv. Borvi) and wheat (Triticum aestivum L. cv. Kraka). For each crop and soil type four plots were irrigated to keep soil water deficit less than approximately 20 mm, while in four other plots the crops were subjected to water stress at various periods by varying the amount of water applied. This was made possible by protecting all plots from precipitation by an automatically moving glass roof. Measured values of air temperature, vapour pressure deficit, wind velocity and global radiation were obtained from the Departmental Climate and Water Balance Station at the immediate vicinity of the field lysimeter. Using the handheld radiometer crop canopy surface temperatures were measured up to four times a day during most of the growing season. The continously measuring radiometers were placed over selected plots and crop canopy surface temperatures measured every minute. The soil water content was determined twice weekly by using the neutron method.

Results

Instant values of crop canopy surface temperatures for fully irrigated and stressed rape grown in the sandy soil, measured before flowering on June 24 at 10.00-11.00 hour, are shown in Fig. 3 as an example. The fully irrigated rape is assumed to have potential transpiration because of low soil water deficit whereas the stressed rape was suffering from severe water stress. Also shown are measured values of global radiation, air temperature, wind speed and vapour pressure deficit. Both crop canopy surface temperatures fluctuate with an amplitude of up to 2 °C. The difference between crop canopy surface temperature and air temperature, $T_c - T_a$, is approximately 4.5 and 1.0 °C for stressed and irrigated rape, respectively. Both global radiation, vapour pressure deficit and air temperature are relatively constant but wind speed fluctuates as common under Danish climatic conditions. Crop canopy surface temperature fluctuations can be inversely related to fluctuations in wind speed because of the cooling effect. However, in cases of rapid changes in wind speed the wind speed may also influence the surface temperature as a result of canopy movement. The true surface temper-

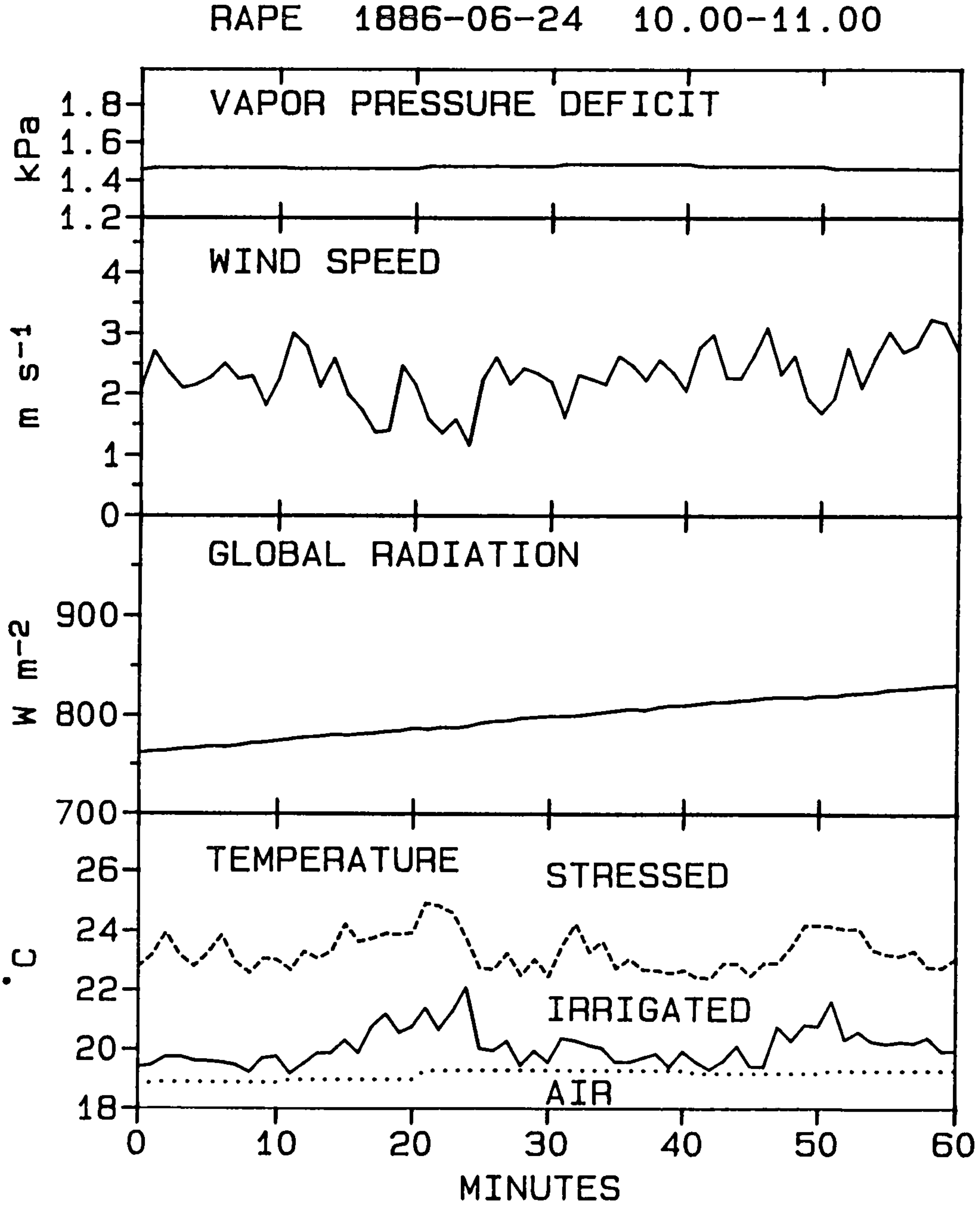

Figure 3: Canopy temperatures of stressed and fully irrigated rape crops and several agrometeorological variables measured 1986-06-24 at 10.00-11.00 h.

ature will in such cases be underestimated as shaded parts of the crop canopy are exposed to the instrument. For high levels of global radiation and vapour pressure deficit it can be concluded that for great differences in soil water content it is possible to detect significant differences in crop canopy surface temperatures.

For high evaporative demands temperature differences between stressed and irrigated crops up to 6 °C have been found.

In cases not shown where the level of global radiation or vapour pressure deficit is low no differences in surface temperatures could be detected even for great differences in soil water content.

During short periods with considerable fluctuations in global radiation resulting from changes in cloud cover the system does not reach steady state and the condition for Eq. (2) is not fulfilled. In such cases crop canopy surface temperatures for both irrigated and stressed crops have been found to fluctuate up to 6 °C within a few minuttes.

Lower base line for fully irrigated crops have been estimated by a linear model Eq. (9) (Jensen et al., 1990), in which a and b have been estimated by linear regression.

$$T_c - T_a = a + b(e_a^* - e_a) \qquad (9)$$

The data used for this purpose were 5-min average values of crop canopy temperature, air temperature and vapour pressure deficits selected from periods with limited temporal changes to ensure approximate steady state conditions.

As an example of this the regression analysis have been made for the whole growing season for rape and for the preflowering and postflowering periods. The results are shown in Table 1. In no case have an acceptable value of the regression coefficient R^2 been found. A reason for this may be that all periods represent different levels of global radiation and wind speed.

Table 1: Linear regression parameters calculated for $T_c - T_a$ versus $(e_a^* - e_a)$ for rape. N is number of observations, a and b is intercept and slope, respectively. s_a and s_b is standard deviation of intercept and slope, respectively, while R^2 is regression coefficient.

Period	a	s_a	b	s_b	R^2	N
Total	4.5	0.8	-2.7	0.6	0.47	28
Preflow.	6.7	1.7	-4.6	1.3	0.62	10
Postflow.	4.5	1.0	-2.6	0.7	0.49	18

Therefore the data have been split according to levels of global radiation and wind speed and regression analysis made for each combination. The results are shown in Table 2 and in Fig. 4.

The effect of splitting according to levels of wind speed shows no clear tendency on the R^2 but high levels of global radiation results in higher values of R^2.

In Fig. 5 theoretical regions for base lines calcutated for $R_n = 600$ Wm^{-2}, $r_a = 15$ sm^{-1} and $r_{cp} = 40$ sm^{-1} are shown. The regions are based on actual temperatures between 10 and 30 °C and vapour pressure deficit between 0 and 3 kPa which are the limits encountered under Danish climatic conditions.

For these constant values of R_n, r_a and r_{cp} the upper region reduces to a line and the best fit throuht the lower region may be estimated with an accuracy of about 0.5 °C.

For a situation where R_n is between 500 and 700 Wm^{-2}, r_a is between 5 and 25 sm^{-1} and r_{cp} is between 20 and 60 sm^{-1} the corresponding theoretical regions are shown in Fig. 6. In this case the upper base line may be estimated with an accuracy of ±6°C and the lower base line with an accuracy of ±3°C.

Table 2: Linear regression parameters for rape at various levels of global radiation S_i and wind speed μ. N is number of observations, a and b is intercept and slope, s_a and s_b is standard deviation of intercept and slope, while R^2 is regression coefficient.

S_i (Wm^{-2})	μ (ms^{-1})	a	s_a	b	s_b	R^2	N
600- 800	all obs.	3.4	1.0	-2.2	0.7	0.38	17
800-1000	all obs.	2.7	0.7	-1.3	0.5	0.54	9
all obs.	2-4	4.6	0.9	-2.6	0.6	0.50	21
all obs.	4-6	5.8	2.3	-4.2	1.7	0.61	6

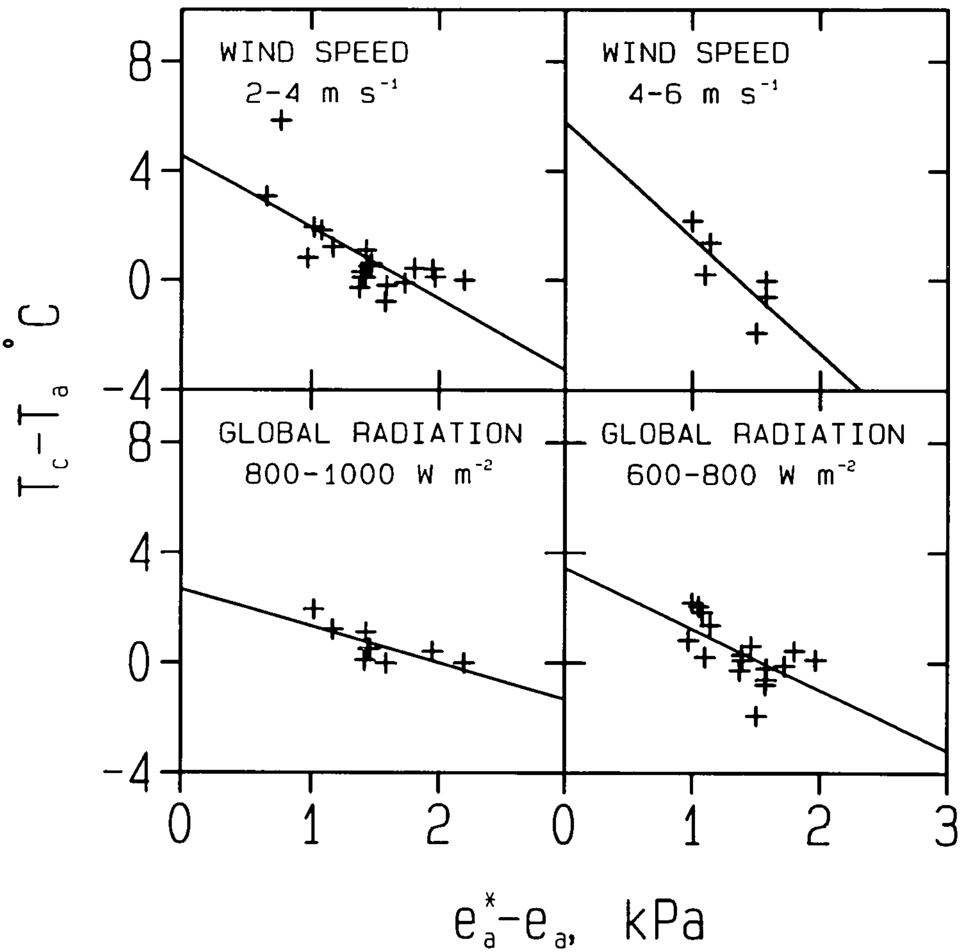

Figure 4: Canopy-air temperatures for fully irrigated rape crop measured at various levels of global radiation and wind speed plotted against vapour pressure deficit.

5

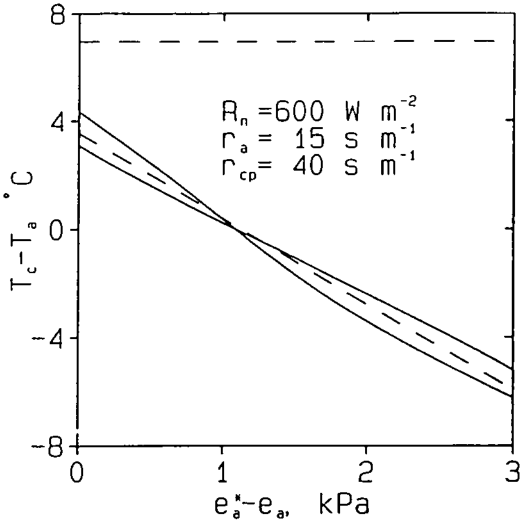

Figure 5: Upper and lower regions of predicted values off crop-canopy-air temperature difference $(T_c - T_a)$ in relation to vapour pressure deficit $(e_a^* - e_a)$ for T_a: 10-30 °C and e_a: 0-3 kPa and for single values of R_n, r_a and r_{cp}. Broken lines are upper and lower base lines.

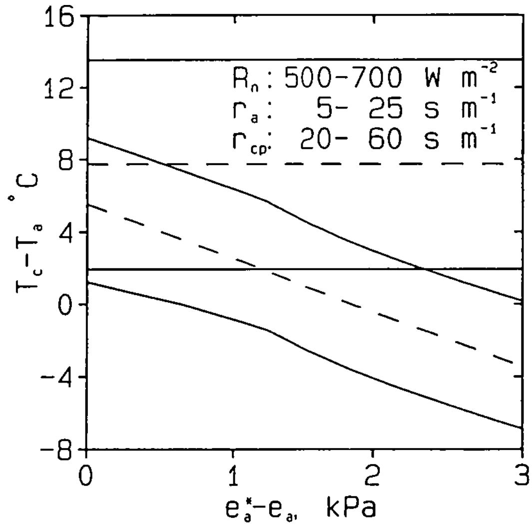

Figure 6: Upper and lower regions of predicted values off crop-canopy-air temperature difference $(T_c - T_a)$ in relation to vapour pressure deficit $(e_a^* - e_a)$ for T_a: 10-30 °C and e_a: 0-3 kPa and intervals of R_n, r_a and r_{cp}. Broken lines are upper and lower base lines.

Conclusion

The fluctuations in global radiation and wind speed during a growing season under humid climatic conditions make it difficult to determine base lines with a reasonable accuracy. In addition maximum of encountered vapour pressure deficit are of the order of 3 kPa which is much smaller than values of 7 kPa reported for arid conditions (Idso, 1982). Thus under the present humid climatic conditions relative small temperature differences need to be measured within a narrow range of vapour pressure deficits and under conditions of fluctuating global radiation and wind speed.

Acknowledgements

This research has been financed in part by the Danish Agricultural and Veterinary Research Council.

References

Blad B.L. and Rosenberg N.J. (1976). Measurements of crop temperature by leaf thermocouple, infrared thermometry and remotely sensed thermal imagery. Agron. J. 68: 635-641.

Ehrler W.L. (1973). Cotton leaf temperatures as related to soil water depletion and meteorological factors. Agron. J. 65: 404-409.

Fuchs M., Tanner C.B. (1966). Infrared thermometry of vegetation. Agron. J. 58: 597-601.

Idso S.B., Jackson R.D., Ehrler W.L. and Mitchell S.T. (1969). A method for determination of infrared emittance of leaves. Ecology 50: 899-902.

Idso S.B., Reginato R.J., Reicosky D.C. and Hatfield J.L. (1981). Determining soil-induced plant water potential depressions in alfalfa by means of infrared thermometry. Agron. J. 73: 826-830.

Idso S.B. (1982). Non-water-stressed baselines. A key to measuring and interpreting plant water stress. Agricultural Meteorology 27: 59-70.

Jackson R.D., Idso S.B., Reginato R.J. and Pinter P.J. Jr. (1981). Canopy temperature as a crop water stress indicator. Water Resources Research 17: 1133-1138.

Jensen H.E., Svendsen H., Jensen S.E. and Mogensen V.O. (1990). Canopy- air temperature of crops grown under different irrigation regimes in a temperate humid climate. Irrigation Science 11: 181-188.

O'toole J.C. and Real J.G. (1986). Estimation of aerodynamic and crop resistances from canopy temperature. Agron. J. 78: 305-310.

Svendsen H., Jensen H.E., Jensen S.E. and Mogensen V.O. (1990). The effect of clear sky radiation on crop surface temperature determined by thermal thermometry. Agricultural and Forest Meteorology 50: 239-243.

Svendsen H., Jensen H.E., Jensen S.E. and Mogensen V.O. (1991). Theoretical analysis of the relationship between crop canopy-air temperature and vapor pressure deficit under temperate humid conditions. Acta Agrc. Scand. 41: 109-117.

Mapping of areal evapotranspiration from high and low resolution satellite imagery

Henrik Søgaard
Institute of Geography, University of Copenhagen
Øster Voldgade 10, DK-1350 Copenhagen, Denmark

Abstract

Based on ground reference data collected over a barley field located near Viborg in Jutland, the so-called simplified relationship between net radiation temperature and evapotranspiration is examined. It is found that the difference between evapotranspiration and net radiation depends on the temperature difference between surface and air and the surface roughness. The derived relationship is applied for monitoring evapotranspiration from surface temperature measured from NOAA-satellite. Finally, the paper examines the resolution problem due to the field size being less than the 1 square km covered by a single NOAA picture element. For a selected day in July this is done by comparing the NOAA data with Landsat TM-data with 120 m resolution in the thermal band.

Introduction

During the recent years increasing emphasis has been put on the development of a methodology which allows satellite-based monitoring of evapotranspiration. In a European agricultural context the application of satellite mapping is already documented in several European cooperation-projects. Also in a wider scientific context e.g. environment management and climatic change studies accurate estimation of areal evapotranspiration is important.

The present applications are generally based on the early models of Jackson (1977) and Seguin et al., (1983). Several studies have confirmed that the difference between evapotranspiration and net radiation can be expressed as a function of the difference between surface and air temperatures in the early afternoon (Riou et al., 1988; Søgaard, 1989; Lagouarde et al., 1991). The relationships of the formula given below have proven to be useful although the coefficients have differed slightly between studies:

$$ET - Rn = b \cdot (T_{s14} - T_{a14}) + a \qquad (1)$$

where ET is the daily evapotranspiration (mm d^{-1})
Rn is the daily net radiation (mm d^{-1})
T_{s14} is the surface temperature at 14 h
T_{a14} is the air temperature at 14 h
b is the slope coefficient (mm d^{-1} °C^{-1})
a is the intercept.

Application of the methodology under Danish conditions was to be examined using the data of Svendsen et al., 1989, by looking at the relationship between surface and air

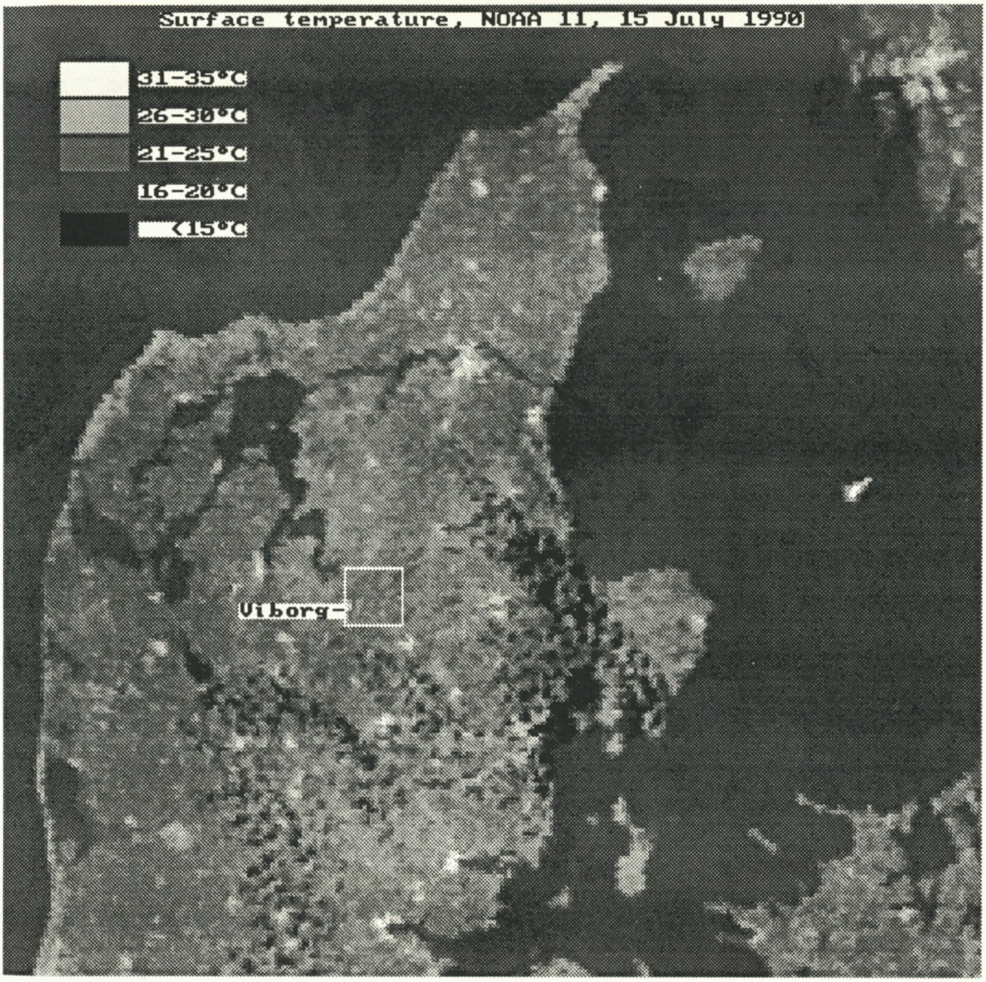

Figure 1: Section of NOAA image showing the 15 by 15 km study area.

temperatures and changes in soil water content. Due to lack of daily values on ET, algorithm (1) could not be examined directly. To overcome this limitation a field experiment was designed by a research group from University of Copenhagen (Højgård et al., 1990) and conducted in cooperation with Dept. of Agrometeorology, in a barley field (cf. Fig. 1 and 7). The measuring equipment was installed in mid-April and the recordings continued until the barley was ready to be harvested by the beginning of August.

Experimental procedure for collecting ground reference data

The methodology for deriving daily values of evapotranspiration (ET) is based on the surface energy budget:

$$Rn = Q_h + ET + Q_g \tag{2}$$

where Rn is the net radiation,
Q_h is the sensible heat transfer (to or from the atmosphere),
ET is the latent heat of evaporation/condensation, and
Q_g is the soil heat flux.

For daily values units are mm evaporated water equivalent, while hourly values are expressed in Wm^{-2}.

The net radiation term, Rn, was measured using a pyranometer (REBS Q*5). Corrections recently reported by Fritschen, 1990, were taken into account. The soil heat flux was measured using 2 heat flux plates (Technical Dienst WS31) placed at a depth of 5 cm.

The estimation of Q_h was based on measurements of wind speed and temperature gradients using the flux profile relationship. One 4 m mast with temperature measurements at two levels and wind speed measurements at three levels was deployed during the whole period. From the middle of June this was supplemented by an additional 9 m mast with three levels. For measuring temperature gradients artificially ventilated thermocouples were used.

All sensors were scanned every 5th second, and integrated by the logger into 15 minute mean values. For the final flux calculations, the data were averaged over 1 hour-intervals.

Calculation of the sensible heat flux from vertical gradients in wind speed and air temperature was based on the Monin-Obukhov similarity and mixing length theory. The total set of algorithms for the calculation of Q_h has been reported in recent studies (e.g. Søgaard, 1988; Vogt et al., 1990).

Supplementary measurements were made of air temperature, rainfall and radiating temperature of the surface, the latter being measured by use of a Heilman K17, infrared thermometer.

Calibration of fluxes using eddy correlation technique

As the flux profile calculation is found to be sensitive to change in surface roughness (roughness length and displacement height), it was found necessary to calibrate the algorithms to the actual conditions. For calibration of the sensible and latent heat fluxes an eddy correlation device was deployed on selected days.

The eddy correlation system consisted of two sensor units, namely a one-dimensional sonic anemometer, CA27, equipped with a fine-wire thermocouple, and a krypton hygrometer, KH20 (Campbell Scientific Inc.).

Both units produce analog signals which are collected and processed on-line by a 21X datalogger (Campbell Scientific) using covariance software and a sampling rate of 10 Hz.

Analysis of NOAA-AVHRR and Landsat TM-satellite data

A total of 20 NOAA-11 scenes were selected to cover the growing season from April to August, 1990. The satellite images have been processed using the CHIPS software (Rasmussen, 1988). The processing consists of the following steps:

1. geometrical registration to a UTM-grid (zone 32) with a spatial resolution of 1 by 1 km.
2. radiometric calibration of raw digital count to albedo or surface temperature neglecting the least significant bit of the NOAA 10-bit-words. The temperature have thus been calculated with a resolution of 0.2 °C.

The NOAA data have been corrected for atmospheric attenuation using the atmospheric transfer model developed by Prince (1983). To study the spatial small-scale variability within each of the 1 by 1 km NOAA picture elements, a Landsat TM scene from July 15, 1990, was purchased as well.

The Landsat image was geometrically corrected to the same UTM coordinate system as applied for the NOAA-data. In the final product the spatial resolution was 30 m. The thermal band 6 with 120 m resolution was also resampled to this grid size.

The Landsat TM-data was radiometric calibrated applying the method given by Wykelic et al., (1989). For the atmospheric correction was used the same method as described for NOAA-AVHRR only the coefficients were adjusted to the Landsat TM5 radiometer.

Results

Calibration of the $ET - Rn$ model

For calibration of the $ET - Rn$ algorithm (1), the measurements of hourly fluxes were supplemented by measurements of barley surface temperature and air temperature during the campaign. The hourly values cover the whole period from April 11 (Julian day 101) to August 2 (Julian day 214). In practice, however, the data set was reduced, mostly due to instrumental problems with the infrared thermometer. However, the final data set consists of more than 90 daily records with measurements of all parameters.

In the calibration of the simplified relationship (1), it is evident that the slope coefficient cannot be assumed constant for the whole period. Several recent studies (Lagouarde, 1991; Lagouarde et al., 1991) have shown that the numerical value of b will increase with increasing surface roughness.

For the barley field studied, it is evident that the aerodynamic roughness increases with height and canopy density of the crop. The technique applied for estimating the roughness length (z_0) from profiles with 3-6 levels of wind speed has been discussed by Jacobs et al., (1988).

The variation in z_0 is visualized in fig. 2 using weekly values of the roughness length, assuming the displacement height to be zero. The roughness length increases from 0.01 m to roughly 0.13 m which is found to accord quite well with the following rule of thumb (Brutsaert, 1984) namely, $h/z_0 = 7$, where h is the vegetation heights.

Due to these changes the calibration procedure has been concentrated to periods with only slowly changing surface roughness, i.e. the first part of May (May 1 to 25) and July (July 9 to August 1).

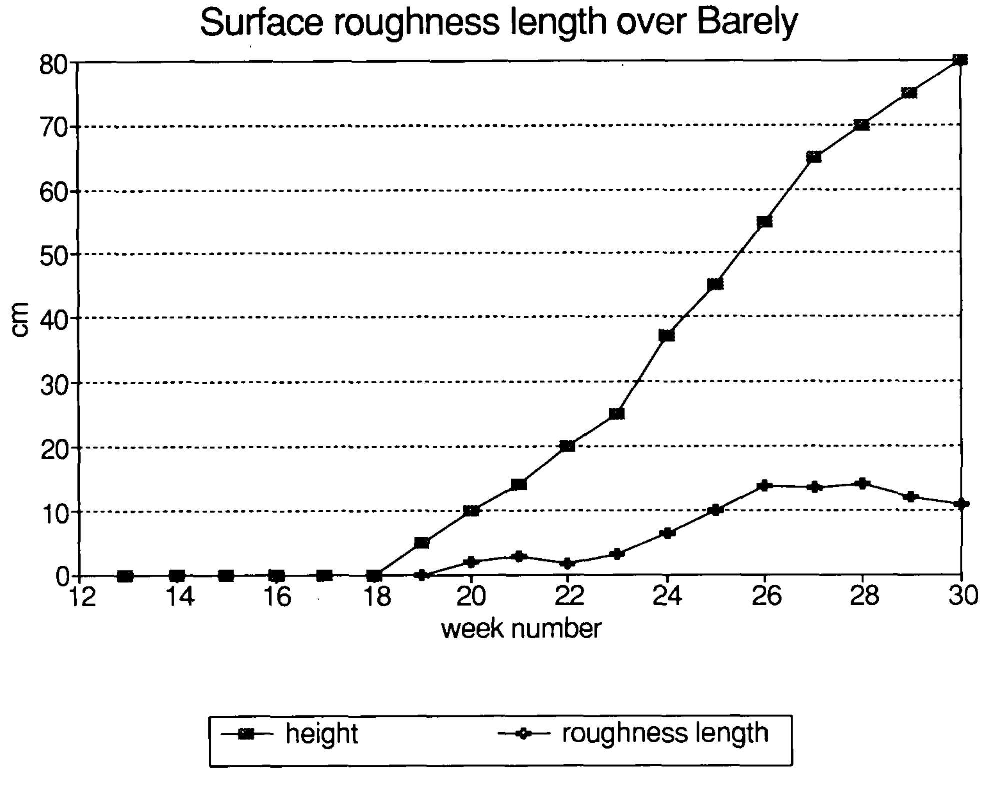

Figure 2: Variation in surface roughness estimated from wind speed measurements at three levels.

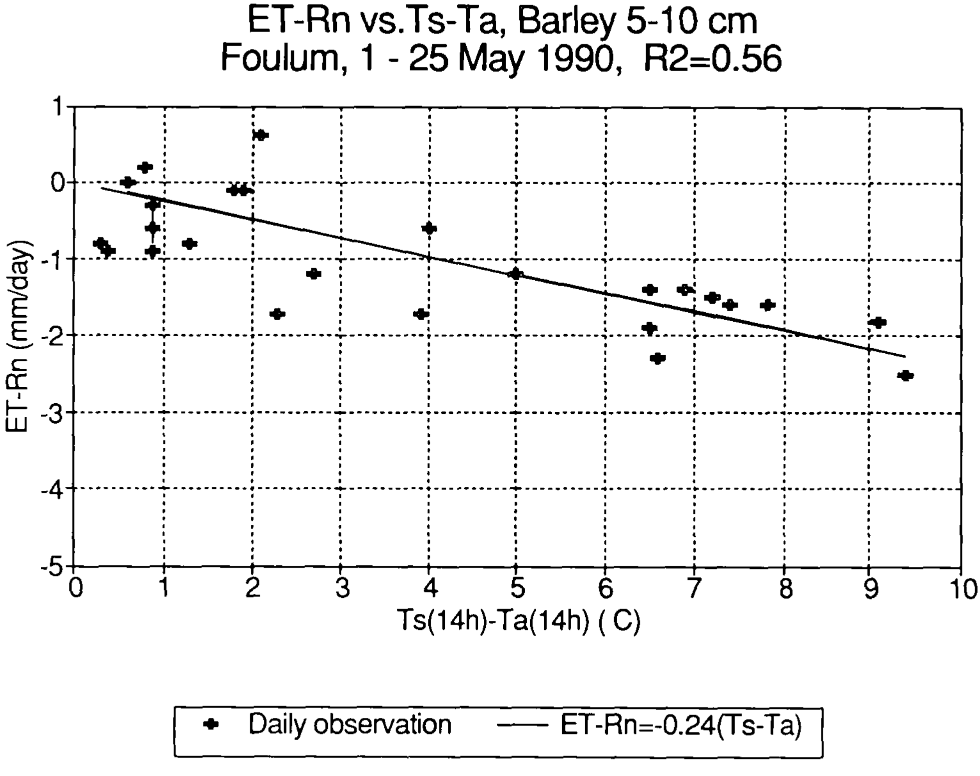

Figure 3: The relationship between $ET - Rn$ and the difference in temperature between surface and air at 14 h during May 1-25.

In fig. 3 is shown a plot for the May period of $ET - Rn$ versus the difference between surface and air temperatures at 14 h, corresponding roughly with time of maximum temperature difference and overpass of the NOAA-satellite. Despite the scatter, the data set confirms the strong linking between $ET - Rn$ and the temperature difference between surface and air. On some days, especially those with daytime rainfall, the 14 h observation is not representative of the diurnal temperature variation, and this is causing some of the scatter in the diagram.

In the analysis of exchange coefficients, it was further assumed that equation (1) could be simplified by setting the intercept to zero, as given below:

$$ET - Rn = c \cdot (T_{s14} - T_{a14}) \qquad (3)$$

where, c is the surface specific exchange coefficient (mm $d^{-1o}C^{-1}$)

Physically, this seems reasonable as the soil heat flux on a daily basis can be neglected, so that the sensible heat flux is equal to $Rn - ET$. On days with no midday excess surface-heating as compared to the air, i.e. $T_{s14} - T_{a14} = 0$, it is a reasonable assumption that $Q_h = 0$.

For the May period the following relation was found:

$$ET - Rn = -0.24 \cdot (T_{s14} - T_{a14}) \qquad (4)$$

Dependency between surface roughness and exchange coefficient

In fig. 4 is shown the result of running the calibration procedure on the data from the last part of the experiment (July). The formula for the 22 days at the end of july is:

$$ET - Rn = -0.62 \cdot (T_{s14} - T_{a14}) \qquad (5)$$

Here the model "explains" even a greater part of the variation, namely 62 %; still, however, there is some scatter in the results. In this data set, one observation day (208) was excluded due to error in the sensible flux estimation. The big difference between fig. 4 and fig. 3 is to be found in the slope or exchange coefficient. If we assume that the increase in slope is due to increasing surface roughness, the values can be compared to the model used by Lagouarde (1991) and it is found that the two points fit in nearly exactly. It should be mentioned that the Lagouarde model is based on both slope and intercept. Here it was found, however, that the model can be more easily explained physically when neglecting the intercept.

Evapotranspiration based on satellite- and ground data

In accordance with (3) the first step in the satellite data analysis is to calculate the net radiation at the earth surface. In the second step, atmospheric-corrected surface temperatures are calculated from the satellite data, while the third step is to combine these data with traditional air temperature measurements using an appropriate exchange coefficient.

This approach was demonstrated by Søgaard (1990), showing each single step in obtaining the surface evapotranspiration. In the present study - which aims at comparing ET-estimates in different scales - some simplification has to be introduced. Only one day is considered, namely July 15, 1990, for which both NOAA, Landsat and ground-reference data are available. Only the region around Viborg and Research Centre Foulum is considered (Fig. 1) and, finally, the ground-based

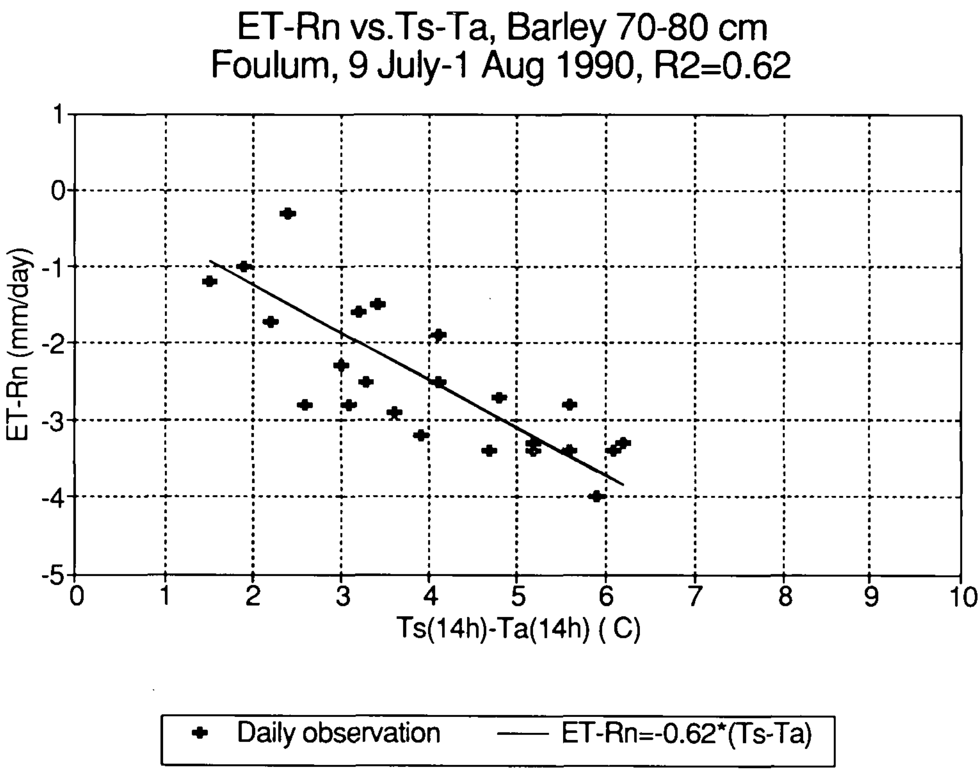

Figure 4: The relationship between $ET - Rn$ and the difference in temperature between surface and air at 14 h July 9 to August 1.

measurements of net radiation and air temperature at Foulum will be applied for all three data sources.

The ground-based estimation of evapotranspiration is found in Fig. 5, showing an energy balance diagram for the actual day together with surface and air temperatures. The evapotranspiration and the sensible heat flux consume a nearly equal amount of energy only at the end of the afternoon. The dense barley canopy restricts the soil flux to roughly 10 % of the net radiation. The total amount of energy during the 24 hours is $Rn = 6.3$ mm, $Q_h = 3.0$ mm, $ET = 3.1$ mm, and $Q_g = 0.2$ mm.

Evapotranspiration based on NOAA-AVHRR and Landsat TM data

In the NOAA-AVHRR case the calculation of ET is relatively straightforward using (4):

$$ET_{NOAA} - 6.3 = -0.62(T_{NOAA} - 20.4) \quad (6)$$

T_{NOAA} is the temperature calculated from NOAA channel 4 corrected for atmospheric attenuation (+3.37 °C) as shown in Fig. 1. The exchange coefficient, 0.62, is used for the whole image as barley is considered the dominating crop in this region. The geographical distribution shown in Fig. 6 will be discussed below.

The Landsat TM-data differs from the NOAA-data in two ways, 1) the spatial resolution and, 2) the time of the satellite overpass is different from the time of thermal maximum signal. While the difference in spatial resolution is obvious when comparing the images, the second point is more problematic, as the basic algorithms for deriving evapotranspiration are based on midday temperatures, while the Landsat overpasses nearly 3 hours earlier. Examples on the use of Landsat for evapotranspiration mapping is found in Stewart et al., (1989).

The diurnal temperature variation on 15 July was examined in order to evaluate if (5) could be applied in the present case. Looking at Fig. 5, it is found that, naturally, the temperature difference between surface and air changes during the day, but in the period between 10 and 14 it is nearly constant on the actual day. Similar studies made in tropical areas with only around 12 hours of daylight show that, at the time of Landsat overpass, the temperature difference is only two thirds of the value found at 14 hour.

In this case it is assumed that (5) can be applied directly using of course the 1030 h value for the air temperature:

$$ET_{Landsat} - 6.3 = -0.62(T_{Landsat} - 18.0) \quad (7)$$

$T_{Landsat}$ is the temperature calculated from Landsat TM band 6 corrected for atmospheric attenuation (+3.71 °C). The difference in correction compared to NOAA is due to different radiometric sensitivity. The resulting ET distribution is shown in Fig. 7. Despite the disturbing scanner errors, the distribution shows a distinct distribution, namely low values in urban areas (Viborg); in fact, most of the villages in the area are low-evaporating areas. As an example east of Viborg, high ET-values are found for the major lakes, while the agricultural areas come up with values around 3 mm. Returning to Fig. 6, the same pattern can be distinguished despite the low spatial resolution.

Discussion

The results from the present study confirm that $ET - Rn$ with reasonable accuracy can be expressed as a function of the temperature difference between surface and air at the

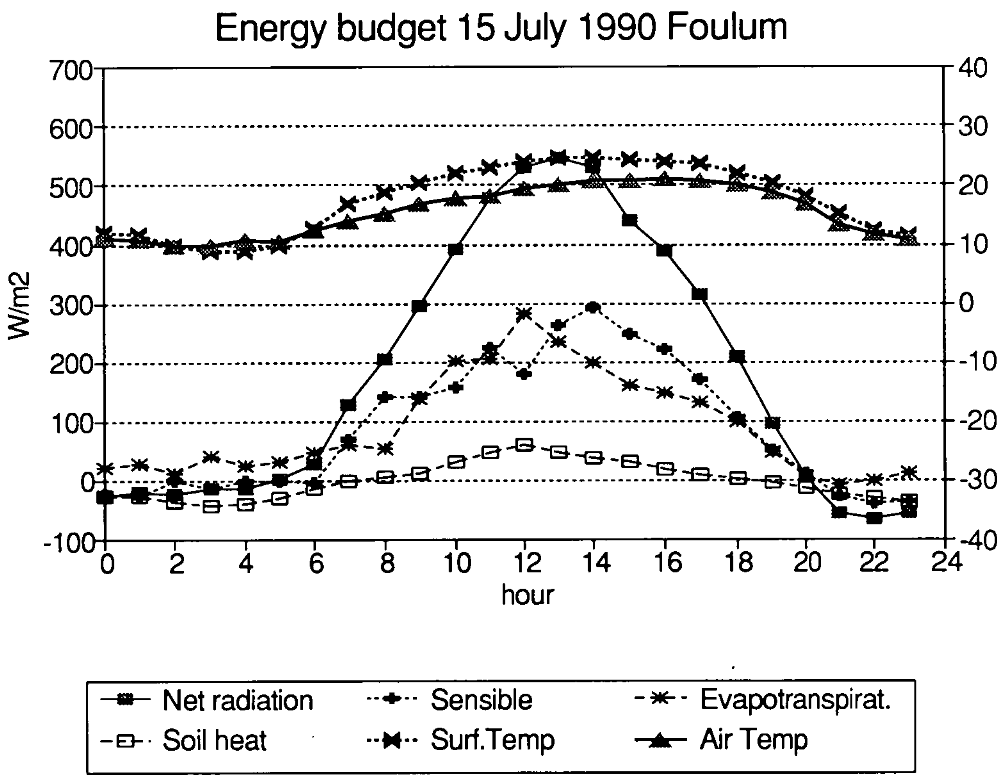

Figure 5: Diurnal variation in energy balance components and temperature on July 15.

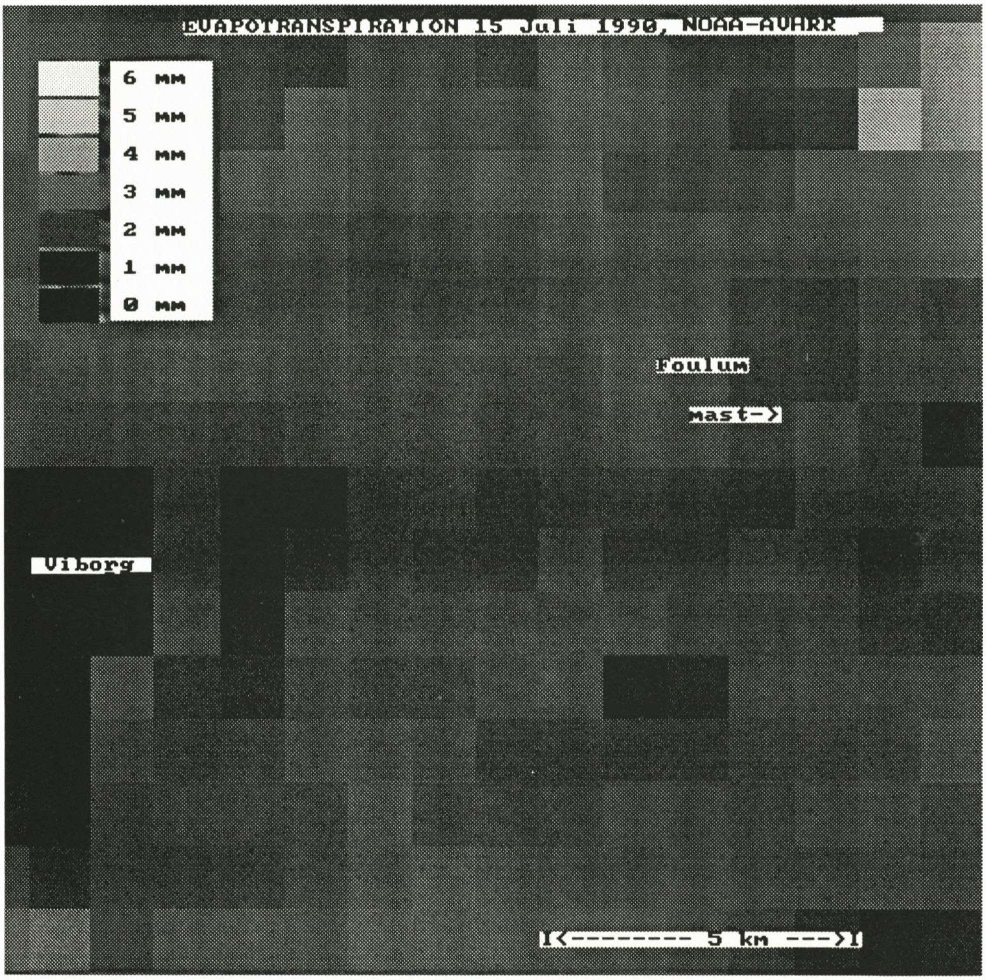

Figure 6: Spatial distribution of ET on July 15 based on NOAA.

Figure 7: Spatial distribution of ET on July 15 based on Landsat TM.

time of the NOAA-satellite overpass in the early afternoon. Without loss of accuracy, the traditional $ET - Rn$ model has been simplified with a physical interpretation of the exchange coefficient. It is found that the numerical value of this coefficient depends on surface roughness, the rougher the surface, the higher the exchange coefficient. The results are thus in contrast to the conclusion drawn by Svendsen et al., (1989) that this methodology is of restricted use under Danish conditions.

For the selected case study it is found that both Landsat and NOAA-AVHRR give results similar to the ground ET-estimations and with a regional distribution which is in accordance with what would be expected. It is obvious that problems still occur and some of these are related to the 1) inaccuracy in the ET-estimation, and 2) the problem of parametrization of the surface roughness. With respect to instrumentation, these ground observations could be improved by adopting the eddy correlation technique in the operational measuring program. The problem about surface roughness might be tackled using the visible and near-infrared Landsat bands for high resolution vegetation mapping.

Acknowledgements

The present study has been funded by SNF grant no. 11-7781. The author would also like to thank Ian Sonne, Charlotte B. Jensen, Tom Jensen and Elin Højgaard for valuable assistance during the field work and for a number of fruitful discussions during the data analysis.

References

Brutsaert, W. (1982). Evaporation into the atmosphere, theory, history, and applications. Dordrecht, The Netherlands, 299 pp.

Fritschen, C. (1990). A comparison of 3 different types of net radiometers. Internal report.

Jackson, R.D., Reginato, R.J. and Idso, S.B. (1977). Wheat canopy temperature: A practical tool for evaluating water requirements. Water Resources Research, 13(3): 651-656.

Højgård, E., Jensen, C.B., Jensen, T. and Sonne, I. (1990). Estimation of evapotranspiration by 4 different methodes. (in Danish) University of Copenhagen, Internal report.

Jacobs, A.F.G. and van Boxel, J.H. (1988). Changes of the displacement height and roughness length of maize during the growing season. Agric. Forest Meteorol. 42: 53-62.

Lagouarde, J.P. (1991). Use of NOAA AVHRR data combined with an agrometeorological model for evaporation mapping. Int. J. Remote Sensing 12(9): 1853-1864.

Lagouarde, J.P. and Mcaneney, K.J. (1991). Daily sensible heat flux estimation from a single measurement of surface temperature and maximum temperature. Boundary Layer Meteorology (in print).

Price, J. (1983). Estimating surface temperature from satellite thermal infrared data. A simple formulation for the atmospheric effect. Rem. Sens. Env. 13: 353-361.

Rasmussen, K. (1988). The chips-image processeing system manual. Copenhagen 70 pp.

Riou, C., Itier, B. and Seguin, B. (1988). The influence of surface roughness on the simplified relationship between daily evaporation and surface temperature. Int. J. Remote Sensing 9(9): 1529-1533.

Seguin, B. and Itier, B. (1983). Using midday surface temperature to estimate daily evaporation from satellite thermal IR data. Int. J. Remote Sensing 4(2): 371-383.

Stewart, J. and Holwil, (1989). Assessment of areal evaporation from Sahelian vegetation using satellite and ground-based SEBEX-data. Inst. of Hydrology, UK.

Svendsen, H., Jensen, S.E., Jensen, H.E. and Mogensen, V.O. (1989). Telemåling i jordbruget (in Danish). Forskningsrapport nr. 1215, The Royal Veterinarian and Agricultural University, Denmark, 228 pp.

Søgaard, H. (1988). Estimation of the surface energy balance in the Sahelian zone of Western Africa. Geogr. Tidsskr. 88: 108-115.

Søgaard, H. (1989). A comparison between satellite derived evapotranspiration and normalized difference vegetation Index in the Sahelian Zone. Proc. of 22nd Int. symp. on Remote Sens. of Env. Abidjan pp. 349-367.

Søgaard, H. (1990). Estimation of evapotranspiration in the Sahelian zone of western Africa based on Meteosat data. 8th Meteosat Scientific Users meeting, EUM P08 pp. 293-298.

Vogt, R. and Jaeger, L. (1990). Evaporation from a pine forest using the aerodynamic method and Bowen Ratio methods. Agric. Forest Meteorol. 50: 39-54.

Wukelic, G.E, Gibbons, E.E., Martucci, L.M. and Foote, H.P. (1989). Radiometric calibration of Landsat thematic mapper thermal band. Rem. Sens. Env. 28: 327-339.

Spectral signatures of danish crops multitemporal signatures derived from hight resolution satellites

Jan Nyholm Poulsen og Thomas Borup Svendsen
Research Centre for Agriculture, Department of Land Data
Enghavevej 2, DK-7100 Vejle
Denmark

Summary

As a part of the European MARS project (Monitoring Agriculture using Remote Sensing), The Department of Land Data made a study concerning multitemporal classification of the most common danish crops. The aim was to distinguish the crops from each other, distinguish the crops from nature areas and to map permanent grasslands.

In the image analysis and in the classifications, the following images were used.

- Landsat TM from 89.06.26, 89.09.21 and 90.05.03
- SPOT MS from 89.05.17, 89.07.04, 89.07.25 and 90.04.08
- SPOT PAN from 89.05.18.

The images were all resampled to UTM with a pixel size of 10 m. Three series of artificial images were created to facilitate the image treatments. Subareas of the original images were mosaicked together to form 512 × 512 and 1024 × 1024 pixel areas containing the training and test areas. This was done for all 31 bands used.

The images were classified (using the CHIPS image processing system) into 11-21 classes using a number of different image analysis methodologies. Vegetation indices and principal components were used and the classification algorithms were minimum distance and maximum likelihood — both applied on a pixel-per-pixel basis. Comparisons were made with respect to image type (TM and SPOT), time of year, classification methodology, use of principal components, and subdivision and merging of classes. Finally the use of additional GIS-data in order to improve classification of permanent grass was demonstrated.

The classification accuracy varied from an overall accuracy of 24.2 % (ML-classification of a SPOT image from 25th of July) to 80.6 % (ML-classification of the 11 most important principal component bands derived from all dates in 1989).

The main conlusions were:

- The most common danish crops can be distinguished from each other (pixel accuracy at least 80 %).
- Nature areas can be distinguished from agricultural crops with high accuracy (pixel accuracy 96.7 %), but not be divided into moor and heath.
- Agricultural grasses as a group can be classified with high accuracy (pixel ac-

curacy 88.7 %), but cannot be divided into permanent and temporary grass.

Finally it was concluded, that the most important aspect of such a classification probably was the collection of sufficient and representative training areas. The variation within a single crop was very large due to differences in management, soils, development phase etc. This variation was obvious between separate fields, while the single fields usually were quite uniform.

Introduction

The ultimate goal of the project described in this report was to analyse the possibilities for using satellite images for:

- making agricultural statistics.
- providing geographically distributed crop data for modelling purposes, and
- mapping permanent grasslands.

To make reliable agricultural statistics it would be necessary to make an accurate classification of the satellite images. A total classification would cause problems especially concerning towns and some forest types vs certain agricultural crops. Using the databases at The Department of Land Data for "masking out" the agricultural areas, the classification could be reduced to discriminating between agricultural crops and a few other land cover types.

The relevant databases (available at The Department of Land Data) would be "forest boundaries", "town limits" and "lakes". The resulting area still contains other land cover types than agricultural, of which the most important are nature areas (heathland, bogs, etc.).

Another important aspect was the permanent grasslands. These areas were of interest for a number of reasons. First of all, these areas are low producing and under minimal agricultural management. Nitrate leaching and erosion is usually negligible and the areas are of interest for a number of other environmental reasons (botanical, ecological, etc.). The permanent grasslands in Denmark are usually either abandoned agricultural land situated on steep slopes or situated in the lower parts of the valleys (organic soils). At The Department of Land Data, three databases could possibly contribute to a mapping/classification of the permanent grasslands. The relevant databases are "low lying areas", "organic soils" and "steep slopes".

Therefore the operational aim of this project was to analyse the possibilities for using multitemporal classification and relevant databases at The Department of Land Data to:

- Distinguish the most common danish crops from each other.
- Distinguish nature areas from crops.
- Distinguish permanent grasslands from other agricultural and natural areas.

Methodology

The following procedures were used:

1. Resampling of images.
2. Selection of classes.
3. Selection of training and test areas.
4. Digitizing and visual editing of training and test areas.
5. Analysis of training and test data.

6. Classification of images.
7. Incorporation of GIS data.
8. Evaluation of results.

Preparation of image and ground truth data

Resampling of satellite images

The selected satellite images from 1989 and 1990 are listed in Table 1 (the bands are numbered according to wavelength in ascending order).

Table 1: Satellite data used in study.

Satellite name	Date of recording	Bands used
SPOT multispectral	89.05.17	1-3
SPOT panchromatic	89.05.18	1
Landsat TM	89.06.26	1-5+7
SPOT multispectral	89.07.04	1-3
SPOT multispectral	89.07.25	1-3
Landsat TM	89.09.21	1-5+7
SPOT multispectral	90.04.08	1-3
Landsat TM	90.05.03	1-5+7

The 22 bands in the 6 images from 1989 and the 9 bands in the 2 images from 1990 were geometrically corrected using cubic convolution resampling. The images were resampled to the UTM coordinate system with rms (root mean sqare) deviations of 0.59-0.75 pixels. All the corrected bands had a resolution of 10 m.

Selection of classes

The work was concentrated on the economically most important crops, and the crops which covered the major part of the agricultural area.

In accordance with this, the classes shown in Table 2 were selected.

The last two classes were nonagricultural nature areas. Class 12 was the wet areas and includes both bog and wet moor. Class 13 was the dry areas and included both heath and dry moor. The two classes were included because they were not separated from agricultural area in the databases at the Department and were expected to be confused with agricultural grass areas in the classification.

The difference between temporary grass and permanent grass is, that temporary grass is under management and has been plowed *within the most recent 5 years.*

After the first classifications it was realized, that a further subdivision of some of the classes, based on the reflection values (pixel values), was needed to improve the classifications. By means of the statistical methods discussed later, 7 of the original classes were expanded into 15 new classes, ending up with a total of 21 classes.

The original classes were still the desired mapping units, so after the classifications using 21 classes but before calculating the classification accuracy, the 21 classes were grouped together into the original 13, and these sometimes even further into 12 or 11 classes.

Specifically class 12 moor and 13 heath were united after some late classifications, in to a new class, which was called class 12x nature area.

Likewise class 9 temporary grass and class 10 permanent grass were joined after the last classification, in to a new class, which was called class 9x agricultural grass.

Collection of training and test areas

The position of more than hundred fields or areas with a land cover belonging to the 13

Table 2: Selected mapping units.

Class	Class name	Spring crop	Winter crop	Permanent "crop"
1	field peas	x		
2	spring barley	x		
3	sugar beets	x		
4	winter wheat		x	
5	winter barley		x	
6	winter rape		x	
7	spring rape	x		
8	rye		x	
9	temporary grass			x
10	permanent grass			x
11	potatoes	x		
12	moor			x
13	heath			x

classes were established for the 1989 data, and almost 30 for the 1990 data. The areas were situated in the middle of Jutland.

The areas were digitized, and grouped together as coloured areas (one class one colour) in an image called an overlay (which could be "laid over" the satellite images in the image processing system CHIPS).

During the digitization and the preliminary statistical analysis problem areas were deleted (due to cloud coverage or change in management), resulting in a total of 82 areas for 1989 and 25 for 1990. These areas were used as training areas for the classifications. The location of the training areas can be seen in fig. 1.

By means of CHIPS the training areas were screened further, before they were actually used in the classifications.

The final 82 training areas for 1989 had an average size of 1.93 ha.

Like the training areas, the test areas were also located in the middle of Jutland, digitized, grouped into an overlay, screened and put through further refinement processes before they were actually used in the classifications.

The final 158 test areas used for 1989, had an average size of 1.42 ha.

Construction of artificial images

From every corrected band, areas matching the training and test areas were cut out, and then mosaicked together to one small training band (1024 × 1024 pixels) and one small test band (512 × 512 pixels), each completely matching the training overlay and the test overlay respectively.

The resulting 22 reduced training bands and 22 reduced test bands were used as the training and test areas in the later image processing (for the 1990 areas the number was $22+9 = 31$ for both training and test bands).

Statistical analysis of training and test areas

All 22 (or 31) reduced bands were put through a statistical analysis for the training and the test areas. This statistical analysis included average, maximum values, min-

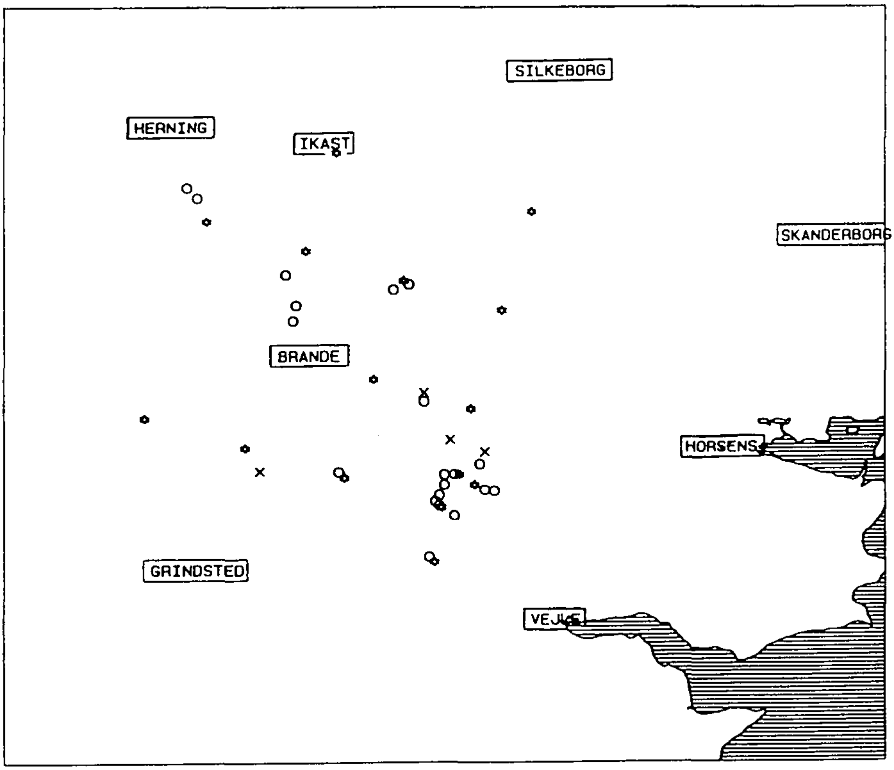

Figure 1: The approximate location of the training and test areas. Circles mean training areas for 1989, crosses mean training areas for 1990 and the stars are test areas. Hatched areas are water.

imum values, confidence intervals, variance, covariance and correlation for each class and for each band. These statistics were the basic statistics used in the later analysis and classification.

Very large variances indicated inhomogenous classes due to either phenological different fields (indicating the need for further subdivision of the classes) or classes, where the fields themselves were inhomogenous (indicating the need for further "cleaning" of the fields in order to avoid wet regions, boundary problems, change in management, etc.).

Histograms

In a similar way histograms of the training and test areas for every class in every band were made. These histograms showed the frequency of pixel values (reflection) in the class and band in question. With this tool, it was possible to identify boundary problems and problems concerning deviant regions (i.e. "wet spots") within the class as a whole.

Furthermore these histograms showed if the distribution of pixel values deviated from the normal distribution (i.e. having two or more peaks or having serious curtosis). This information could be used for further subdivision of the classes.

Single field analysis

As the last refinement process statistical analysis of single fields were used. This analysis returned values like mean pixel value, standard deviation and min./max. pixel values. In this way single fields which deviated from the class mean or having boundary problems and problems concerning deviant regions (wet spots etc.) could be located.

Vegetation indices

From the mean values, normalized difference vegetation indices (NDVI) were calculated for the training areas.

The NDVI was defined as:

$$NDVI = \frac{NIR - R}{NIR + R}$$

where NIR was the reflection in the near infrared band (SPOT channel 3 and Landsat TM channel 4) and R was the reflection in the red band (SPOT channel 2 and Landsat TM channel 3). The NDVI is positively correlated to the above ground biomass.

The NDVI's could naturally be grouped into three groups — spring crops (field peas, spring barley, sugar beets, spring rape and potatoes), winter crops (winter wheat, winter barley, winter rape and rye) and permanent crops (temporary grass, permanent grass, moor and heath). The result is shown in fig. 2, where the NDVI for the different dates is shown for a typical representative of each crop group.

Spring crops usually have a very low NDVI in the spring. Depending on the time of harvest, the NDVI is rising during midsummer and then dropping in the fall.

The winter crops usually have a relatively high NDVI in the spring. As can be seen, winter crops are normally harvested/mature before 25th of July.

The permanent crops have in general a rather constant NDVI throughout the year. In general the grasslands have a higher NDVI than the nature areas.

Formation of "principal component" bands

It became clear, that the more bands used, the better the classification would be.

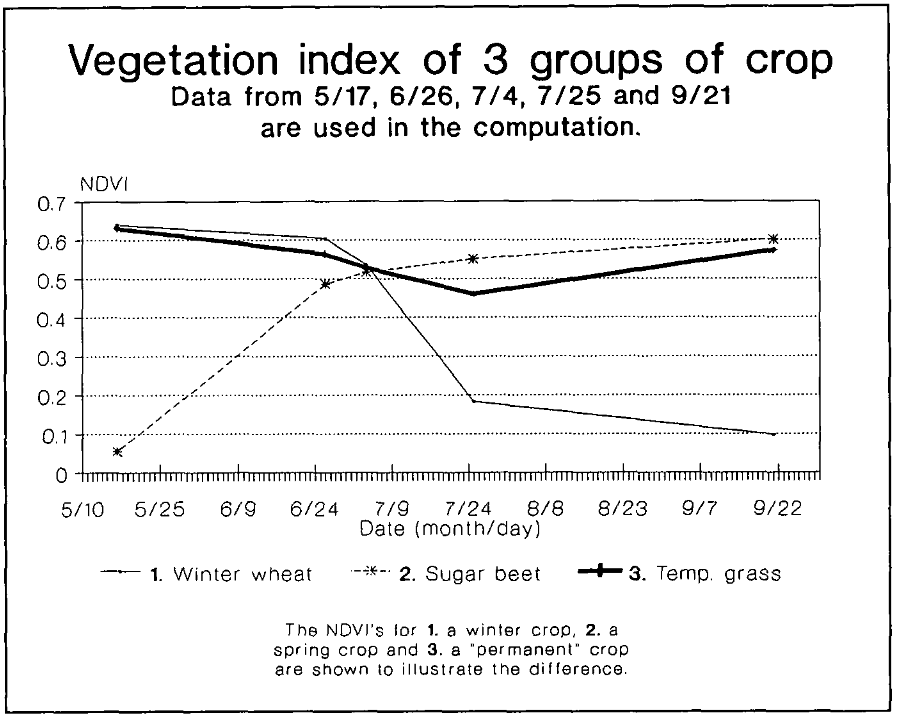

Figure 2: NDVI's for a typical representative of spring crops (sugar beet), winter crops (winter wheat) and permanent crops ("temporary" grass).

Therefore the Karhunen-Loeve transformation was used to transform the 22 original training and 22 original test bands, fundamentally into 22 new "principal component" training bands and 22 new "principal component" test bands.

This transformation was, both for training and test data, based on statistics from the 22 original training bands, excluding areas with cloud cover.

These new bands, numbered from 1 to 22 according to their information content, retained all the information contained in the original bands, but the information was distributed in a new compressed way among the bands. That meant, that the information content was by far the largest in the first bands, rapidly declining in the following bands until near zero in the last bands. This was a way to reduce the number of bands, and still retain most of the information from all the 22 original bands.

Overview of the classifications

All the following classifications were made using the image processing system CHIPS (the software only allowed maximum likelihood classification with maximum 11 bands).

Altogether 18 classifications with different combinations of bands were made. Two different classification methods were used: "minimum distance" classification (MD) and "maximum likelihood" classification (ML).

In Table 3 an overview of the 18 classifications is shown.

The arrow → indicates that the classified number of classes, on the left side of the arrow, were reduced by merging classes together to the final number on the right side of the arrow.

The column overall accuracy % shows the weighted means of the pixel accuracies of all classes. The pixel accuracy of a class indicates how often a classified pixel (pixel = picture element = area unit) is classified and located correctly. In this way the accuracy shows the overall success of the classification.

Fig. 3 shows some of the results graphically.

Application of post-classification-methods using GIS-data

Following the supervised classification several attempts were made to improve the results further by using a Geographical Information System (GIS).

The main problem to solve was the poor discrimination between temporary grass and permanent grass.

Three parameters were selected, which in advance appeared promising:

1. organic soils (soil type humus, often wet).
2. steep slopes.
3. low lying areas (very often wet).

The idea was to sort out permanent grass, because if the classification showed grass on steep slopes, in low lying areas or in areas with humus soil, then it probably was permanent grass and not temporary grass.

Three new overlays that fitted the test area background were made. One with lines encircling humus soil areas, one with lines encircling areas with inclinations of more than 6 % and one with lines bounding low lying areas.

Classification no. 15 was then selected as the best possible, and on the classified image grass areas lying under one or more of the overlay areas could now be identified.

Table 3: Results from image classification.

Clssif. nos.	Clssif. type	Satell. name	Date of record	Bands used	No. of class.	Overall accu. %	Remarks
1	ML	SPOT	05.17	1-3	13	45.7	
2	ML	Land.	06.26	1-5+7	13	39.2	
3	ML	SPOT	07.04	1-3	13	25.3	
4	ML	SPOT	07.25	1-3	13	24.2	
5	MD	SPOT	05.17	1-3	13	47.8	
			05.18	1			
			07.04	1-3			
			07.25	1-3			
		Land.	06.26	1-5+7			
			09.21	1-5+7			
6	MD	SPOT	05.17	1-3	21→13	50.1	
			05.18	1			
			07.04	1-3			
			07.25	1-3			
		Land.	06.26	1-5+7			
			09.21	1-5+7			
7	ML	SPOT	05.17	2-3	13	54.3	
			07.04	2-3			
			07.25	2-3			
		Land.	06.26	3-5			
8	ML	SPOT	05.17	2-3	13	93.4	obs! trained on test statistics.
			07.04	2-3			
			07.25	2-3			
		Land.	06.26	3-5			
9	MD	both	every	1-9	21→13	52.3	principal component bands used.
10	ML	both	every	1-9	21→13	68.1	principal component bands used.
11	ML	both	(every)	1-9	21→13	64.9	principal component bands used. Landsat bands from 09.21 not used in the formation.
12	ML	both	every	1-9	21→12	74.2	principal component bands used.
13	ML	both	every	3-5+7	21→13	54.8	principal component bands used.
14	ML	both	every	1-10	21→13	68.1	principal component bands used.
15	ML	both	every	1-11	21→13	71.4	principal component bands used.
16	ML	both	every	1-11	21→12	77.4	principal component bands used.
17	ML	both	every	1-11	21→11	80.6	principal component bands used.
18	ML	SPOT	05.17	2-3	2	86.1	The only classification using bands from both 1989 and 1990 (04.08 and 05.03) and only two classes (9 and 10).
			07.04	2-3			
			07.25	3			
		Land.	09.21	3-4			
		SPOT	04.08	2-3			
		Land.	05.03	3-4			

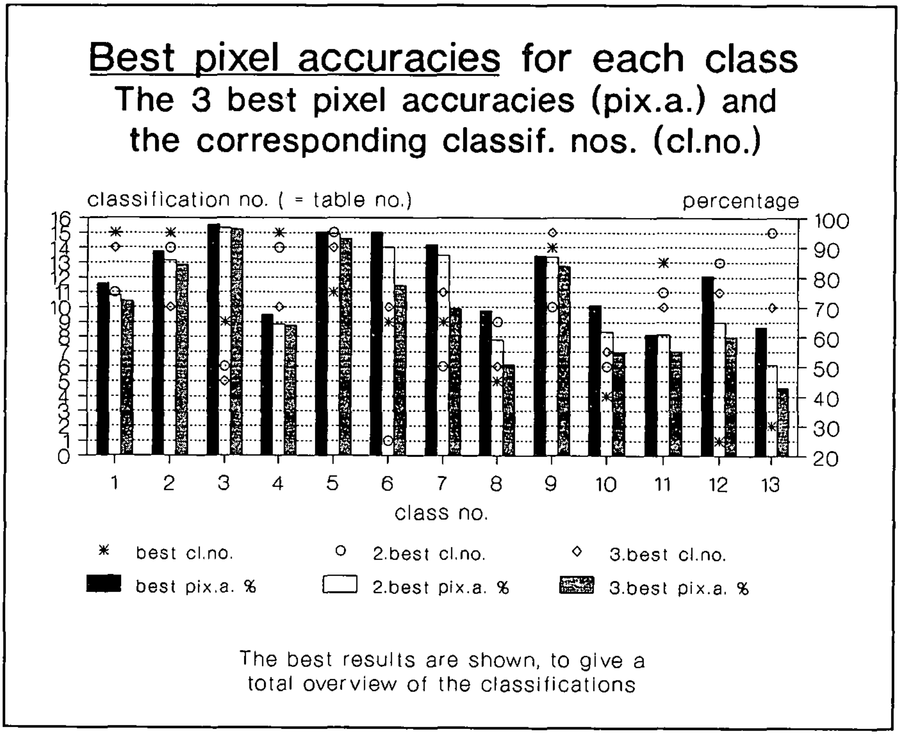

Figure 3: For each class is shown: a) the 3 best pixel accuracies, and b) the numbers of classifications these accuracies derive from.

Humus areas and low lying areas showed to be more or less identical within the regions concerned, with the low lying areas being a little wider and a little more detailed. Therefore low lying areas and sloping areas turned out to be the important factors.

The result of this post-classification-method was:

1. 28 pixels rightly classified as temporary grass were wrongly changed to permanent grass.

2. 78 pixels incorrectly classified as temporary grass were correctly changed to permanent grass.

This gave a total shift of 106 pixels and a net improvement of 50 pixels.

The impact of this improvement on the classification accuracy is listed in Table 4.

Altogether it was an accuracy improvement, though not a major one, so the method worked. If test areas had been selected specifically in both hilly and low lying regions, surely a greater improvement would have been obtained. Anyhow, this way of choosing test areas would have given a non-representative selection of fields, which was undesirable.

Conclusion

Main conclusions

The following main conclusions can be drawn from the analysis of available satellite imagery:

- The most common Danish crops can be distinguished from each other with an overall accuracy of at least 80 %. Some of the crops could in this project be classified with higher accuracy (spring barley, sugar beets and winter barley) and some with less accuracy (rape, wheat and rye). If the aim is area statistics, they can be compiled with a total area accuracy of more than 90 % (total area accuracy is: the total accuracy for estimation of the area for all classes without taking the position into consideration).

- The nature areas can be classified with high accuracy (pix. acc. 96.7 %), and can rather easily be distinguished from the crops and from the agricultural grasses. Due to the rather loose definition of the nature classes and due to the fact that these classes were very inhomogenous (and overlapping), it proved very difficult to distinguish between moor and heath.

- The permanent grasslands proved very difficult to distinguish from especially temporary grass. If permanent grass was grouped together with temporary grass, the classification could be done with high accuracy (pix. acc. 88.7 %). Use of images from both 1989 and 1990 did not improve the classification of permanent grass in this test. Use of GIS-data (organic soils, steep slopes and low lying areas) did only give a marginal improvement concerning classification of permanent grassland. The main problems seems to be the actual definition of temporary grasslands — managed and under plow within the most recent 5 years. This makes it very difficult to distinguish permanent from temporary grass. Finally the classes themselves are very inhomogenous. Temporary grass covers a wide range of species, and is used for a number of different purposes (seed production, grazing, grass for silage and hay). Permanent grass areas are generally grazed, but they vary considerably concerning the composition of plant

Table 4: Accuracy of classification of surface type "grass".

	Temporary grass			Permanent grass			total		
	before		after	before		after	before		after
Pixel accuracy	83.7	→	82.6	9.4	→	20.0			
Overall accuracy							71.4	→	71.6

species.

Lessons learned

During this project a number of lessons were learned. Some of the lessons were anticipated — others were not.

The following lessons/conclusions are primarily meant as recommendations for future work concerning multitemporal classification of crops:

- The number of training fields should be at least the double of what is expected to be necessary to use in the later classifications. There is a number of reasons for this. First of all the variation between the different fields is actually very large, due to different conditions concerning irrigation, fertilizers, development phase, varieties, soil types etc. If this variation has to be covered, a large number of training fields is needed. Furthermore a number of training fields will be discarded due to cloud cover, changes in management, etc. Finally it can be stated, that the need for training fields increases with the number of images (number of dates) available.

- Subdivision of classes is a good way to improve the classification. In general the more classes involved in the classification and the fewer final classes involved in the evaluation (classes grouped together) the better the result.

  The more bands (the more dates) used in the classification — the better the result. Using principal component bands and thus compressing the information from more bands into fewer bands, this can be done without using excessive computer resources.

  Use of maximum likelihood classification improves the result considerably compared to minimum distance classification.

  Landsat TM is significantly better for classification purposes than SPOT. Images from a date in spring (here 17th of May) is better than images from later in the growing season (here 26th of June, 4th of July, and 25th of July).

  Depending on the "nature" of the training and test sets, some classes are either "collecting" pixels from the other classes or "spreading" the pixels to a number of other classes. A typical example of a "collecting" class is spring barley. In almost all classifications, quite a few other pixels have been classified as spring barley. This is probably due to a "too wide" definition through the training areas of the class. Typical examples of "spreading" classes are spring rape and rye. This is due to inhomogenous test areas (large variation between fields) and great difference between training and test areas.

Future improvements

The classification accuracy can be improved by first of all ensuring, that the training areas are representative for their mapping unit.

This would imply a considerably larger number of training areas.

Furthermore, the classification accuracy could be improved by using an additional number of data treatments. The most important improvements would be to apply different filtering techniques, apply context/texture classifications and to use a "two-phase classification".

This two-phase classification strategy could be to use the result of a first classification (phase-1) to subdivide the image into one or more groups, and then use second classifications (phase-2) to classify each group separately. Such a separated group could for instance be spring crops, classified using only the May image. Subsequently all the pixels belonging to the spring crop group could be classified into individual crops using all available images. A similar approach could be applied for the winter and permanent crops.

Finally, the classification result could be improved by using more GIS-data. When the land cover database for Denmark is finished, the classification will only have to deal with the annual crops (and temporary grass). The classes permanent grass, moors and heath will be registered in the database, and the classification will only have to be carried out for the purely agricultural areas.

Soil degradation assessment in semi-arid tropical areas — satellite image methodology

Pia Frederiksen
Institute of Geography, Socioeconomic Analysis and Computer Science
Roskilde University, DK-4000 Roskilde
Denmark

Introduction

Satellite images offer a potentially very useful tool for environmental monitoring due to the regular recording intervals and the large areas covered.

For monitoring rangelands in developing countries this give some major advantages due to the characteristics of these areas, e.g.:

- the frequent lack of data on the natural resources
- the high climatic variability where drought appears a norm rather than a special event. This creates a need for time series in order to detect treds and changes in the environmental conditions
- the large areal coverage of the semi arid and arid lands which would yield tremendously high costs if regular sampling should be carried out in the field or by air photos.

The objective of the present study has thus been to investigate the potentials of digital image processing and interpretation for the assessment and monitoring of soil erosion in these environments. The satellite system used has been the Landsat Multispectral Scanner, which offers historical data for the development of change detection methods at relatively low costs.

Study area

The study area is located in the lowland part of Kitui District, Eastern Kenya, where population growth and changes in land use have lead to accelerating land degradation. It is covering around 3000 square kilometers and is situated in the Eastern part of Kenya in the lowland plains. This region is semi arid and offers a marginal potential for agricultural activity. The semi natural vegetation consists of various shrub species forming dense bush and thicket, and the vegetation is under heavy pressure due to population growth and immigration into the lowlands. Clearing and overgrazing is substantial and the traditional farming systems are under pressure.

Soil degradation in the area is principally related to water erosion. When the semi natural bush is cleared or overgrazing occurs, water erosion becomes very severe due to the climatic conditions. The annual rainfall of around 5-700 mm is divided into two rainy seasons with 70 % of the total rain falling during the first 30 days, when both the natural vegetation cover and crop cover are thinnest (Fisher, 1978). The variability of the rainfall is great, giving rise to harvest failures in one out of every 3-4 seasons, and the intensity of the rainfall is often high.

The area consists of a few major combinations of geomorphology and soils, namely a large floodplain with gray and grayish brown soils and erosional plains and uplands formed on precambric basement rock with predominantly brownish red soils.

Loss of top soil and organic matter, sealing and compaction are as well causes as effects of the soil erosion, which is taking place on all the major soil types of Ferralsols, Luvisols and Cambisols distributed on floodplain and erosional plains and uplands.

Soil erosion and vegetation cover

Soil erosion is in itself not easily detected on the Landsat MSS images, and it is thus nescessary either to estimate the soil loss by using models, or assess the degradation by means of indicators.

The vegetation cover is of paramount importance as a protective agent against soil erosion. This effect is not only related to the interception by leaves and stems, but also to the ground cover of grasses, herbs and litter, which improves infiltration and hydraulic conditions and enhances incorporation of organic matter into the soil due to biological activity. Finally it is related to the physical binding of soil by stems and roots (Spanner 1982, Stocking 1988, Styckzen 1988).

For mathematical models of soil erosion the most well known is the Universal Soil Loss Equation (USLE). This model is an empirically derived equation including multiplication of the parameters affecting the soil loss: soil erodibility, topography, vegetation (crop) cover and soil management. In the present study the topographical effect has been sought eliminated by choosing the lowland part as study area, and the vegetation cover has been chosen as the parameter under investigation — either for use as indicator of soil eroison, or as input layer to a soil erosion model. In fig. 1 the relationship between vegetation cover and soil loss is illustrated.

The objective of the project has thus been operationalized in a few major investigation areas:

- to review and investigate the information in the Landsat MSS spectral data for the purpose of vegetation cover estimation
- to investigate the spectral response of the soil types present and the soil factors that are responsible for the major spectral contributions
- to analyse the spectral changes following soil erosion
- to investigate the possibility of detecting changes in the vegetation cover.

This paper concentrates mainly on the first two aspects.

Background

Estimation of vegetation cover along with other vegetation related factors have a long history of research within the satellite related research environment — especially due to the interest in crop monitoring. The estimators — or vegetation indices — have commonly built on a two dimensional data space represented by the red and NIR spectral range, as green vegetation has its most prominent features here, and as it has been argued, that the Landsat MSS data space is essentially bidimensional. (Band ranges in the Landsat MSS system are shown in table 1).

Fig. 2 shows the distribution of spectal signatures drawn from Kitui area field plots of

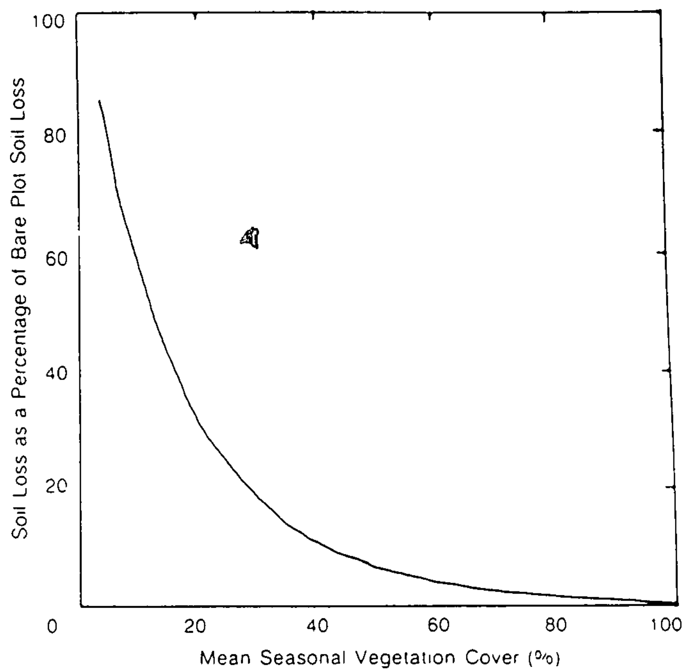

Figure 1: Relative soil loss as a function of vegetation cover (after Stocking, 1988).

Table 1: The characteristics of the Landsat MSS spectral bands.

	Band 4 (B4) green	Band 5 (B5) red	Band 6 (B6) NIR	Band 7 (B7) NIR
spectral range (nm)	500-600	600-700	700-800	800-1100

known soil and vegetation cover. (See appendix A for a description of data aquisition, field work and image correction).

This general pattern of data distribution is normally seen from various environments, and the before mentioned indices build on this distribution as illustrated by the indices in fig. 3. These are widely used as they correlate rather well to a range of vegetation parameters. For the present purpose however they have serious drawbacks:

- estimation of dead vegetation is not supported
- the shrub vegetation of these areas do not exhibit the high NIR reflectance
- the soil background contribution is important in low cover estimation. Different soils gives different contributions, and these are not only additional but also interfering in high cover signatures.

Based on work in rangelands in Australia, Botswana and Arizona several researchers have suggested the red band 5 as the best estimator of vegetation cover (Pech at al., 1986; Ringrose et al., 1987; Musick, 1984) - but figs. 2 and 3 illustrates obvious sources of error:

- different red absorption (B5) of green vegetation and litter
- different soil reflections in the actual band (soil end points in the B5 direction).

A major obstacle to the estimation of vegetation cover from brightness is thus the soil background contribution to the spectral signature. The soil reflectance in the semi arid Tropics is related to factors such as the organic matter content, mineralogy, iron content, particle size and salt precipitation. Hereby the background contribution to the vegetation signal varies significantly from dark to light soils.

The soil background problem has been studied in several works (e.g. Graetz et al., 1982; Huete et al., 1983, 1986 and 1987, Ezra et al., 1984; Heilman et al., 1986; Ringrose et al., 1987). It has lead to new vegetation index propositions such as the Soil Adjusted Vegetation Index (SAVI) derived from the NDVI (Huete, 1988).

In the rangeland context this problem has most extensively been treated in work form the Botswana savannah. Recent work (Ringrose, 1989) has shown, that the soil background interferes with the vegetation signal for multiple leaf layers (up to LAI=2.5), and thus that the traditional vegetation indices do not normalize for soil reflectance. On this background it is again proposed to estimate green leaf content using the darkening effect in the red band (B5).

A potential problem for vegetation cover assessments in general is thus, that information of the background soil is required. Even if this information was present, the major problem in this context is still, that most investigations concentrate on the green parts of the vegetation, and thus give no indication of how to estimate total ground cover including litter.

Model and method

In order to approach the problems described above, it was decided to use the information in all four bands and to investigate, to which extent the information of soils and vegetation could be separated in different dimensions. The data used consist of a test dataset with ground thruth on soils, vegetation cover, erosion status, a.o. collected during field work in 1987 and 1989 (see appendix A).

Data classification values are tabulated in

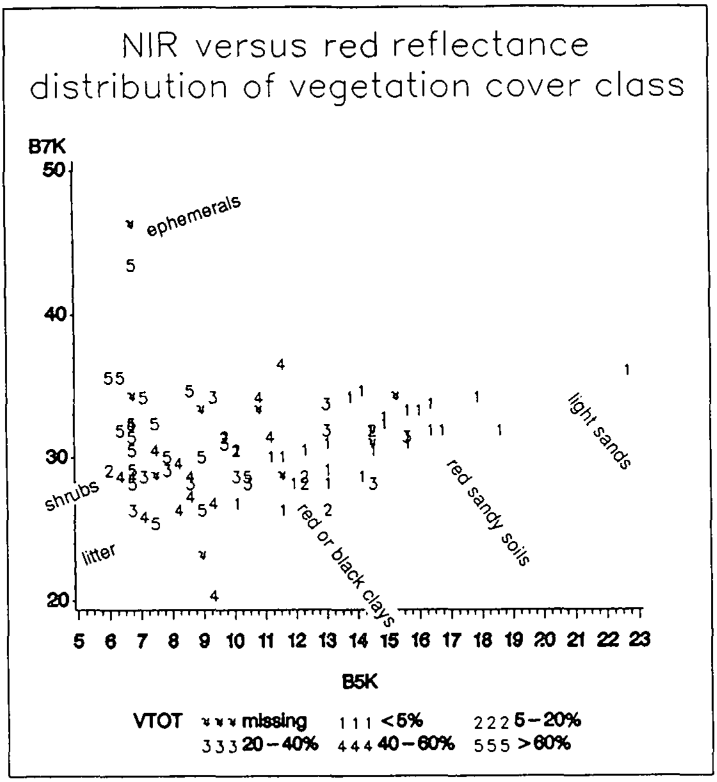

Figure 2: Distribution of surface classes in the B7 versus B5 dataspace — test data from Kitui District.

Table 2: Data classification values.

Vegetation cover (Symbol=VTOT)	Degradation class (Symbol=EROS)	Soil colour (Symbol=FARVE)
1) 0-5 %	1) none	1) red
2) 5-20 %	2) slight	2) browny red
3) 20-40 %	3) moderate	3) brown
4) 40-60 %	4) severe	4) dark brown
5) 60-100 %	5) very severe	5) yellowish brown
		6) brownish grey
		7) dark grey, black
Geomorphological/soil units (Symbol=GS)		
1) floodplain, alluvial soils		
2) plain and upland, clayey soils		
4) plain and footslopes, sandy soils		

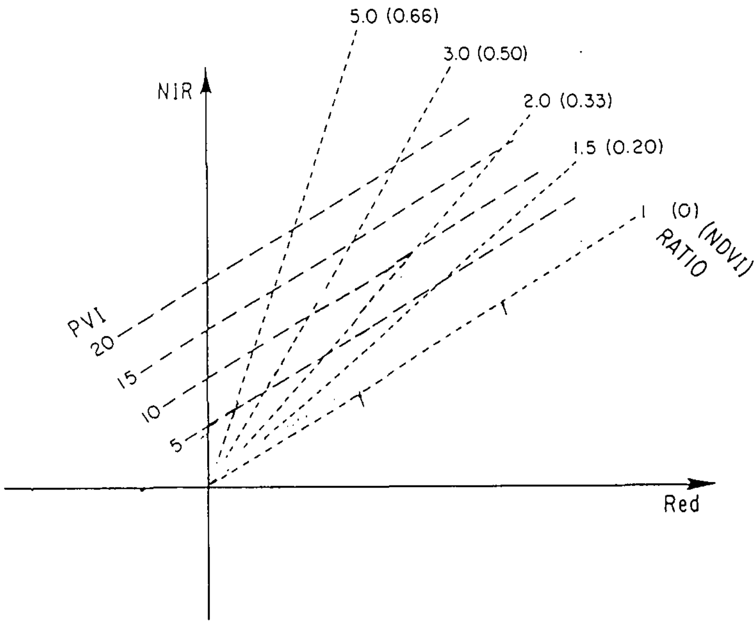

Figure 3: Vegetation Index isolines: Normal Difference Vegetation Index (NDVI).

table 2.

First an attempt to "equalize" the green and gray vegetation as a zero point for vegetation cover assessment over a given soil was made.

Fig. 4 shows the distribution of the test dataset in a dataspace expanded by the first and second principal components derived from a principal component analysis (PCA) on all four bands. It is seen, that soils (VTOT=1) are scattered along the brightness line (P2) and full cover vegetation (VTOT=5) along a line with both a greenness and a brightness component. The data in between is thus mixels of vegetation (gray and green) and different soils.

The idea followed was then to extract the data representing total vegetation cover (gray and green) and to carry out a PCA on this subsample, in order to find a rotation matrix, which would come out with a first axis collecting the variation of green and gray vegetation and a modified brightness axis as the second. This idea is sketched on fig. 4 in two dimensions as stipulated lines.

The total data set was thus transformed by this matrix giving axes P1 (greenness), P2 (modifies brightness) and P3. The fourth axis was left out of further analysis. P2 was now tested as a vegetation cover estimator.

The second problem described was the case of lacking soil information. Would there be information in the image spectral signatures which could help in differentiating the soil background?

It was anticipated, that by transforming the total dataset in the above mentioned way, the major vegetation information was collected in the plane expanded by the first and second axis. (Greenness and brightness characteristics of the vegetation). Therefore the information in the third axis was investigated

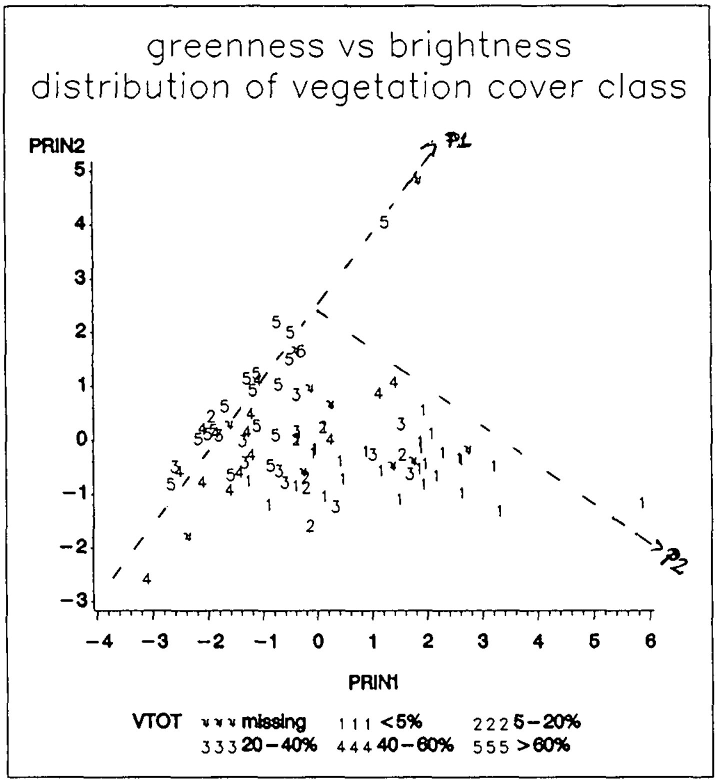

Figure 4: Datadistribution in the dataspace expanded by 1. and 2. principal axis.

Table 3: Spearman correlations of P2 and VTOT within GS units, 1987 and 1989.

	without fields		with fields	
	P289	P287	P289	P287
GS1	-0.8189	-0.8752	-0.7613	-0.7475
N	36	47	43	55
GS2	-0.8970	-0.9134	-0.9027	-0.8606
N	19	33	28	40
GS4	-0.9515	-0.8973	-0.9589	-0.9238
N	15	18	23	26

for information content on soils.

This part of the work was supported by investigations of the soil spectral signatures as measured by radiometer and correlated to different soil factors such as organic matter, free iron, colour, texture and particle size. (Further details on the analysis of the relationship between the various parameters and the spectral response of the band ranges represented in the Landsat MSS system will be published in a forthcoming Ph.D. thesis).

Results

P2 as vegetation cover estimator

Fieldplot signatures were subdivided into the three GS units and a Spearmann correlation analysis between P2 and vegetation cover class was carried out on each subsample. Both the 1987 and 1989 samples were used, as the 1989 image is rather cloud covered, anticipating, that the vegetation cover did not change a lot during this period. The result is seen in table 3, and it shows significant correlations in each unit.

The results are presented both with and without the fieldplots representing fields, as the fields located on the alluvial soils present a problem. Establishment of fields on this soil changes the soil surface very much from grayish brown to black - especially on ploughed fields. It is apparent, that exclusion of fields in unit 1 improves the correlations.

A linear regression of the P2 values versus the midpoint of the VTOT classes from the test data set was carried out, and as a preliminary investigation had indicated, that the relationship over red clays might be curvilinear, a log linear regression was also tried. Soil endpoints were established by these regressions.

The improvement in vegetation cover estimation as compared to estimation based on red band 5 (with endpoint defined as min/max within each GS unit) is shown in table 4. The improvement compared to this - rather rough - estimation can be seen to be substantial - especially assessment of vegetation cover on red clays is strongly improved. This improvement is even greater if a log linear relationship is used. Thus the idea of "zeroing" the green and gray vegetation seems promising.

P3 as soil separator

The colour of the soils showed up to be interesting for separation in this area. It was clearly related to the two geomorphological/soil units through the iron coating of the soils on the erosional plains, and the grayish colours of the alluvial floodplain. Slight differences in colour shades from red to brown and light to brown in these soils were related to the organic matter, such that erosion of the top soil actually made the surface more red on the erosional plains, and more light (and bright) on the floodplain, see table 5. Thus - at least in this special case - the major soil units might possibly be differentiated by spectral characteristics.

Table 4: Accuracy of different vegetation cover estimators.

	GS1*)	GS2	GS4
Number of fieldplots	36	28	23
C2 linear estimation	66 %	61 %	87 %
B5 linear estimation	63 %	48 %	53 %
C2 log-linear for GS2 and GS4	66 %	75 %	74 %

*) Without fields

Table 5: Means of organic matter and free iron versus colour class.

	Means		
colour class	org. matter (%)	free iron (ppm)	N
red (1)	0.7	84	4
browny red (2)	1.7	52	9
brown (3)	2.5	50	19
pale-yell.brown (5)	0.8	22	5
brownish gray (6)	1.8	32	11
gray/black (7)	1.9	20	3

Especially interesting was then, that this difference showed up in the third axis, which became a kind of "redness axis". This is due to the spectral characteristics of iron oxide (in the haematitic form). While generally darkening the spectral signal, it has an inflection on the curve in the range around 600 nm which gives rise to a local maximum in the B5 in the Landsat space (Zafyriadis, 1986). Thus the difference in B4 and B5 expresses to some extent the "redness" of the soil (which is not totally correlated to the iron content, as it is the coating of the single particles, which define the colour), and this difference is exactly what is expressed in the third axis of the above transformation. Interestingly, the same information is found in the third axis of a PCA based on a sample of bare soil reflections (even if the loadings are a little different). Thus it seems as if the dominant characteristics of the soil-vegetation complex is collected in the greenness/brightness space, while minor, but important information on the soils can be found in a dimension which is dominated by the spectral characteristics of B4 and B5. Fig. 5 shows the relationship of the third axis (P3) and the colour classes.

This colour separation was tested against vegetation cover class, and it showed, that the soil effect was actually significant under rather densely covered conditions. Unfortunately, the separation of the two major colour groups seemed to shift upwards under denser vegetation (exceeding around 50%), hampering the possibility of differentiating the soils in the image.

The reddness dimension thus supports a division of soil endpoints into the two geomorphological units, but it does not solve the question of different endpoints within these units. For the area under study, this present problems of differentiating red clayey soils from red sandy soils, which is imperative for the improvement of the estimation of vegetation cover over red clays. Also fields cleared and ploughed on the floodplain present a methodological problem, as they appear as grayish black soils not distinguishable from

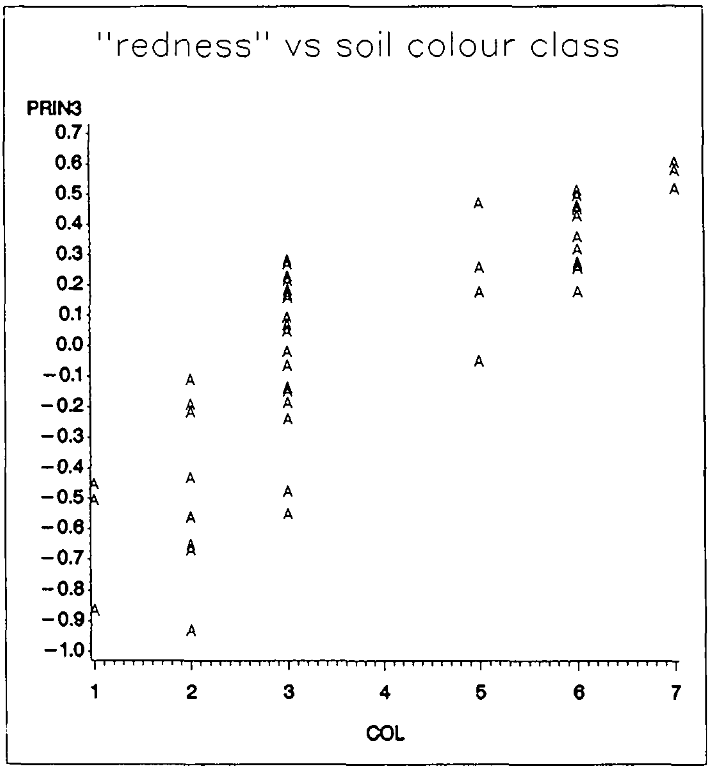

Figure 5: Distribution of P3-values in colour classes.

dense vegetation cover in this estimation.

Summary and discussion

Vegetation cover in rangeland areas is best estimated by some kind of brightness measure. This is due partly to the decreased reflectance in the NIR from the shrub vegetation, partly to the variation in the state of decay, which must be expected to be found both within and between different satellite scenes. Prerequisite for a good result is a former subdivision into major soil units.

It has been shown, that a brightness measure derived from the perpendicular distance from a vegetation line defined by a subset of dense vegetation covers (from non-shrub gallery forest over green shrubs to defoliated bush and litter), gave reasonable results as cover estimator. The improvement compared to other classifications (supervised classification and single band 5) was substantial. The result was further improved by establishing a log-linear relation over the red clayey soils.

The model used is rather simple, and a number of factors can possibly explain the reasons for non-linear relationships:

- the shadow effect of the vegetation may change significantly over different soils due to changes in phenology. The impression from the field was for instance, that the more small-leafed, thorny species dominated on the degraded parts of the floodplain compared to other sites.

- The soil endpoints must change progressively during the vegetation thinning due to the increased soil erosion, shifting towards brighter values with increased compaction or due to removal of smaller (darker) soil particles, leaving a thin sheet of sand.

Another significant result of the study was the apparent division of soil colours which was seen in the third dimension of the transformation. This dimension is at the same time orthogonal on the plane collecting most of the vegetation information, thereby opening a possibility of separating soil colour units without interference from the vegetation. It was shown, that for vegetation covers beneath around 50 %, red, iron coated soils could be separated from grayish floodplain soils. The separation existed even for denser covers, but moved upwards in C3-value. It should be further investigated if a vegetation neutral separation could be established, but at present, the soil separation can at least be supported by the information contained in this dimension.

The importance of the results on the soil differentiation is thus highly dependent on the amount of information available for a given area beforehand. If no soil maps are present, valuable information can probably be obtained by the above described transformation, and in the present case, where soil maps only exist for part of the area, interpretation of the satellite image based on this additional information aids in the delimitation of rough GS units.

References

Ezra, C.E., Tinney, L.R. & Jackson, R.D. (1984). Effect of Soil Background on Vegetation Discrimination Using Landsat Data. Rem. Sens. Env. 16: 233-242.

Fisher, N.M. (1978). Cropping Systems for Soil Conservation in Kenya. In: Soil and Water Conservation in Kenya, Inst. f. Dev. Studies and Faculty of Agric., Paper 28.

Frederiksen, P. (1991). The influence of soil factors on the spectral signature. Contribution to Ph.D. Thesis to be published.

Graetz, R.D. & Gentle, M.R. (1982). The Relationship between Reflectance in the Landsat Wavebands and the Composition of an Australian Semi-Arid Shrub Rangeland. Photogramm. Eng. Rem. Sens. 48(11): 1721-1730.

Heilman, J.L. & Boyd, W.E. (1986). Soil Background Effects on the Spectral Response of a Three-component Rangeland Scene, Rem. Sens. Env. 19: 127-137.

Huete, A.R., Post, D.F. & Jackson, R.D. (1983). Soil Spectral Effects on 4-space Vegetation Discrimination. Rem. Sens. Newsletter 83(1): 1-5, Univ. of Arizona.

Huete, A.R. (1986). Separation of Soil-Plant Spectral Mixtures by Factor Analysis. Rem. Sens. Env. 19: 237-251.

Huete, A.R. & Jackson, R.D. (1987). Suitability of spectral indices for Evaluating Vegetation Characteristics on Arid Rangelands. Rem. Sens. Env. 23: 213-232.

Huete, A.R. (1988). A Soil-Adjusted Vegetation Index (SAVI). Rem. Sens. Env. 25: 295-309.

Marker, B.L. & Barkham, J.L. (1987). Radiometric Properties of U:S: Processed Landsat MSS Data. Rem. Sens. Env. 22: 39-71.

Musick, H.B. (1984). Assessment of landsat Multispectral Scanner Spectral Indexes for Monitoring Arid Rangeland. Trans. Geosc. and Rem. sens. (6): 512-519.

Pech, R.P., Graetz, R.D. & Davis, A.W. (1986). Reflectance Modelling and the derivation of Vegetation Indices for and Australian semi-arid shrubland. Int. J. Rem. Sens. 7(3): 389-403.

Richardson, A.J., Wiegand, C.L. (1977). Distinguishing Vegetation from Soil Background Information, Photogramm. Eng. Rem. Sens. 43(12): 1541-1552.

Ringrose, S. & Matheson, W. (1987). Spectral Assessment of Indicators of Range Degradation in the Botswana Hardveld Environment. Rem. Sens. Env. 23: 379-396.

Ringrose, S., Matheson, W., Mogotsi, B. & Tempest, F. (1989). The Darkening Effect in Drought Affected Savannah Woodland Environments Relative to Soil Reflectance in Landsat and SPOT Wavebands, Rem. Sens. Env. 30: 1-19.

Robinove, C.J. (1982). Computation with Physical Values from Landsat Digital Data. Photogramm. Eng. Rem. Sens. 48(5): 781-784.

Spanner, M.A. (1982). Soil Loss Prediction in a Geographic Information System Format. Thesis in Geography, Univ. of California.

Stocking, M.A. (1988). Assessing Vegetative Cover and Management Effects. In: Lal R: Soil Erosion Research Methods, Publ: Soil and Water Conservation Society, Iowa.

Stycksen, M. (1988). Vandforårsaget erosion: En kort oversigt over: processer, kvantificering, jordbundsmæssige ændringer.

Zafyriadis, J-P. (1986). Satellitoptagelser til hydrogeologiske formål i semi-aride områder. Inst. for teknisk geologi, DtH.

Appendix A

Image acquisition

Landsat MSS imagery was acquired in order to cover as long a time span as possible, and recorded as close as possible to the two field work periods. The actual images were from June 1979, February 1987 and October 1989, representing different seasons with very different degrees of vegetation senescence.

Field work

Field work data were collected in two periods: the first in December 1987 and January 1988 and the second in September to november 1989. Data collected included total cover of vegetation and litter, ground cover type, terrain in major geomorphological types, soil texture and colour, erosion features, photos of all field plots.

During the first field work period all the roads and tracks in the area were travelled and data collection performed at three levels: Primary field plots were selected to represent all major surface types, as defined from available material: topographical maps (1:250.000), soil maps (National Soil map of 1:1.000.000 and a reconnaissance soil map of 1:250.000 covering a part of the area) and a NDVI image derived from the 1979 image data. On these plots the above mentioned data, except ground cover type and geomorphological type, were collected, and a soil sample was taken for laboratory analysis.

Secondary field plots denote systematic registrations for every five kilometers along all the major tracks. The registrations included total vegetation cover, soil colour, texture and signs of soil erosion.

Tertiary field plots were drawn from comments made on dictaphone along the routes followed, and they were used for supplementing the information on low cover/bare soil sites. The total number of field plots used in the analysis came to 93.

During the second field work period three areas representing the major geomorphological/soil (GS) types were selected, and the data collection was conducted along routes traversed by foot in order to avoid the "road bias". The total number of field plots analyzed from this period was 115.

Image correction

The Landsat satellite is passing over the area at about 9.30 local time, thereby recording a scene, where shadows influence the presentation of the area.

The first received image from 1979 was geometrically corrected to the UTM grid and resampled to a pixel size of 80 x 80 metres. The other images were geometrically corrected by an image to image registration based on the 1979 image. Each of the images has then been corrected for sun elevation and sensor sensibility on basis of the method of Robinove (1982) and the correction parameters of Markham and Barker (1987).

As the area contains absolutely no surfaces which are surely unchanged from year to year, a final band offset of the 1987 and 1989 image to the 1979 image was carried out based on shadow signature.

Participants

Arne Jensen	Department of Environmental Research Research Centre Risø P.O. Box 49 DK-4000 Roskilde
Bent Lorenzen	Botanical Institute University of Aarhus Norlandsvej 68 DK-8240 Risskov
Henrik Søgaard	Institute of Geography University of Copenhagen Øster Voldgade 10 DK-1350 Copenhagen K
Thomas Borup Svendsen Jan Nyholm Poulsen	Department of Land Data Enghavevej 2 DK-7100 Vejle
Henry E. Jensen Carsten Petersen Henrik Svendsen	Department of Agricultural Sciences The Royal Veterinary and Agricultural University Thorvaldsensvej 40 DK-1871 Frederiksberg C
Anton Thomsen Jens Grønbech Hansen	Department of Agrometeorology Research Centre Foulum P.O. Box 25 DK-8830 Tjele
Svend Christensen	Department of Weed Control Flakkebjerg DK-4200 Slagelse
Birte Boelt	Department of Industrial Plant and Seed Production Ledreborg Allé 100 DK-4000 Roskilde
Mathias Andersen	Department of Soil Physics, Soil Tillage and Irrigation Flensborgvej 22, Jyndevad DK-6360 Tinglev

Peter Frederiksen Pia Frederiksen Bernd Munier	Inst. of Geography, Socioeconomic Analysis and Computer Science Roskilde University DK-4000 Roskilde
Michael A. Hardisky	University of Scranton Department of Biology Scranton Pennsylvania 18510 4625 USA
Jürgen Schellberg	Institut für Pflanzenbau der Rheinischen Friedrich-Wilhelms Universität Katzenburgweg 5 5300 Bonn 1 Germany

Afdelinger under Statens Planteavlsforsøg

Direktionen

Direktionssekretariatet, Skovbrynet 18, 2800 Lyngby	45 93 09 99
Afdeling for Biometri og Informatik, Forskningscenter Foulum, Postbox 23, 8830 Tjele	89 99 19 00

Landbrugscentret

Centerledelse, Fagligt Sekretariat, Forskningscenter Foulum, Postbox 23, 8830 Tjele	89 99 19 00
Afdeling for Grovfoder og Kartofler, Forskningscenter Foulum, Postbox 21, 8830 Tjele	89 99 19 00
Afdeling for Industriplanter og Frøavl, Ledreborg Allé 100, 4000 Roskilde	42 36 18 11
Afdeling for Sortsafprøvning, Teglværksvej 10, Tystofte, 4230 Skælskør	53 59 61 41
Afdeling for Kulturteknik, Forskningscenter Foulum, Postbox 23, 8830 Tjele	89 99 19 00
Afdeling for Jordbiologi og -kemi, Forskningscenter Foulum, Postbox 23, 8830 Tjele	89 99 19 00
Afdeling for Planteernæring og -fysiologi, Forskningscenter Foulum, Postbox 23, 8830 Tjele	89 99 19 00
Afdeling for Jordbrugsmeteorologi, Forskningscenter Foulum, Postbox 23, 8830 Tjele	89 99 19 00
Afdeling for Arealdata og Kortlægning, Enghavevej 2, 7100 Vejle	75 83 23 44
Askov Forsøgsstation, Vejenvej 55, Askov, 6600 Vejen	75 36 02 77
Borris Forsøgsstation, Vestergade 46, 6900 Skjern	97 36 62 33
Jyndevad Forsøgsstation, Flensborgvej 22, 6360 Tinglev	74 64 83 16
Rønhave Forsøgsstation, Hestehave 20, 6400 Sønderborg	74 42 38 97
Silstrup Forsøgsstation, Oddesundvej 65, 7700 Thisted	97 92 15 88
Tylstrup Forsøgsstation, Forsøgsvej 30, 9382 Tylstrup	98 26 13 99
Ødum Forsøgsstation, Amdrupvej 22, 8370 Hadsten	86 98 92 44
Laboratoriet for Biavl, Lyngby, Skovbrynet 18, 2800 Lyngby	45 93 09 99
Laboratoriet for Biavl, Roskilde, Ledreborg Allé 100, 4000 Roskilde	42 36 18 11

Havebrugscentret

Centerledelse, Fagligt Sekretariat, Kirstinebjergvej 10, 5792 Årslev	65 99 17 66
Afdeling for Grønsager, Kirstinebjergvej 6, 5792 Årslev	65 99 17 66
Afdeling for Blomsterdyrkning, Kirstinebjergvej 10, 5792 Årslev	65 99 17 66
Afdeling for Frugt og Bær, Kirstinebjergvej 12, 5792 Årslev	65 99 17 66
Afdeling for Planteskoleplanter, Kirstinebjergvej 10, 5792 Årslev	65 99 17 66
Laboratoriet for Forædling og Formering, Kirstinebjergvej 10, 5792 Årslev	65 99 17 66
Laboratoriet for Gartneriteknik, Kirstinebjergvej 10, 5792 Årslev	65 99 17 66
Laboratoriet for Levnedsmiddelforskning, Kirstinebjergvej 12, 5792 Årslev	65 99 17 66

Planteværnscentret

Centerledelse, Fagligt Sekretariat, Lottenborgvej 2, 2800 Lyngby	45 87 25 10
Afdeling for Plantepatologi, Lottenborgvej 2, 2800 Lyngby	45 87 25 10
Afdeling for Jordbrugszoologi, Lottenborgvej 2, 2800 Lyngby	45 87 25 10
Afdeling for Ukrudtsbekæmpelse, Flakkebjerg, 4200 Slagelse	53 58 63 00
Afdeling for Pesticidanalyser og Økotoksikologi, Flakkebjerg, 4200 Slagelse	53 58 63 00
Bioteknologigruppen, Lottenborgvej 2, 2800 Lyngby	45 87 25 10

Centrallaboratoriet

Centrallaboratoriet, Forskningscenter Foulum, Postbox 22, 8830 Tjele	89 99 19 00

Frederiksberg Bogtrykkeri a·s 921101